Government of **Western Australia**
Department of **Mines, Industry Regulation and Safety**

RECORD 2019/3

METAMORPHIC HISTORY OF THE MOUGOODERRA FORMATION, YILGARN CRATON, WESTERN AUSTRALIA

by
S Parmenter
University of Waterloo, Canada

Geological Survey of Western Australia

UNIVERSITY OF WATERLOO

Government of **Western Australia**
Department of **Mines, Industry Regulation and Safety**

RECORD 2019/3

METAMORPHIC HISTORY OF THE MOUGOODERRA FORMATION, YILGARN CRATON, WESTERN AUSTRALIA

by
S Parmenter
University of Waterloo, Canada

PERTH 2019

Geological Survey of Western Australia

REFERENCE
The recommended reference for this publication is:
Parmenter, S 2019, Metamorphic history of the Mougooderra Formation, Yilgarn Craton, Western Australia: Geological Survey of Western Australia, Record 2019/3, 148p.

ISBN PDF 978-1-74168-839-9 (online)
ISSN 2204-4345 (online)

Grid references in this publication refer to the Geocentric Datum of Australia 1994 (GDA94). Locations mentioned in the text are referenced using Map Grid Australia (MGA) coordinates, Zone 50. All locations are quoted to at least the nearest 100 m.

About this publication
This Record is a Masters thesis researched, written and compiled as part of an ongoing collaborative project between the Geological Survey and Resource Strategy (GSRS) and the University of Waterloo, Canada. Although GSRS has provided field support for this project, the scientific content of the Record, and the drafting of figures, was the responsibility of the author. No editing has been undertaken by GSRS.

Published 2019 by the Geological Survey of Western Australia
This Record is published in digital format (PDF) and is available online at <www.dmp.wa.gov.au/GSWApublications>.

Further details of geological products and maps are available from:
Information Centre
Department of Mines, Industry Regulation and Safety
100 Plain Street
EAST PERTH WESTERN AUSTRALIA 6004
Telephone: +61 8 9222 3459 Facsimile: +61 8 9222 3444
www.dmp.wa.gov.au/GSWApublications

Cover image: Sunset over the Yalgoo Mineral Field. Photograph by T Ivanic, DMIRS

Metamorphic History of the Mougooderra Formation, Yilgarn Craton, Western Australia

by

Stacey Parmenter

A thesis

presented to the University of Waterloo

in fulfilment of the

thesis requirement for the degree of

Master of Science

in

Earth Sciences

Waterloo, Ontario, Canada, 2018

Author's Declaration

I hereby declare that I am the sole author of this thesis. This is a true copy of the thesis, including any required final revisions, as accepted by my examiners.

I understand that my thesis may be made electronically available to the public.

Abstract

Sedimentary sequences are common in granite-greenstone belts of Archean terranes. In the Yilgarn Craton of Western Australia, the Mougooderra Formation is an extensive sedimentary sequence that preserves low-variance metamorphic mineral assemblages and unconformably overlies older greenstone material within the Murchison Domain. Geochemical, mineral composition, and geochronological data is presented in combination with pressure-temperature estimates of the Mougooderra Formation to give insights into the geodynamic conditions of this region at the time of metamorphism.

Metamorphic rocks from the Mougooderra Formation display a range of metamorphic mineral assemblages that relate to different bulk compositions. Variations in the bulk compositions of these rocks can be largely attributed to variations in the amount of Fe, Mg, Ti, Al, and K. Taking into account the variation between these elements, the metamorphic rocks of the Mougooderra Formation can be separated into a high Fe-Mg group, a high Al group and an average pelitic group, each of which displays different metamorphic mineral assemblages. Results of thermobarometry and phase equilibrium modelling agree in terms of *P–T* estimates and indicate that the Mougooderra Formation experienced temperatures of 550–570°C and pressures of 2.2 to 3.3 kbar, while select samples of greenstone material near Mt Mulgine experienced *P–T* conditions of 610–650°C and 4 to 7.2 kbar. Garnet Lu-Hf and Sm-Nd geochronology returned respective ages of 2686±18 Ma (MSWD of 0.87) and 2611±35 Ma (MSWD of 0.51) for the Mougooderra Formation and ages of 2685±15 Ma (MSWD of 1.5) and 2590±21 Ma (MSWD of 0.24) for the greenstone material near Mt Mulgine, indicating simultaneous metamorphism. The difference in ages between the two garnet chronometers is consistent with slow cooling from the peak of metamorphism across this region. The metamorphic ages obtained in this study are considerably different than those of the granitic rocks within the surrounding area, including the cross-cutting Seeligson monzogranite, and suggests metamorphism was not triggered by the emplacement of post-tectonic granitic intrusions.

Calculated apparent thermal gradients of the rocks from the Mougooderra Formation and greenstone material near Mt Mulgine range between 1700 and 2300 °C/GPa and 900 to 1600°C/GPa, respectively, and are consistent with other apparent thermal gradients from the western Yilgarn Craton. These ages, *P–T* conditions, and high apparent thermal gradients can be used to infer a thin continental lithosphere and the presence of a large, long-lived heat source at the time of metamorphism. This is compatible with a plume-dominated tectonic regime in the Yilgarn Craton during the Neoarchean.

Acknowledgements

I would first like to thank my supervisor, Dr. Chris Yakymchuk, for his guidance, encouragement, and time throughout this project.

I would also like to thank Dr. Tim Ivanic and the Geological Survey of Western Australia for the opportunity to work on this project, and for the support offered both in the field and throughout the process of this thesis.

Additionally, I would like to thank Dr. Audrey Bouvier for her assistance and guidance during the acquisition of my garnet Lu-Hf and Sm-Nd data at Western University's GEOMETRIC Lab. I would also like to thank Dr. Wanda Aylward, David Grant, and Dylan Goudie from Memorial University for their assistance in gathering microprobe data and the creation of the MLA maps.

Thank you to Jill Kendrick for the many metamorphic discussions had in our office, and for reviewing many of the figures and text throughout this thesis.

Finally, thank you to the other grad students of the Earth Science Department for your friendship during these last two years, and to my family and friends for the continued support.

Table of Contents

List of Figures

List of Tables

List of Abbreviations

g: Garnet

st: Staurolite

q: Quartz

mu: Muscovite

ru: Rutile

liq: Liquid

pl: Plagioclase

bi: Biotite

cd: Cordierite

cu: Cummingtonite

gr: grunerite

mt: Magnetite

ilm: Ilmenite

chl: Chlorite

sill: Sillimanite

and: Andalusite

als: aluminosilicate

ep: Epidote

Chapter 1: Introduction

1.1 Introduction

Remnants of the Archean Eon are reported from across the globe and include well-known cratons such as the Superior Province of Canada, the Pilbara and Yilgarn cratons of Australia, the Kaapvaal craton of south Africa, and several others (Abbott et al., 2013). These terranes generally consist of several dominant rock types including alternating felsic and mafic greenstone sequences, granitic intrusions, and sedimentary sequences that unconformably overlie greenstone material (Anhaeusser, 2014). Greenstone belts within these Archean terranes are often heavily mineralized areas that can host world-class mineral (e.g. gold, base metal) deposits, however, despite the attention that these regions receive, a consensus on the mechanisms behind the formation and tectonic evolution of many of these terranes has not yet been reached (e.g. Bedard, 2018; Wyman, 2018). The Yilgarn Craton, like many Archean cratons, has two endmember tectonic models which attempt to explain the formation and evolution of the craton. The first model invokes uniformitarian tectonic processes and involves subduction and the accretion of terranes onto an older portion of continental crust (i.e. Youanmi Terrane; Fig. 1.1) where the large intrusions observed throughout the craton relate to melting of subducting oceanic crust (Myers, 1993; 1995; Wilde, 1996; Krapez and Barley et al., 2008; Standing, 2008). The second model involves thinning of the continental lithosphere, heating of the deep to middle crust, and diapiric and sagduction processes due to the presence of a large mantle plume at the base of the crust (Van Kranendonk et al., 2013). This model does not include subduction, which suggests a different plate tectonic regime compared with the modern day (e.g. Bedard, 2018).

In the Yilgarn Carton, the debate surrounding the topic stems largely from the age, poor exposure and preservation of outcrops, and lack of research in less mineralized regions of the craton (Van Kranendonk, et al., 2013).

The Yilgarn Craton consists of six terranes, three of which are heavily mineralized north-south-trending terranes known collectively as the Eastern Goldfields Superterrane (Cassidy et al., 2006). The majority of research within the Yilgarn Craton has been focused on these Au-rich regions, and previous studies in all terranes of the Yilgarn Craton have largely been focused on the timing and lithostratigraphy of the volcanic sequences and granitic suites. In contrast to this, metasedimentary sequences have received little attention. In addition to the sandstone and conglomerate units that dominate these sedimentary sequences, fine-grained material with *P–T* sensitive metamorphic mineral assemblages can also be found. These sequences provide key information on the thermal and burial history of the sedimentary packages. However, analysis of these metamorphic rocks is rarely undertaken. The aim of this study is to characterize the metamorphic history of an epiclastic sedimentary sequence known as the Mougooderra Formation in the Murchison Domain of the Yilgarn Craton. The characterization of these rocks will give the first *P–T* estimates for this region of the Murchison Domain and will help determine if these types of metamorphic rocks are useful recorders of tectonic events within the region. Characterization of the Mougooderra Formation was achieved using a variety of methods, including: petrography, whole-rock geochemical analysis using X-ray fluorescence (XRF), analysis of major element compositions using an electron probe microanalyzer (EPMA), and false coloured images using a scanning electron microscope (SEM) and Mineral Liberation Analysis (MLA) software. The data gathered from these methods was then used with phase equilibrium modelling and classic thermobarometry calculations to determine the pressure and

temperature conditions of the Mougooderra Formation. Coupled garnet Lu-Hf and Sm-Nd geochronology was used to constrain the timing of metamorphism within the region. The results of these analyses are tested against various tectonothermal models of the evolution of the Yilgarn Craton.

This thesis consists of six chapters. The remaining sections of Chapter 1 will briefly outline the geology of the Yilgarn Craton, the Murchison Domain, and the study area, followed by the major objectives of the project. Chapters 2 and 3 provide the methodology and results of the techniques mentioned. Chapter 4 presents the *P–T* estimates obtained from phase equilibrium modelling and thermobarometry. Chapter 5 discusses the geological significance of the *P–T* estimates and geochronology with respect to the Murchison Domain. Chapter 6 outlines and discusses potential future studies.

1.2 Background Geology

1.2.1 The Yilgarn Craton

The Yilgarn Craton (Fig. 1.1 inset) of western Australia is one of three Archean cratons located within the Australian continent and is also one of the largest Archean cratons in the world. The craton consists of six terranes that have previously been interpreted to have formed as the result of Archean orogenesis and amalgamation (Myers, 1993; 1995; Wilde, 1996; Krapez and Barley et al., 2008; Standing, 2008). Two of the terranes are made up dominantly of older gneissic material, while the remaining four contain low-grade granite-greenstone belts typical of Archean terranes (Cassidy et al., 2006).

The two dominantly gneissic terranes are known as the Narryer Terrane and the Southwest Terrane and are found in the northwestern and southwestern areas of the Yilgarn Craton (Fig. 1.1; Cassidy et al., 2006). Both are made up of high-grade granitic gneiss with ages between 3.2 and 2.6 Ga, and contain minor granodiorite, tonalite, layered intrusions, and overlying metasedimentary rocks (Myers, 1993; Cassidy et al., 2006). These terranes contain some of the oldest geological components on Earth. In addition to the well-known Jack Hills conglomerate, which contains Hadean detrital zircon (Compston and Pidgeon, 1986), the Narryer terrane also hosts the oldest known rocks in Australia, the 3.73 Ga Meeberrie Gneiss and the 3.73 Ga Manfred Igneous Complex (Cassidy et al., 2006). The three eastern most terranes are collectively known as the Eastern Goldfields Superterrane (Fig. 1.1) and each contains granite-greenstone belts that range in age from 2.81–2.66 Ga, as well as tholeiitic and komatiitic mafic–ultramafic rocks, felsic volcaniclastics, epiclastic sedimentary sequences, and large granitic intrusions (Cassidy et al., 2006).

The final terrane, known as the Youanmi Terrane, is the largest terrane within the craton and is comprised of two smaller domains that include the Murchison Domain to the west and the Southern Cross Domain to the east (Fig. 1.1; Cassidy et al., 2006). The two domains are separated by the Youanmi Fault system; however, they display similar ages and lithostratigraphic units that suggest a shared tectonic history between the two (Myers 1993; Chen et al., 2003; Cassidy et al., 2006). Both domains comprise north-trending greenstone belts made up of several cycles of ultramafic to felsic volcanic rocks (~3.05–2.70 Ga), and numerous granitic and mafic-ultramafic intrusions (Cassidy et al., 2006; Ivanic et al., 2010; Ivanic et al., 2012; Van Kranendonk et al., 2013). The presence of inherited >4.0 Ga zircons in both the Murchison and Southern Cross Domains, and Nd model ages from granitic rocks greater than 3.0 Ga suggests

that the Youanmi Terrane may have been built on an older crustal component with the Narryer and Southwestern Terranes (Nelson et al., 2000; Champion and Cassidy, 2007; Van Kranendonk et al., 2013).

1.2.2 The Murchison Domain

Despite the important geological features within the terranes of the western Yilgarn Craton, research within domains such as the Murchison has been neglected for the more mineral-rich terranes of the Eastern Goldfields Superterrane. In addition to the debate about the overall tectonic setting of the Yilgarn Craton, smaller terrane scale questions still remain, such as the relationship between the older gneissic terranes and the Murchison Domain, the origin of the greenstone belts and granitoid intrusions, the relationship between epiclastic sedimentary sequences and granitic intrusions, and the general metamorphic histories of these domains.

Previous work in the Murchison Domain began in the early 1990s, the majority of which focused on general mapping of the area or understanding the timing relationships between the greenstone belts and granitic intrusions (Myers, 1993, 1995; Wang, 1998; Watkins and Hickman, 1990; Wilde et al., 1996; Yeats et al., 1996). In addition to these studies, in 2005 the Geological Survey of Western Australia (GSWA) began a 1:100 000 scale mapping project within the Murchison Domain with the aim of better understanding the tectonic history of the region. The project is still ongoing but has so far resulted in a better understanding of the timing of granitic and mafic intrusions, better constraints on the lithostratigraphic scheme of the greenstone material, and a better idea of the overall evolution of the domain (e.g. Van Kranendonk and Ivanic, 2009; Ivanic et al., 2010; Ivanic 2012; Van Kranendonk et al., 2013).

A lithostratigraphic scheme that incorporates the new data acquired during the mapping project with previous work was put forward in 2009 (Van Kranendonk and Ivanic, 2009). This

work has been built upon and thus-far has identified four volcano-sedimentary sequences displaying typical dome and keel structures within the region. These include the 2950 Ma Mount Gibson Group, the 2814–2800 Ma Norie Group, the 2785–2734 Ma Polelle Group, and the 2724–2700 Ma Glen Group (Van Kranendonk and Ivanic, 2009). The later three greenstone sequences have been interpreted to represent nearly 225 Ma of continuous plume-related magmatism that transitions from mafic to felsic compositions over time (Van Kranendonk et al., 2013).

In addition to the volcano-sedimentary sequences, large ultramafic-mafic and granitic intrusions are found throughout the Murchison Domain (Van Kranendonk and Ivanic, 2009; Ivanic et al., 2010; Ivanic et al., 2012). The mafic-ultramafic intrusions make up a large volume of the rocks found in the northern portion of the Murchison Domain, are host to V, Cr, Ni, Cu, and PGE mineralization, and are considered to be coeval with the early stages of greenstone formation (Ivanic et al., 2010). The ultramafic–mafic intrusions and the ultramafic–mafic rocks within greenstone belts are interpreted to be partial melts of mantle material at varying depths and sources based on trace element compositions (Van Kranendonk et al., 2013). Older ultramafic–mafic rocks have been interpreted to represent partial melting of deep, primitive mantle sources, while the younger ultramafic–mafic rocks have been interpreted to represent shallower mantle melts affected by greater amounts of crustal contamination over time (Van Kranendonk et al., 2013).

While ultramafic-mafic intrusions are associated with the start of the greenstone cycles, granitic intrusions have been interpreted to be coeval with the latter stages of greenstone cycles (Ivanic et al., 2012). In general, the older granitic intrusions of the Murchison Domain have relatively low concentrations of SiO_2, and high concentrations of MgO and Ni, whereas younger

granites have compositions consistent with a more fractionated magma, including increased concentrations of SiO_2 and K_2O as well as larger Eu anomalies (Ivanic et al., 2012). The variation seen within the granitic suites has been interpreted to be the result of continuous re-melting of lower crustal components at progressively shallower crustal levels that resulted in the production of increasingly more fractionated granitic melts over time (Ivanic et al., 2012).

1.3 Study Area

The study area for this thesis is located within the Murchison Domain, near the town of Yalgoo, Western Australia (Fig. 1.1). This thesis focuses on the Mougooderra Formation within the Ninghan area (Fig. 1.2). The formation is a 2–3 km thick metasedimentary unit that unconformably overlies greenstone material of the Polelle and Norie groups (Zibra et al., 2018). Samples for this thesis have been taken primarily from the sedimentary layers within the Mougooderra Formation, however, select samples of the greenstone material from the Polelle Group near Mt Mulgine were also analysed (Fig. 1.1-1.2; Table 1.1). Sample locations and further information can be found in Appendix A.

The Mougooderra Formation is part of the Glen Group and is composed of a range of lithologies including interbedded conglomerate, sandstone, and siltstone, with minor banded iron formation, chert, and basalt (Fig. 1.3a; Watkins and Hickman, 1990). These rocks display a normal, upward fining sequence that has previously been interpreted as the transition from a shallow shelf environment to a distal, deeper marine environment (Watkins and Hickman, 1990). Detrital zircon and Th/U analyses from the Mougooderra Formation near the Yalgoo Dome indicate similar ages and Th/U ratios to those of the nearby Kynea Tonalite and granitic rocks of the Rothsay Suite (Zibra et al., 2018). In addition, structural studies of the Yalgoo Dome, and

associated granitoids such as Mt Mulgine, have documented doming fabrics and indicate that sediments of the Mougooderra Formation may have been sourced from these granitic rocks and overlying greenstone material (Zibra et al., 2018).

This thesis examines the metapelitic material within the Mougooderra Formation (Fig. 1.3b, c), which display a range of mineralogical assemblages with respect to bulk composition. In order to reach a better understanding of the tectonic evolution of the Yilgarn terrane and Archean terranes in general, robust pressure-temperature (*P*–*T*) constraints from metamorphic rocks with useful mineral assemblages are required to assess the timing of burial and heating. The metamorphic assemblages found within the metapelitic rocks of the Mougooderra Formation allow for the first detailed *P*–*T* constraints of the Ninghan area to be determined, which is critical for characterizing the tectonometamorphic history of the region.

1.4 Research Objectives

Original work within the Murchison domain suggested that horizontal tectonics was the major geodynamic process (Myers, 1993; 1995; Wilde, 1996; Krapez and Barley et al., 2008; Standing, 2008), and therefore the driving force behind the deposition and metamorphism of this material. However, more recent work within the domain suggests that an alternative tectonic regime may have been responsible for the development of the granites and greenstones found within the Murchison Domain (Van Kranendonk et al., 2013). In addition to the well-studied granitic and greenstone material in the region, metasedimentary sequences stratigraphically overlie the greenstone belts. The Mougooderra Formation is one of the largest metasedimentary sequences within the region, and besides mapping in the 1990s by Watkins and Hickman (1990) that noted characteristics such as the sedimentary sequence and clast types, very little work on

this metasedimentary sequence has been done until recently. Much of the history of the Mougooderra Formation still remains unknown including the provenance of much of the sedimentary material within the Ninghan area, the metamorphic conditions, and the overall geodynamic environment at the time of metamorphism. The purpose of this thesis is to constrain the metamorphic history of the Mougooderra Formation through petrography, mineral analysis, phase equilibrium modelling and garnet geochronology, and use this information to test the current tectonic models of the Murchison Domain. Understanding the metamorphic histories of these metasedimentary sequences is an important step towards fully understanding the tectonic setting of the Murchison Domain and the tectonic evolution of Archean cratons in general.

This study aims to better understand the metamorphic history of the Mougooderra Formation through three major objectives, these include (1) to characterize the metamorphic rocks and mineral assemblages within the Ninghan area, (2) to determine the pressure and temperature conditions under which those mineral assemblages formed, and (3) to determine the timing of metamorphism by dating specific metamorphic minerals (i.e. garnet) within these rocks.

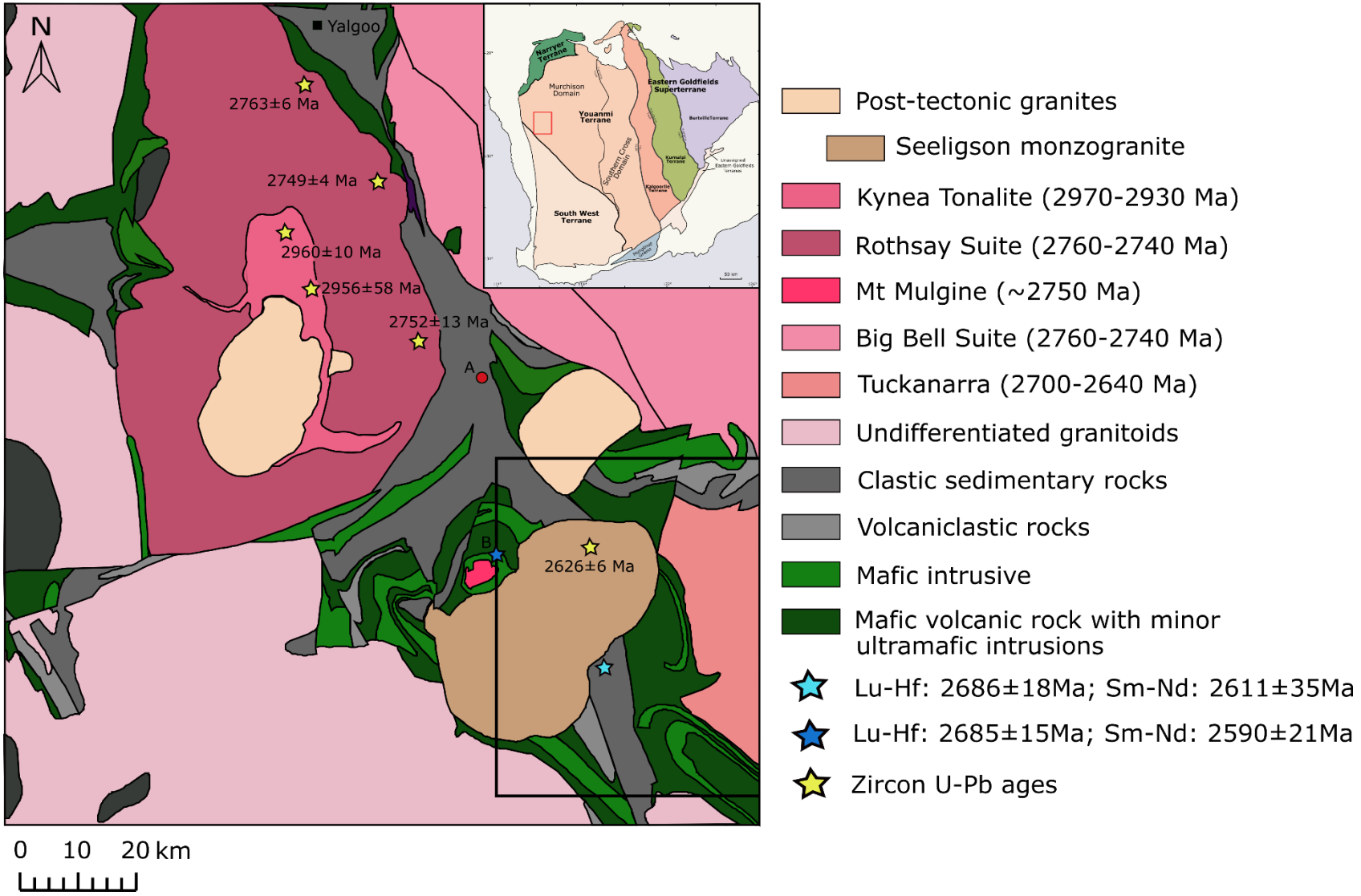

Figure 1.1. Bedrock map of the Yalgoo and Ninghan areas downloaded and modified from the GSWA's online interactive geological map (GeoVIEW) with dates from Clos et al. (2018). Inset shows the domains and terranes of the Yilgarn Craton modified after Cassidy et al. (2006). The black outline indicates the location of Figure 1.2, while letters A and B represent sample locations that are outside the limits of Figure 1.2. Letters A and B represent relative sample localities, see Table 1.1 for exact sample locations.

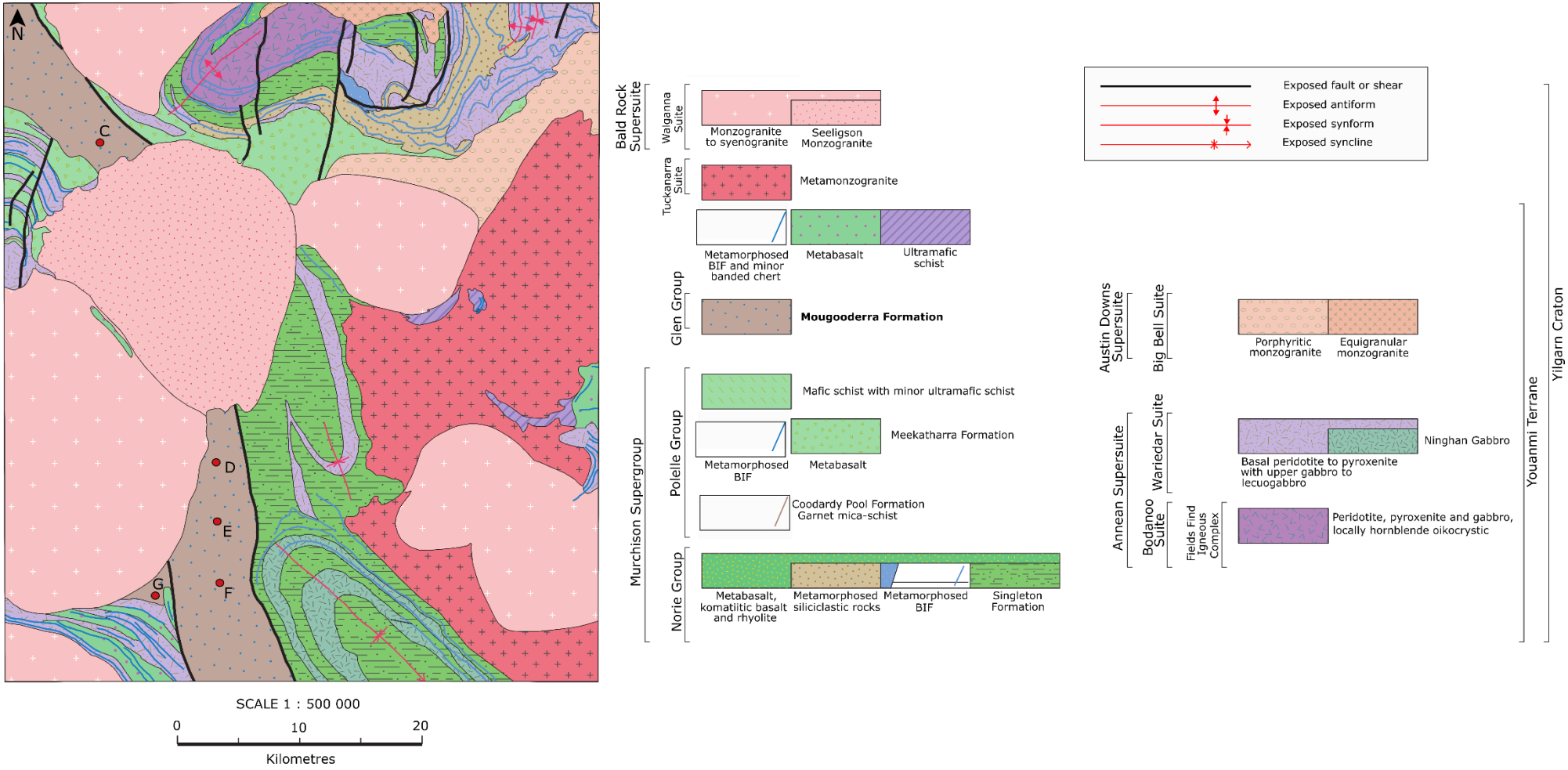

Figure 1.2. Interpreted bedrock map of the Ninghan area modified with sample localities after Ivanic (2018). Letters C-G represent relative sample localities, see Table 1.1 for exact sample locations.

Table 1.1. Sample locations and major metamorphic minerals.

Sample Locality	Sample	Easting	Northing	Major Metamorphic Minerals
A	**207691**	500197	6801963	Andalusite
	207697	500197	6801963	Andalusite
	229105	500197	6801963	Andalusite
B	**207690**	500499	6772698	Garnet, amphibole
	229151	500499	6772698	Garnet, amphibole
	229146	501062	6772484	Cordierite
	229148	497923	6771884	Amphibole, biotite
	229149	497923	6771884	Amphibole
C	**207602**	507755	6780386	Andalusite
	229106	509123	6780266	Andalusite
	229107	509123	6780266	Andalusite
	229109	509658	6779783	Andalusite
	229137	509616	6779803	Cordierite
	229152	503577	6781411	Cordierite
D	**207695**	517089	6757120	Andalusite, cordierite
	207692	516595	6756846	Garnet, cordierite, amphibole
	207694	516888	6756813	Cordierite
	207693	516664	6756852	Garnet, amphibole
	229101	516597	6756844	Garnet, cordierite
	229111	516588	6756937	Garnet, Cordierite
	229112	516588	6756937	Garnet, Cordierite
	229113	516648	6756904	Andalusite, biotite, cordierite
	229114	516834	6756895	Andalusite, cordierite
	229115	516916	6756901	Garnet, chlorite
	229116	516953	6756901	Cordierite
	229117	517089	6756978	Cordierite, andalusite
	229119	516597	6756844	Garnet, cordierite
	229120	516597	6756844	Garnet, cordierite, amphibole
	229124	516959	6756401	Garnet, amphibole
	229125	517116	6756110	Andalusite
	229126	517268	6755655	Andalusite
	229155	516996	6755779	Cordierite, andalusite
	229157	517216	6755692	Andalusite
	229158	517216	6755692	Andalusite

Table 1.1. (continued).

Sample Locality	Sample	Easting	Northing	Major Metamorphic Minerals
E	**229130**	518043	6752074	Andalusite, chlorite
	229132	518076	6751728	Andalusite
	229127	518293	6751231	Andalusite
F	**229110**	518345	6745826	Andalusite
G	**211117**	512517	6744201	Cordierite
	211116	512517	6744201	Andalusite, cordierite
	229133	512564	6744224	Andalusite
	229134	512564	6744224	Andalusite
	229135	512295	6744251	Andalusite
	229136	512382	6744132	andalusite, cordierite

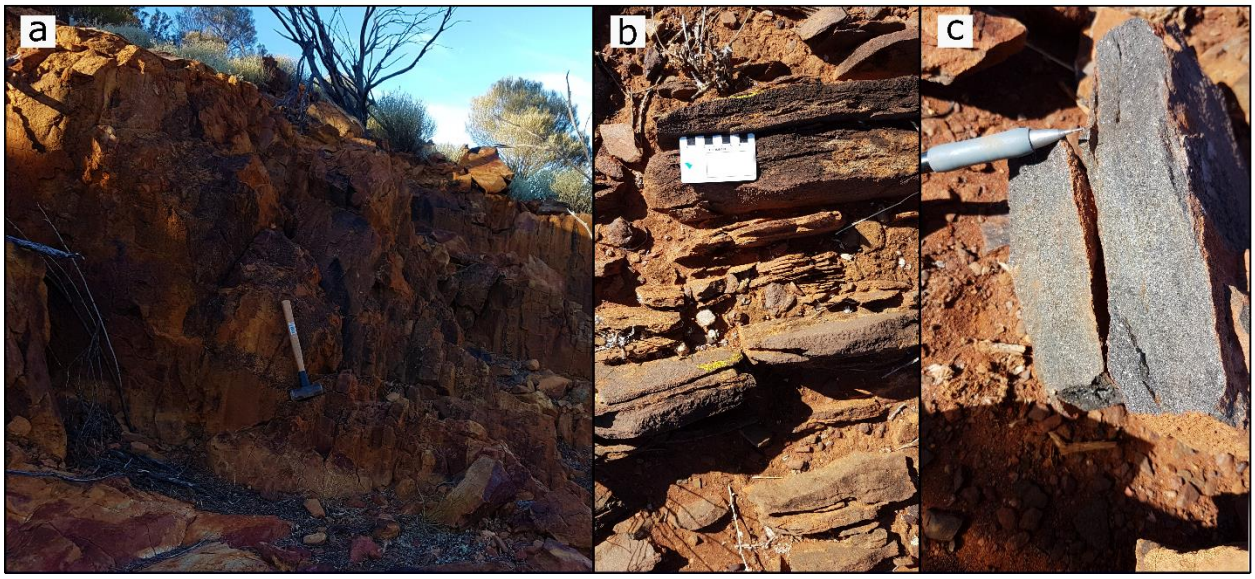

Figure 1.3. Field photos of the Mougooderra Formation: (a) A large conglomerate and sandstone package, (b) metapelitic material (sample 229111) from the Mougooderra Formation are commonly more heavily eroded and weathered, however, still preserve relatively unaltered rock (c).

Chapter 2: Methods

2.1 Geochemistry

Whole-rock geochemical analysis for thirty-three samples was completed by Bureau Veritas Minerals (Perth, Australia). Major element analyses were completed through the use of X-ray fluorescence (XRF) on a glass disc fused with 12:22 Lithium-borate flux for each sample (BV Minerals analysis type: XF202) with an elemental precision better than ±1% of reported values. Trace elements were determined through fused bead LA-ICP-MS (BV Minerals analysis type: LA101), and FeO concentrations were determined through acid digestion and volumetric titration (BV Minerals analysis type: GC101). Bureau Veritas Minerals quality assurance is achieved through the use of blanks, duplications, and the analysis of certified international standards. To assure quality data within each batch, the GSWA also includes 10% standards and 10% blanks in addition to the standards and blanks used by the lab. Both whole rock geochemistry and ferrous iron concentrations were required for the calculation of pseudosections and to constrain pressure and temperature conditions.

2.2 Scanning Electron Microscope (SEM) and Mineral Liberation Analysis (MLA)

An FEI Quanta 400 scanning electron microscope (SEM) was used with Mineral Liberation Analysis (MLA) software at Memorial University of Newfoundland to collect false coloured images and backscatter images for a select number of samples. Samples were analysed using an accelerating voltage of 25kV, and a beam current of 10nA. The false coloured images produced by MLA software allows for a better understanding of the textural and mineralogical distributions of a sample than traditional petrography can achieve on its own. This is because the

MLA software is capable of mapping very fine-grained mineral relationships and because of its ability to differentiate between minerals with similar optic properties. The SEM-MLA was used in combination with optical petrography to understand the mineralogy and textures of samples from the Mougooderra Formation.

2.3 Electron Probe Microanalyzer (EPMA)

Major element compositions of the main phases within garnet-bearing samples were determined using the JEOL JXA-8230 electron probe microanalyzer (EPMA) at the Department of Earth Sciences, Memorial University of Newfoundland. Synthetic and natural standards were used for calibration and data reduced using ZAF correction online by the JEOL software. The main minerals of interest include garnet, amphibole, biotite, chlorite, cordierite, and feldspar. Minerals were analysed with an accelerating voltage of 15kV, a beam current of 20nA, a beam diameter of 1μm for non-hydrous minerals, and a beam diameter ranging between 3-15μm for hydrous minerals. X-ray compositional maps of garnet porphyroblasts were collected to determine any zoning patterns within the grains with respect to Ca, Fe, Mn, and Mg. Mapping conditions of 15kV and 200nA were used with a dwell time of 150ms and step sizes that ranged between 3.5 to 6.5μm depending on the size of the garnet porphyroblast. Because mineral compositions are sensitive to changes in pressure and temperature, the EPMA results were used in conjunction with pseudosections and garnet-biotite thermometry to constrain the *P–T* conditions.

2.4 Thermobarometry

Temperature estimates for the Mougooderra Formation were determined using measured mineral compositions (EPMA data) combined with seven garnet-biotite thermometer calibrations (Thompson, 1975; Holdaway and Lee, 1977; Ferry and Spear 1978; Perchuk and Lavrent'eva. 1983; Dasgupta et al., 1991; Bhattacharya et al., 1992; Holdaway, 2000), while pressures were determined through the garnet-biotite-Al_2SiO_5-quartz barometer calibration of Wu (2017).

2.5 Phase Equilibrium Modelling

Phase equilibrium diagrams were calculated using bulk compositions obtained through XRF. The rocks from the Mougooderra Formation were used to model mineralogical relationships and in conjunction with EPMA data were used to determine peak metamorphic conditions. Phase equilibrium diagrams were calculated using Thermocalc 3.33 (Powell and Holland, 1988) and internally consistent data set tcds55 (Holland and Powell, 1988; updated 2003). Diagrams were constructed in the MnO-Na_2O– CaO–K_2O–FeO–MgO–Al_2O_3–SiO_2–H_2O–TiO_2–Fe_2O_3 (MnNCKFMASHTO) system with clino-and orthoamphibole a-x models of Diener et al. (2007), garnet, biotite, and ilmenite-hematite a-x models of White et al. (2005), cordierite, epidote, and staurolite a-x models of Holland and Powell (1998), plagioclase and K-feldspar a-x models of Holland and Powell (2003), muscovite a-x model of Coggon and Holland (2002), melt model of White et al. (2007), and magnetite a-x model of White et al., (2000). The use of this system allows both H_2O content and ferric iron to be considered during calculations. For this study, since the rocks being considered are subsolidus H_2O was considered to be in excess (e.g. Webb et al., 2015). A ferric iron value was assigned based on iron values obtained through

titration methods and ranged between 0.35 and 4.0 mol% Fe_2O_3 depending on the sample being considered.

2.6 Garnet trace element zoning

Trace element zoning in garnet was measured using 4–14 points across garnet grains from samples chosen for garnet geochronology. Transects across three garnets were measured from sample 207692, three grains from sample 229151, and two grains from sample 207690 (same locality as sample 229151). Garnet in thin section was analyzed using an Analyte G2 193nm laser ablation system coupled to an Agilent 8800 QQQ-ICP-MS operating in single-quadrupole mode in the Metal Isotope Geochemistry Laboratory at the University of Waterloo. Garnet was ablated using a 50 μm spot, a 5 Hz repetition rate and a fluence of 5 J/cm^2 (measured at the surface of the sample). Ablation occurred in a He atmosphere in a Helex2 chamber. The aerosol was transported to the torch using 0.5 L/min He and 1.5 L/min Ar makeup gas that was added in a T-junction between the chamber and the torch. NIST612 was used as the external standard (measured every ~5 unknown analyses) and ^{29}Si was used as the internal standard using an assumed concentration of 16.9 wt.% Si in garnet. The following masses were measured all with 10s dwell times: ^{29}Si, ^{139}La, ^{140}Ce, ^{141}Pr, ^{146}Nd, ^{147}Sm, ^{153}Eu, ^{157}Gd, ^{159}Tb, ^{163}Dy, ^{165}Ho, ^{166}Er, ^{169}Tm, ^{172}Yb, ^{175}Lu, ^{178}Hf. A 20s gas background was measured prior to a 30s ablation of the garnet. Data were reduced using Iolite (v3.1) and the "Trace_element_IS" data reduction scheme (Paton et al., 2011). BHVO-2G was monitored as a secondary standard and REE were within 10% of the preferred values from the GeoRem database (Jochum et al., 2016).

2.7 Garnet Lu-Hf and Sm-Nd Geochronology

Rock samples were crushed to ~1mm and garnet grains were then hand picked under a binocular microscope. Whole-rock powders were prepared by milling ~15 ml of crushed sample in an agate jar using a Retsch PM200 planetary ball mill.

Chemical processing and column chemistry were carried out at the GEOMETRIC Lab at the University of Western Ontario. All teflonware was Savillex® PFA beakers and PTFE Teflon vessels for the Parr® vessel dissolution. At the GEOMETRIC Lab, chemicals used for processing were BDH® Aristar Ultra for HF, $HClO_4$, and H_2O_2, while HCl and HNO_3 were house distilled from BDH® Aristar Plus in Savillex DST-1000 stills. Water was purified to a resistivity of 18.2 MΩ using a Millipore Advantage 10 system and QPOD Element dispenser. Chemistry was carried out in a Class 10 vertical laminar flow polypropylene fume hood. Total analytical blanks were <10pg for Hf and <5pg for Nd, Sm and Lu, which are negligible.

For samples 207692 and 229151, garnet splits were processed along with each corresponding whole-rock powder for each sample in two batches. For whole-rocks, two acid dissolution methods on hot plate and Parr® bomb vessels were used to obtain partial or total dissolution of refractory minerals respectively. A first split was dissolved using Parr® vessel dissolution at 180 ºC (at the University of Waterloo) with a 3:1 HF:HNO_3 mix to ensure that all refractory minerals including zircons were fully dissolved. A second split was dissolved in beakers at 120 ºC on table top hot plate at atmospheric pressure to avoid the dissolution of refractory minerals which may be at isotopic disequilibrium.

For each garnet sample, five fractions were prepared for trace element analysis and Sm-Nd and Lu-Hf geochronology according to the methods described in Zirakparvar et al. (2010).

About 0.09 to 0.20 g of hand-picked crystals were first acid washed at room temperature in 1M hydrochloric acid (HCl), sonicated for 5 minutes, rinsed in H_2O, sonicated for 5 minutes, and water was pipetted off. Concentrated 15M nitric acid (HNO_3), ultrapure 29M hydrofluoric acid (HF) (1:10 of HNO_3:HF), were added to the beakers for digestion for 24-48 hours at 120 ºC on hot plate, repeated one more time for the first batch of garnets for 207692. For 229151, garnet grains were slightly crushed within an agate mortar before leaching to facilitate the dissolution process.

All samples (garnet and whole-rock) were dried, covered with perchloric acid and evaporated at 150-180 ºC. For whole-rock and garnet samples, the final dissolution step consists of uptaking samples in 6M HCl and H_2O_2. After that, solutions were dried and then dissolved again in 6M HCl. A fraction of the whole-rock and garnet solutions were used for quadrupole ICPMS trace element analysis (Thermo iCAP Q at the Western GEOMETRIC Lab) to optimize spike addition. Mixed enriched ^{149}Sm-^{150}Nd and ^{176}Lu-^{180}Hf spikes for whole-rocks and garnets were added to each sample solution in ideal proportions (to reach $^{150}Nd/^{144}Nd$=0.35, and $^{180}Hf/^{177}Hf$=2.3), fluxed together, and once again dried down to ensure sample-spike equilibration.

The column chromatography protocols used for Hf-REE separation from the sample matrices and elemental purification are described in Bouvier et al. (2008, 2015). In summary, ~8.7 ml of Biorad AG50W-X8 200-400 mesh cation exchange resin was loaded in Savillex® PFA Teflon columns to separate Hf and other high field strength elements (in 0.1M HF-1M HCl) from the sample matrix (in 2.5M HCl) and from the REE (in 6M HCl) sequentially. Hafnium was further purified using a 0.6 ml Eichrom Ln-spec resin chemistry protocol in house-made shrinkable Teflon columns following the protocol described in Bouvier at al. (2008). The

fractions containing REE were further processed to extract sequentially Nd (in 0.2M HCl), Sm (in 0.4M HCl) and Lu (in 6M HCl) with 25-50% of Yb (to correct internally the instrumental mass bias) from the rest of the REE on a 1ml Eichrom Ln-spec resin bed in quartz columns.

Purified fractions of Sm, Nd, Hf and Lu with Yb were analyzed using a Thermo Neptune Plus MC-ICPMS coupled with an Aridus II desolvating system at Laboratoire Magmas et Volcans in Clermont-Ferrand (France). The average $^{143}Nd/^{144}Nd$ ratios and 2 standard deviation (2SD) for the JNd_i Nd isotopic standards measured in static mode (60 ratios) during two analytical sessions were respectively 0.512042 ± 0.000004 (2SD, at 50 ppb Nd), 0.512056 ± 0.000006 (2SD, at 40 ppb Nd). The Nd isotopic compositions of the samples were normalized for each session to the accepted JNdi-1 Nd standard value of 0.512115. The average $^{176}Hf/^{177}Hf$ ratios and 2SD for the JMC 475 Hf isotopic standards measured in static mode (60 ratios) during two analytical sessions were respectively 0.282160 ± 0.000009 (2SD, at 10 ppb Hf), 0.282205 ± 0.000012 (2SD, at 20 ppb Hf). The Hf isotopic compositions of the samples were normalized for each session to the accepted JMC 475 Hf standard value of 0.282160. To verify the accuracy of cup bias corrections, a BCR-2 was also measured with a corrected composition at $^{176}Hf/^{177}Hf$= 0.282874 ± 0.000002 which is in agreement with the reported average value of 0.282870± 0.000008 for BCR-2 by Weis et al. (2007). A block of 30 ratios was measured for the Sm samples, along with the SRM 3147 Sm standard at 10ppb to control stability and accuracy. The Lu fractions were analyzed with ~25-50% of the Yb to correct for instrumental mass bias on $^{175}Lu/^{176}Lu$ using the method described in Vervoort et al. (2004). For age calculations, we used the external reproducibility of ±0.000010 for $^{143}Nd/^{144}Nd$ isotopic ratios and ±0.000010 for $^{176}Hf/^{177}Hf$ isotopic ratios (or the internal precision if higher) and of ±0.5% for $^{147}Sm/^{144}Nd$ and $^{176}Lu/^{177}Hf$ based on repeated measurements of BCR-2 standards using the same isotopic dilution

method. Isochron ages were calculated using the Isoplot macro 4.14.11 for Excel by Ludwig (2011).

Chapter 3: Results

3.1 Geochemistry

Whole-rock geochemical analyses of various sedimentary rocks from the Mougooderra Formation and select samples from the Polelle Group near Mt Mulgine are presented in Table 3.1. Whole-rock data for pelitic to semi-pelitic rocks are presented in terms of Fe + Mg + Ti mol%, Al mol% and K mol% in Figure 3.1. Whole-rock trace element data can be found in Appendix B. Measured whole-rock compositions define three general groups, including a high Fe + Mg group, a high Al group, and an average pelitic group.

Rocks of the high Fe-Mg group have concentrations of SiO_2 that range between 44.18 and 59.83 wt%, and concentrations of Al_2O_3 ranging from 7.42 to 19.20 wt%. Concentrations of Fe and Mg between these samples vary, with FeO values ranging between 5.00 and 31.80 wt%, and MgO concentrations of 3.56 to 18.20 wt%. The majority of these samples have consistent FeO and MgO values that fall within the 11–17 wt% and 3–6 wt% ranges, respectively. However, samples 229124 and 207693 are considerably more FeO enriched with respective values of 31.80 and 24.16 wt%. Samples 229148 and 229149 are relatively FeO depleted and have MgO values of 17.37 wt% and 18.20 wt%. The concentrations of the other major elements for the rocks of the high Fe-Mg group are generally consistent with Fe_2O_3 values <5.00%, TiO_2 concentrations <0.83wt%, MnO values <0.22 wt%, CaO+Na_2O values <2.59 wt%, and K_2O values between 0.05 and 2.73 wt%. Exceptions to this are sample 229148 which has a CaO+Na_2O value of 9.16 wt%, and sample 229149 which has a K_2O value of 6.54 wt%.

While samples from the high Fe-Mg group have SiO_2 values consistently < 60 wt%, and Al_2O_3 values consistently < 20 wt%, samples from the high Al group are considerably more enriched in SiO_2 and Al_2O_3 concentrations. Samples within this group have SiO_2 values that

range from 61.32 to 77.99 wt%, and Al_2O_3 concentrations between 13.53 and 31.23 wt%, with the majority of samples having concentrations of Al_2O_3 greater than 20.00 wt%. The rocks of the high Al group are relatively depleted in almost all other major element concentrations and have FeO, MgO, MnO, CaO, and Na_2O values all less than 1.00 wt%. TiO_2 and K_2O concentrations are slightly higher with values that range from 0.61 to 2.05 wt% and 0.04 to 4.38 wt%, respectively.

Samples from the average pelitic group have major element compositions broadly similar to the pelitic samples of Shaw (1956) and have major element compositions that fall between the major element ranges observed within the high Fe-Mg and high Al groups. Rocks from this group have SiO_2 values that range from 53.05 to 79.12 wt%, and Al_2O_3 concentrations between 13.44 and 25.39 wt%. The rocks of this group also show slight variation with respect to iron concentrations and have FeO values ranging from 0.37 to 7.77 wt% and Fe_2O_3 values between 0.46 and 10.26 wt%. Concentrations of other major element are generally consistent with TiO_2 values <1.35 wt%, MgO values <2.78 wt%, MnO values <0.17 wt%, CaO+Na_2O values <0.6wt%, and K_2O values <5.00 wt%. Exceptions to this are samples 229152 and 229131, which have CaO+Na_2O values of 1.58 and 6.76 wt% respectively.

3.2 Petrography

Metamorphic mineral assemblages within the rocks of the Mougooderra Formation and associated greenstone units vary with respect to surrounding rock types and the geochemical groups they fall within. The most common mineral assemblage in the rocks of the high Fe-Mg group include garnet + biotite + cordierite + quartz ± grunerite ± chlorite ± plagioclase. In these rocks garnet and cordierite porphyroblasts are randomly distributed throughout a fine-grained

groundmass of quartz and biotite (Fig. 3.2a). In some samples, minor foliation is defined by the slight elongation of cordierite porphyroblasts. Cordierite porphyroblasts are prevalent throughout the samples, are up to 1mm in size, and are often altered to very fine-grained pinite (i.e. fine-grained aggregates of white mica) assemblages. A large proportion of fine-grained opaque minerals can be found concentrated at the cores of these cordierite grains, and in some samples aluminosilicate material is also found in the core of cordierite grains (Fig 3.2b). In areas where cordierite grains are present in large proportions, garnet porphyroblasts are hypidioblastic -to-idioblastic, range in size from 0.5 to 2mm, are often surrounded by a small rim of quartz, and have inclusion-rich cores. Where garnet is associated with more quartz-rich areas, grains are smaller (0.2–0.5mm) and do not have well-formed boundaries. Inclusions within garnet porphyroblasts are made up largely of quartz, but also include minor chlorite, ilmenite, and accessory apatite grains throughout. In addition to the cordierite and garnet porphyroblasts, hypidioblastic -to- idioblastic grains of grunerite and chlorite are distributed randomly throughout the groundmass. Grunerite grains are well-formed and display platy to needle-like textures (Fig. 3.2c), while chlorite grains form in aggregates displaying radial textures (Fig. 3.2d), a pattern often observed at the cores of garnet porphyroblasts (Fig 3.2e) and are often associated with cordierite grains. Plagioclase is a rare matrix component of the rocks of the high Fe-Mg group and is commonly absent from samples all together.

Other mineral assemblages within the high Fe-Mg group include chlorite + muscovite + garnet + quartz, grunerite + garnet + quartz + magnetite ± feldspar, and biotite + quartz + amphibole. Samples that contain the grunerite + garnet + quartz ± feldspar assemblage have very high concentrations of iron and are generally made up of a matrix of randomly oriented quartz and grunerite, with sericite altered plagioclase, and randomly distributed garnet porphyroblasts

(Fig 3.2f). Samples that contain the biotite + quartz + amphibole assemblage are found exclusively at the contact between the Mt Mulgine granitic intrusion and the surrounding greenstone units. These samples are Mg-rich and are made up dominantly of medium-grained biotite, lesser amounts of quartz, randomly distributed and oriented amphibole grains, and large accretions of iron oxide material.

Samples from the high Al group can be found throughout the Mougooderra Formation. Within the region of the Seeligson monzogranite, rocks from the high Al group are found between 1 and 5 km from the interpreted boundaries of the Seeligson monzogranite. However, samples from this group can also be found further north, up to 7.5km from any granitic intrusion. The rocks from this group display only one major mineral assemblage that includes andalusite + quartz + opaque minerals ± biotite ± muscovite (Fig 3.3). These rocks include a matrix that is made up of fine-grained quartz, a large proportion of opaque minerals, and in some samples, randomly distributed biotite. Randomly distributed throughout the groundmass are well-formed andalusite porphyroblasts that range in size from 0.5mm to 1cm in length. Textures and alteration of andalusite grains vary but include well-formed chiastolite grains to less well-formed poikiloblastic grains with a large proportion of quartz inclusions. In some samples there is no observed foliation and quartz grains have polygonal texture, while in others the foliation is defined by the alignment of opaque minerals and elongate quartz (Fig. 3.3). In samples with poikiloblastic andalusite grains, the internal inclusion pattern is aligned with the matrix foliation.

Samples from the average pelitic group display two common mineral assemblages. These assemblages include biotite + cordierite + quartz + opaque minerals, and biotite + cordierite + quartz + opaque minerals + andalusite. Cordierite and andalusite porphyroblasts occur within a matrix of fine-grained quartz, biotite, and minor opaque minerals (Fig 3.4). Cordierite grains are

often replaced by very fine-grained pinite assemblages, are 0.5–2mm in size, and contain numerous inclusions of biotite and quartz. Andalusite grains display similar characteristics, including replacement by fine-grained muscovite aggregates, inclusions of quartz and opaque minerals, and range in size from 0.5mm to 1cm in size. The alignment of biotite within the samples often defines a weak foliation that can be observed wrapping around cordierite porphyroblasts.

3.3 SEM and MLA Results

After initial examination of samples using a petrographic microscope, false coloured images, backscatter images, and modal proportions were obtained for four samples with low variance metamorphic assemblages (samples 207692, 229115, 229120, and 229151) using a scanning electron microscope and mineral liberation analysis (SEM-MLA) to better constrain the mineralogy and textures.

Sample 207692 is a representative sample of the garnet-bearing rocks near the Seeligson monzogranite and belongs to the high Fe-Mg group. The false coloured image (Figure 3.5) shows that the matrix of the sample is made up dominantly of fine-grained quartz, cordierite, and biotite with no observed foliation. Cordierite grains within the sample have been altered to very fine-grained muscovite and chlorite. Xenoblastic-to-hypidioblastic garnet porphyroblasts are distributed randomly throughout the sample and are relatively small (~1mm) with a consistent diameter. Garnet grains are surrounded by a small rim of quartz and contain a large proportion of quartz inclusions with minor amounts of apatite and ilmenite.

Sample 229120 (Fig. 3.6) is located roughly the same distance away from the Seeligson monzogranite and also belongs to the high Fe-Mg group. Similar to the previous sample, sample

229120 is made of a matrix of quartz, cordierite, grunerite, and biotite, and shows no evidence of preferred mineral alignment. Unlike the previous sample, sample 229120 displays compositional layering. The first layer has a matrix that contains cordierite, biotite, and chlorite grains throughout, with minor amounts of an aluminosilicate mineral (likely andalusite). Garnet porphyroblasts are randomly distributed throughout the matrix in this layer, are generally idioblastic, 2–3mm in diameter, and contain numerous ilmenite and quartz inclusions. The second layer contains a larger proportion of quartz, less cordierite, has no chlorite or aluminosilicate minerals, and unlike the first layer, contains a small proportion of feldspar and grunerite. Grunerite grains are bladed, up to 1.5mm in length and are randomly distributed and oriented throughout the quartz-rich matrix. A few small (<0.5mm in diameter) xenoblastic garnet porphyroblasts are present in this layer. Accessory minerals throughout both layers include pyrrhotite, ilmenite, and apatite.

Sample 229115, from the high Fe-Mg Group, has a matrix made up dominantly of chlorite, quartz, and muscovite, with lesser amounts of biotite and minor amounts of plagioclase (Fig. 3.7). A weak foliation is defined by the alignment of chlorite and muscovite grains. Garnet porphyroblasts are randomly distributed throughout the sample, are up to 1mm in diameter, and are surrounded by a rim of quartz. Garnet grains are generally xenoblastic and include numerous quartz and chlorite inclusions. No cordierite or aluminosilicate were found in this sample. Magnetite lenses up to 1mm in size and minor amounts of ilmenite are also randomly distributed throughout the sample.

Sample 229151 was taken from a garnet-bearing layer from the greenstone material near Mt Mulgine and is from the high Fe-Mg group. The false colour map shows that the sample is made up largely of four minerals and includes quartz, amphibole, feldspar, and garnet (Fig. 3.8).

Matrix minerals are made up largely of quartz, feldspar, and amphibole, and display no foliation throughout the thin section. Feldspar grains throughout the matrix have been heavily altered to sericite. The high proportion of amphibole (~29.01 area%) in the matrix of sample 229151 makes it different than sample 229120 (~2.38 area% amphibole). Xenoblastic garnet porphyroblasts are randomly distributed throughout the sample. Garnet grains are surrounded by a small rim of quartz, and host numerous quartz, apatite, ilmenite, and pyrrhotite inclusions. No cordierite or aluminosilicate were found in this sample.

3.4 EPMA: Mineral Compositions

Compositional ranges of garnet and biotite analyses are presented in Tables 3.2-3.3, while representative analyses for cordierite, amphibole, feldspar, chlorite, and muscovite can be found in Table 3.4. The full dataset is in Appendix C.

Garnet porphyroblasts within all samples are dominantly Fe-rich (e.g. almandine-rich) but vary with respect to endmember proportions and major element zoning. Garnet porphyroblasts within sample 207692 have Ca-rich cores (Fig 3.9a) with $X_{(Grs)}$ (molar Ca/[Ca+Mg+Mn+Fe]) decreasing from ~0.059 in the cores to ~0.030 in the rims. Zoning of other major elements within garnet porphyroblasts from sample 207692 is less obvious with slight concentrations of Fe and Mg in the rims, and very little Mn variation throughout. Similar to sample 207692, sample 229111 has garnet grains with cores that are Ca-rich. Garnet grains within this sample also have cores that are enriched in Mn, while rims are Fe and Mg -rich (Fig. 3.9b). Garnet grains from sample 229111 show concentric zoning with multiple Ca-rich zones and $X_{(Grs)}$ values of 0.059 that decrease to 0.035 in the rim of the grains. Unlike the Ca-zoning, Mn is concentrated only near the core and does not show more than one Mn-rich zone. $X_{(Sps)}$

(molar Mn/[Fe+Mg+Mn+Ca]) proportions decrease from 0.022 in the core to 0.009 in the rim of the grains. $X_{(Alm)}$ (molar Fe/[Fe+Mg+Mn+Ca]) and $X_{(Pyp)}$ (molar Mg/[Fe+Mg+Mn+Ca]) increase from core to rim with respective values of 0.799–0.83 and 0.12–0.14. Garnet grains within sample 229119 show major element zoning similar to that of the previous sample, with Mn-rich cores and multiple Ca-rich zones (Fig. 3.9c). However, Fe concentrations within garnet grains of sample 229119 show little variation between the core and the rim. Endmember proportions are comparable to that of samples 207692 and 229111 with $X_{(Alm)}$ values ranging between 0.79 and 0.82, $X_{(Pyp)}$ values ranging from 0.10 to 0.15, $X_{(Sps)}$ values of 0.008–0.025, and $X_{(Grs)}$ values between 0.048 and 0.066. Sample 229120 has similar garnet endmember proportions as the previous samples, however, major element zoning within garnet grains of this sample are slightly different. In addition to the Mn and Ca-rich cores, the core of the garnet grains are also Mg-rich (Fig. 3.9d).

Sample 229115 has garnet porphyroblasts that show slightly different major element zoning and endmember proportions. Cores of the garnet grains are enriched in Mn, Mg, and Ca, with $X_{(Pyp)}$ values of 0.085, $X_{(Sps)}$ values of 0.079, and $X_{(Grs)}$ values of 0.0433 that decrease to $X_{(Pyp)} = 0.074$, $X_{(Sps)} = 0.049$, and $X_{(Grs)} = 0.027$ in the rim (Fig. 3.9e; Table 3.2). Rims of the garnets are enriched in Fe with $X_{(Alm)}$ values increasing from 0.794 in the core to 0.843 in the rims. Garnet porphyroblasts within this sample have spessartine endmember proportions considerably higher than other samples from the other analysed samples. $X_{(Sps)}$ values within this sample range between 0.049 to 0.079, whereas all other samples have $X_{(Sps)}$ values less than 0.02.

Garnet porphyroblasts from more iron-rich samples (207693 and 229151) display similar zoning to that of the more aluminous samples (Fig. 3.10). Garnet porphyroblasts within samples 207693 and 229151 have Ca-rich cores but show little variation with respect to Fe and Mn

concentrations throughout and display Mg enrichment only in the outer margin of the grains. Sample 229151 has similar zoning. The cores of these grains are Ca and Mg-rich, while Mn and Fe show little variation throughout. Unlike the more pelitic rocks, garnet porphyroblasts within samples 207693 and 229151 have larger proportions of $X_{(Alm)}$ and the lower $X_{(Pyp)}$ proportions with values that range from 0.81–0.901 and 0.06–0.106, respectively.

The matrix mineral assemblages between garnet-bearing samples vary, but are generally dominated by biotite, cordierite, amphibole, and chlorite. Biotite is found mainly within the matrix, but also within garnet porphyroblasts (Table 3.3). Al(VI) values of biotite grains are similar for grains in the matrix and within garnet porphyroblasts, with ranges between 0.39–0.46 and 0.29–0.52 a.p.f.u. (atoms per formula unit), respectively. In general, biotite inclusions in garnet porphyroblasts display lower $X_{(Fe)}$ ratios and concentrations of Ti than those found within the matrix. Amphibole grains within these samples are monoclinic, rich in Fe and Mg and display little compositional variation (Fig. 3.11). Cordierite grains also show very little variation throughout samples, with $X_{(Mg)}$ (molar Mg/[Mg+Fe]) values ranging from 0.57–0.62. Similarly, chlorite grains also display little variation with samples having an $X_{(Mg)}$ range between 0.39–0.53.

In addition to the major matrix minerals mentioned above, samples 229120 and 229151 also contain minor amounts of feldspar, while sample 229115 contains muscovite within the matrix. Feldspar grains within sample 229120 have dominantly plagioclase endmembers with $X_{(An)}$ (molar Ca/[Na+Ca+K]) values that range from 0.63-0.90, $X_{(Ab)}$ (molar Na/[Na+Ca+K]) values that range from 0.10–0.37, and $X_{(Ksp)}$ (molar K/[Na+Ca+K]) values less than 0.005. Feldspar grains within sample 229151 have endmembers values that are less dominated by

plagioclase endmembers with X_{An} values that range from 0.034–0.056, $X_{(Ab)}$ values of 0.43 to 0.51, and $X_{(Ksp)}$ values between 0.44 and 0.54.

3.5 Garnet trace elements and Lu-Hf and Sm-Nd geochronology

Coupled garnet Lu-Hf and Sm-Nd geochronology was completed for one sample of the Mougooderra Formation (sample 207692) and for one sample from a garnet-bearing layer within the associated greenstone of the Polelle Group near Mt Mulgine (sample 229151). Isotope data can be found in Appendix D. Laser ablation analysis for sample 207692 was completed on randomly selected euhedral garnet grains from the garnet separate. For this sample, it was attempted to expose the centre of the garnet grains during polishing. Laser ablations analysis for sample 229151 was completed on a polished thin section. Garnet trace element data can be found in Appendix E.

Garnet grains from sample 207692 display relatively flat garnet profiles with respect to Lu and Hf and have only a slight enrichment of Lu in the core for two garnet grains relative to the outermost rims (Fig. 3.12). All analysed grains have Lu values less than 5ppm and Hf values that range between 0.27 and 4.8ppm. The Sm and Nd profiles of these garnet grains display minor zoning, with the exception of two analyses (point 5 from garnet A and point 3 from garnet B) that show a spike in the concentrations of Sm and Nd. Point 5 from garnet A has a Nd concentration of 240±120 ppm and a Sm concentration of 52±25 ppm, while point 3 of garnet B has a Nd concentration of 69±76 ppm and a Sm concentration of 14±13 ppm. These points were removed from the diagram so that the zoning from the other points may be observed. The high Sm and Nd concentrations from these points may be related to an analysis that drilled through a mineral inclusion in garnet with elevated light rare earth element (LREE) such as monazite.

Therefore, these analyses are excluded from the discussion of garnet zoning patterns. Sm concentrations range from 1.1 to 10.6 ppm for garnet A, from 0.7 to 3.6 ppm for garnet B, and from 1.3 to 2.2 ppm for garnet C.

The Lu-Hf isochron of sample 207692 returned an age of 2686±18 Ma with an MSWD of 0.87 and initial $^{176}Hf/^{177}Hf$ of 0.280990±0.000015 (Fig. 3.13a). The Sm-Nd age of the garnet grains form this sample are considerably younger with an age of 2611±35 Ma, an MSWD of 0.51, and an initial $^{143}Nd/^{144}Nd$ of 0.509130±0.000040 (Fig. 3.13b). For this sample, the whole-rock bomb sample was excluded from the regression as it was in disequilibrium with the system. The reasons for this are unclear, but it may be the result from the dissolution of refractory minerals (e.g. zircon?) that were not in isotopic equilibrium with garnet.

Garnet grains from sample 229151 show slight zonation with respect to Lu and Hf. Garnet A has Lu concentrations that increase from rim to core and has a range of 0.13 to 1.3 ppm (Fig. 3.14). The Sm concentrations of garnet A have values of 0.52–4.19 ppm. Points with the highest Sm concentrations are found between the rim and the core. Garnet B has Lu concentrations of 0.3–1.1 ppm with the higher concentrations near the core of the grain, and with Sm concentrations of 2.5 to 4.8 ppm with the points of highest Sm and Lu concentration being located in the same location. Garnet C has Lu concentrations that range from 0.02 to 2.3 ppm with the highest concentrations located at the rim of the grain, and Sm concentrations ranging between 2.3 to 6.3 ppm with the highest concentrations located at the core of the grain. The variable zoning patterns may relate to sectioning of the garnet; some profiles may not represent cross sections through the cores of the garnets. Sample 207690 was taken from the same location as 229151 during the 2016 field season. Concentrations of Lu within garnet A from this sample range from 0.2 to 1.9 ppm, while Sm concentrations range from 1.5 to 4.3 ppm (Fig. 3.15). Lu is

strongly concentrated within the core of the grain, while Sm is concentrated between the rim and the core. For garnet B, Lu ranges between 0.2 and 1.89 ppm and is strongly concentrated within the core of the grain, while Sm is concentrated near the rim of the grain and ranges between 3.2 to 6.1 ppm.

The Lu-Hf isochron from sample 229151 returned an age of 2685±15Ma with an MSWD of 1.5 and initial $^{176}Hf/^{177}Hf$ of 0.280883±0.000010 (Fig. 3.16a). The Sm-Nd age of the garnet grains from this sample are also considerably younger with an age of 2590±21Ma, an MSWD of 0.24, and an initial $^{143}Nd/^{144}Nd$ of 0.509041±0.000026 (Fig. 3.16b).

Table 3.1. Major element compositions for rocks of the Mougooderra Formation and select underlying greenstone material in wt%.

	Sample	SiO_2	TiO_2	Al_2O_3	FeO	Fe_2O_3	MgO	MnO	CaO	Na_2O	K_2O	P_2O_5	SO_3	LOI	Total
High Fe-Mg group	229101	59.83	0.73	12.12	12.30	1.58	6.14	0.22	0.25	0.16	0.54	0.16	0.02	4.31	98.35
	229111	48.01	0.77	19.20	17.40	1.23	5.79	0.10	0.50	0.29	2.39	0.11	0.03	2.24	98.06
	229115	53.82	0.83	16.84	12.20	1.91	6.13	0.23	0.11	0.12	1.79	0.04	0.02	4.68	98.72
	229119	56.81	0.63	16.70	12.10	1.40	4.70	0.08	0.44	0.28	2.54	0.10	0.16	2.77	98.71
	229120	51.68	0.74	18.53	14.40	1.33	5.61	0.10	0.51	0.25	2.78	0.10	0.02	2.33	98.38
	229124	44.18	0.61	10.11	31.80	1.85	6.93	0.20	1.62	0.10	0.06	0.06	0.04	0.00	97.55
	229151	56.44	0.78	12.29	16.00	3.47	3.72	0.14	1.76	0.83	1.55	0.07	–	1.57	98.62
	207693	58.58	0.40	7.42	24.16	1.98	5.29	0.15	0.56	0.03	0.05	0.02	0.07	–	98.72
	207692	55.36	0.67	17.17	11.46	2.48	5.14	0.08	0.49	0.37	2.73	0.11	0.10	2.22	98.38
	207690	57.05	0.74	11.72	17.14	2.75	3.56	0.14	1.72	0.82	1.66	0.09	0.63	0.74	98.76
	229148	44.70	0.61	11.96	5.00	5.02	17.37	0.10	1.50	0.11	6.54	0.04	–	5.18	98.13
	229149	49.75	0.46	8.04	5.89	3.00	18.20	0.20	8.74	0.42	1.42	0.03	0.03	2.37	98.55
High Al group	229105	63.77	2.05	31.23	0.19	0.10	0.04	–	0.02	0.17	0.08	0.075	0.02	2.27	100.01
	229109	68.38	0.98	19.53	0.35	1.75	0.12	0.01	0.03	0.39	4.38	0.021	0.02	3.64	99.60
	229127	61.32	1.26	29.39	0.26	0.00	0.14	0.00	0.42	0.45	1.67	0.052	0.47	4.44	99.87
	229135	77.99	0.61	13.53	0.29	1.78	0.12	0.01	0.16	0.10	1.21	0.023	0.17	3.78	99.77
	229138	64.59	1.04	30.01	0.20	0.48	0.09	0.01	0.04	0.08	1.57	0.03	0.07	1.55	99.76
	207602	67.11	0.76	20.84	0.30	0.89	0.21	–	0.04	0.86	4.18	0.032	0.12	3.80	99.13
	207691	71.45	1.69	23.88	0.08	–	–	–	0.01	0.10	0.04	0.142	0.01	2.02	99.38
Average pelitic group	229131	68.81	0.69	15.06	3.02	0.92	2.05	0.04	1.3	0.28	4.24	0.05	0.04	2.75	99.25
	229130	53.05	1.13	21.14	7.77	1.77	2.78	0.17	1.79	1.24	2.58	0.018	0.07	5.41	98.92
	229146	64.67	0.92	16.13	0.39	8.57	1.00	0.03	0.25	0.15	1.04	0.021	0.04	6.43	99.64
	229147	64.25	0.98	15.57	–	10.26	0.25	0.01	0.30	0.07	0.16	0.06	0.04	7.75	99.69
	229152	54.11	0.61	15.35	–	10.18	0.82	–	6.35	0.41	2.35	0.041	0.10	9.41	99.73
	211117	74.43	0.24	15.09	0.85	0.86	1.18	0.02	0.16	0.16	4.75	0.033	0.02	1.93	99.72
	207694	58.24	1.05	19.49	0.37	9.31	1.05	0.02	0.08	0.24	4.93	0.028	0.09	4.69	99.58

Table 3.1 (continued)

	Sample	SiO_2	TiO_2	Al_2O_3	FeO	Fe_2O_3	MgO	MnO	CaO	Na_2O	K_2O	P_2O_5	SO_3	LOI	Total
Average pelitic group continued	229113	54.07	1.35	25.39	6.45	3.11	2.37	0.06	0.06	0.10	3.99	0.034	0.03	2.20	99.21
	229117	61.60	1.25	24.10	7.16	0.46	1.69	0.10	0.26	0.28	0.471	0.142	0.02	1.56	99.09
	229136	74.15	0.50	13.44	0.79	2.26	0.69	0.02	0.15	0.16	3.81	0.029	0.09	3.39	99.48
	229157	62.62	0.99	22.35	2.91	3.59	0.94	0.07	0.08	0.24	2.28	0.029	0.10	3.14	99.34
	229158	61.77	0.93	21.22	5.80	6.63	1.30	0.07	0.04	0.07	2.71	0.087	0.02	1.65	102.30
	211116	79.12	0.50	11.62	0.57	1.75	0.65	–	0.13	0.15	2.78	0.03	0.022	2.39	99.71
	207695	60.68	0.93	22.07	7.45	0.83	2.17	0.12	0.27	0.32	2.20	0.128	0.561	1.56	99.29

– Indicating below detection limit; LOI – Loss on ignition

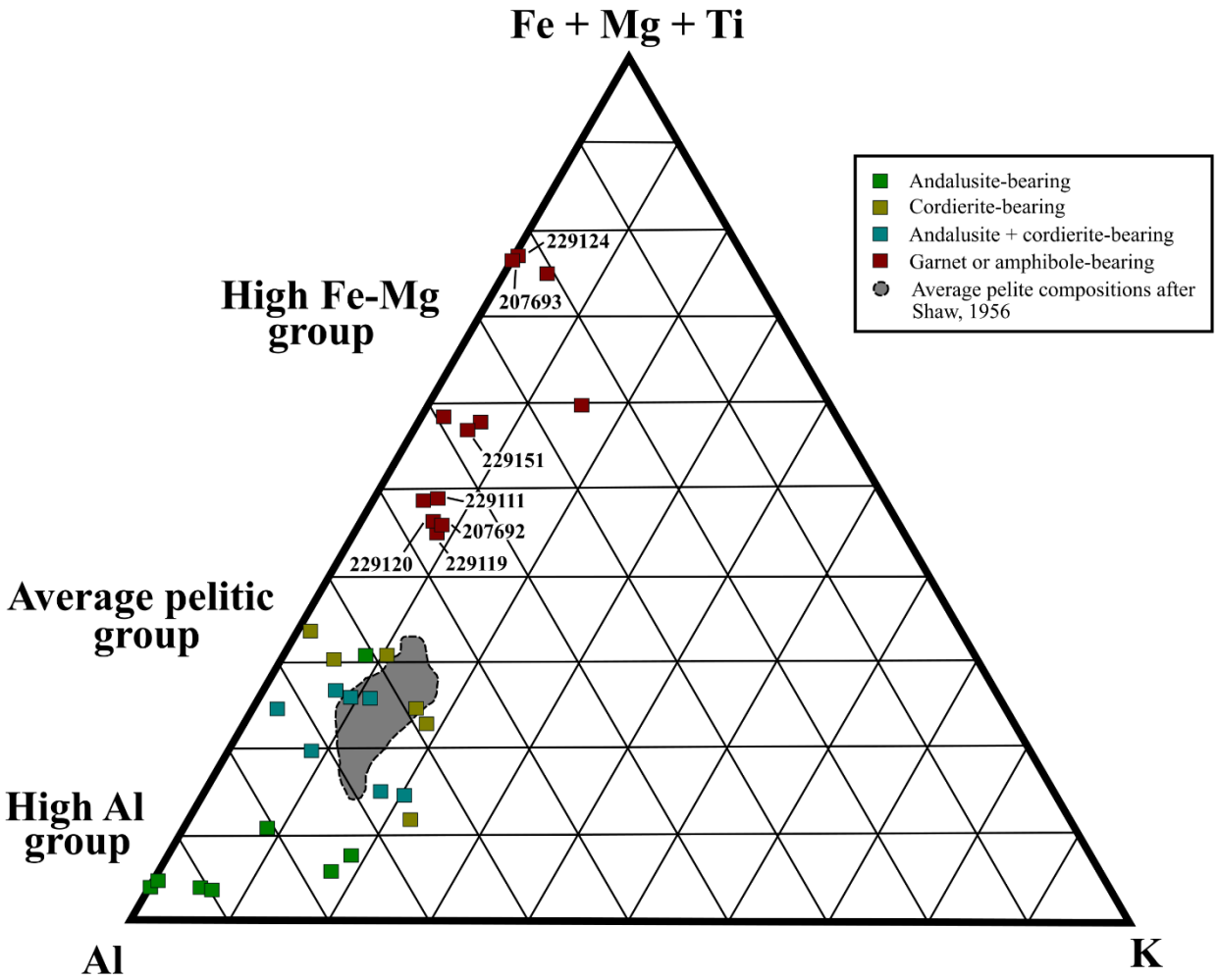

Figure 3.1. Ternary diagram showing whole-rock compositions expressed in terms of Fe + Mg + Ti mol%, Al mol%, and K mol%.

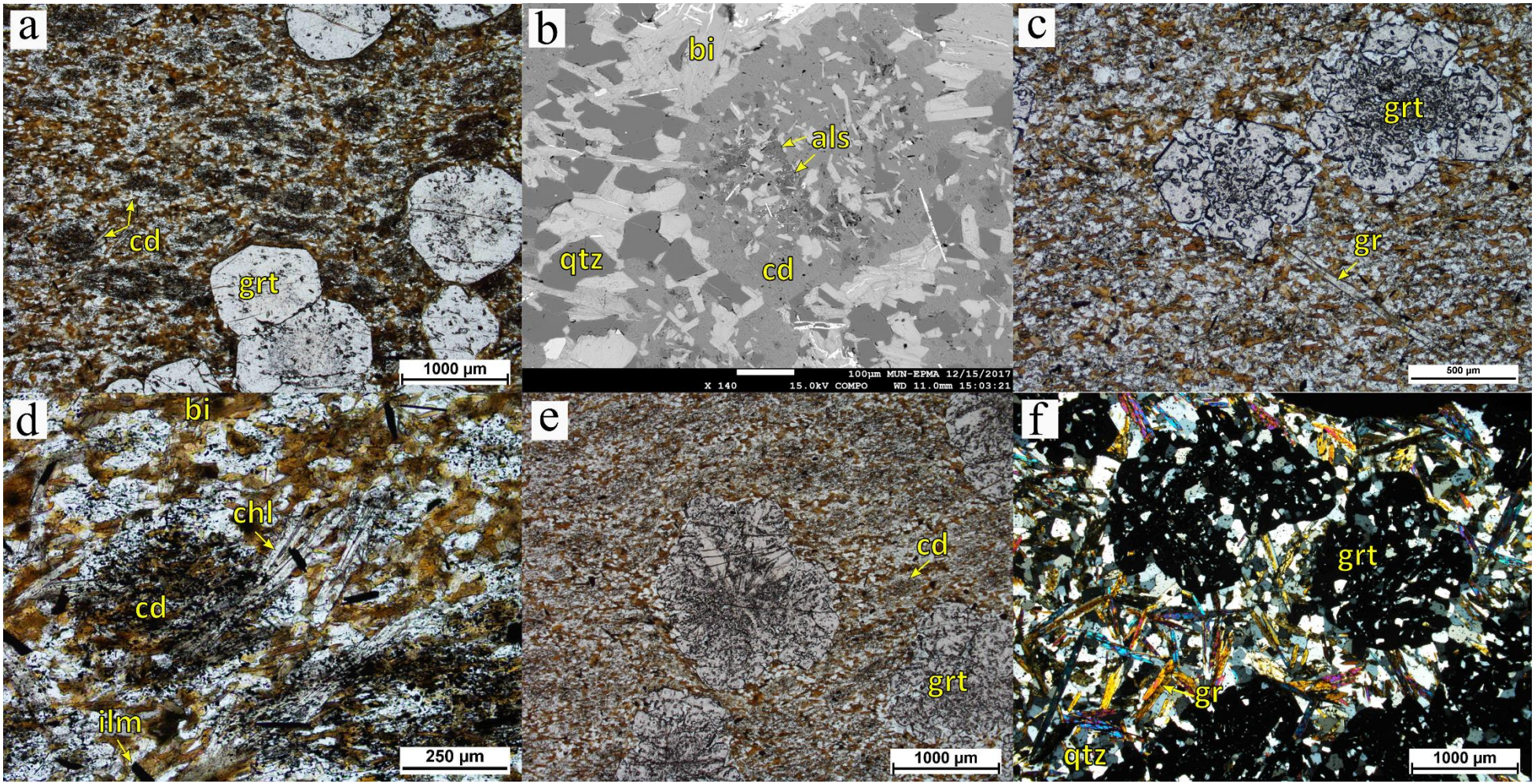

Figure 3.2. Mineral assemblages from the high Fe-Mg group including: (a) sample 229111 showing garnet and cordierite porphyroblasts distributed throughout a matrix of biotite and quartz with minor fine-grained chlorite (b) an electron probe micro-analyzer image of sample 229119 showing a cordierite porphyroblast within a matrix of biotite and quartz, with micaceous and aluminosilicate inclusions, (c) sample 207692 showing grunerite and garnet grains randomly distributed throughout a quartz and biotite-rich matrix, (d) sample 229111 showing chlorite and cordierite grains within a matrix of quartz and biotite, (e) sample 229112 showing the radial pattern observed within the cores of garnet, (f) sample 229151 showing garnet porphyroblasts and grunerite grains throughout a matrix of quartz.

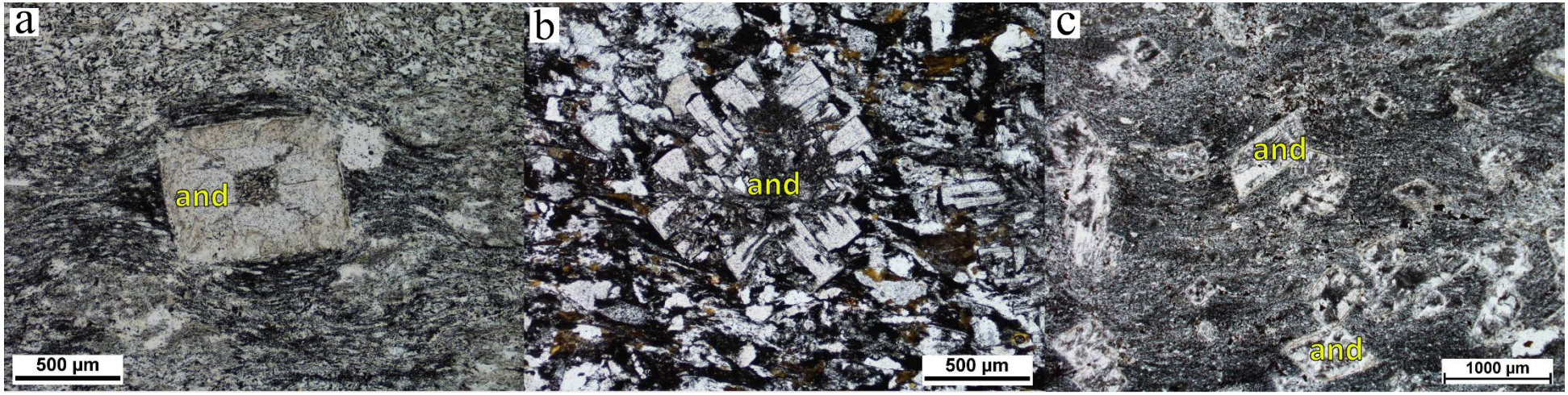

Figure 3.3. Samples (a) 229133, (b) 229132, and (c) 229135 from the high Al group showing the textures of andalusite and a foliation defined by the alignment of quartz and opaque minerals of the matrix.

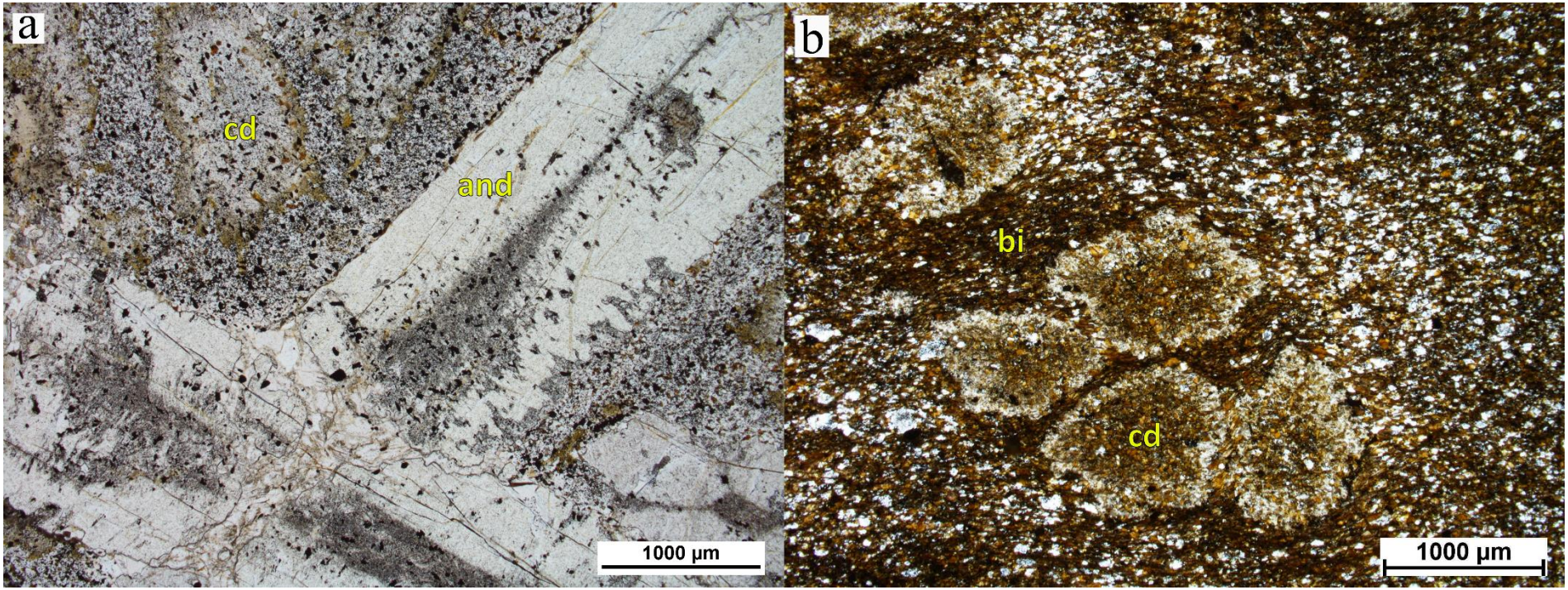

Figure 3.4. (a) Sample 229117 showing andalusite and cordierite porphyroblasts within a matrix of quartz and opaque minerals, and (b) sample 229155 showing the texture of cordierite porphyroblasts within a biotite and quartz matrix from a cordierite only sample from the average pelitic group.

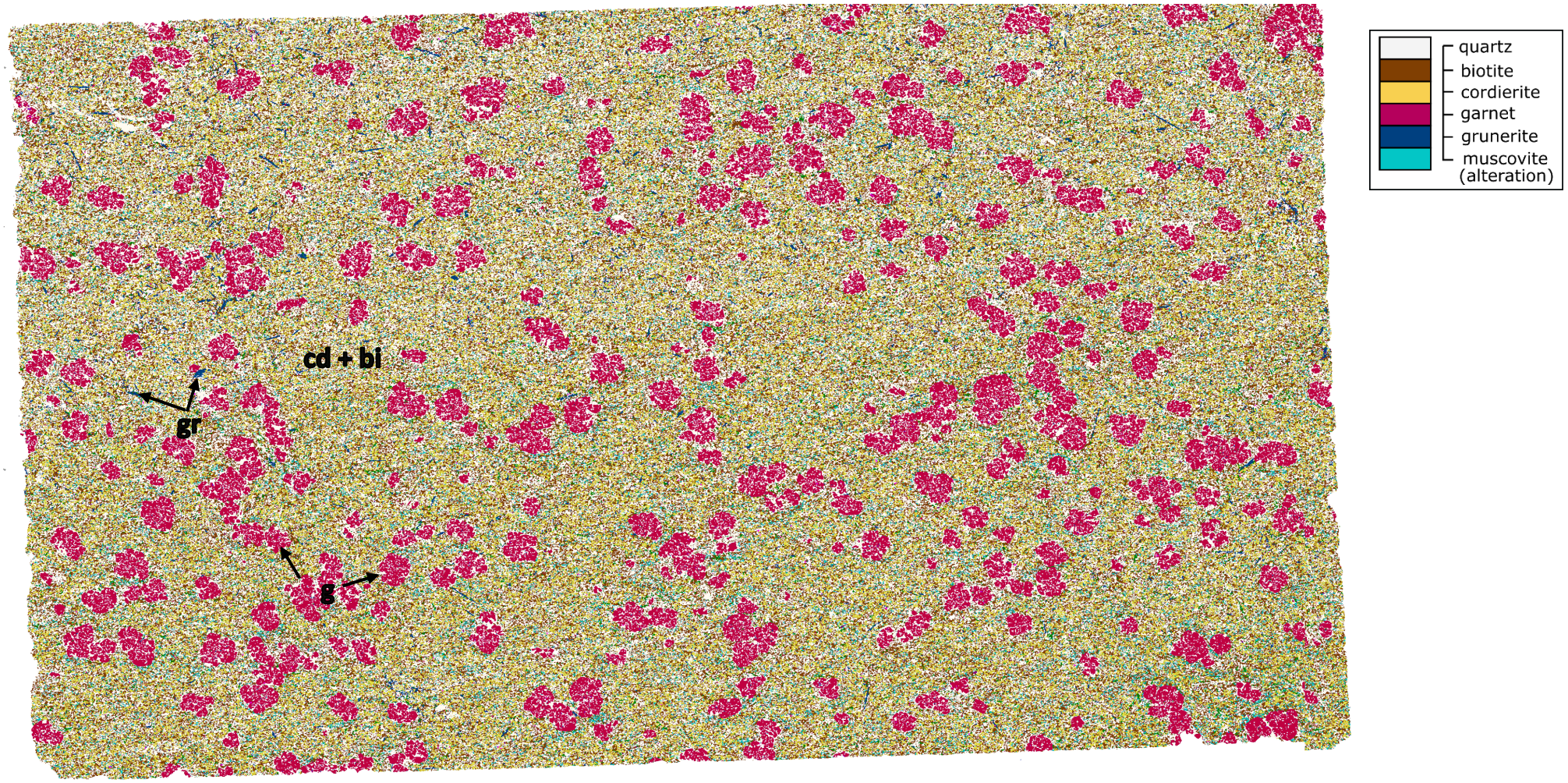

Figure 3.5. SEM-MLA false coloured map of sample 207692 showing pink garnet porphyroblasts within a fine-grained matrix of yellow cordierite and brown biotite. The false coloured map was made of a thin section that is 4cm x 2cm in size.

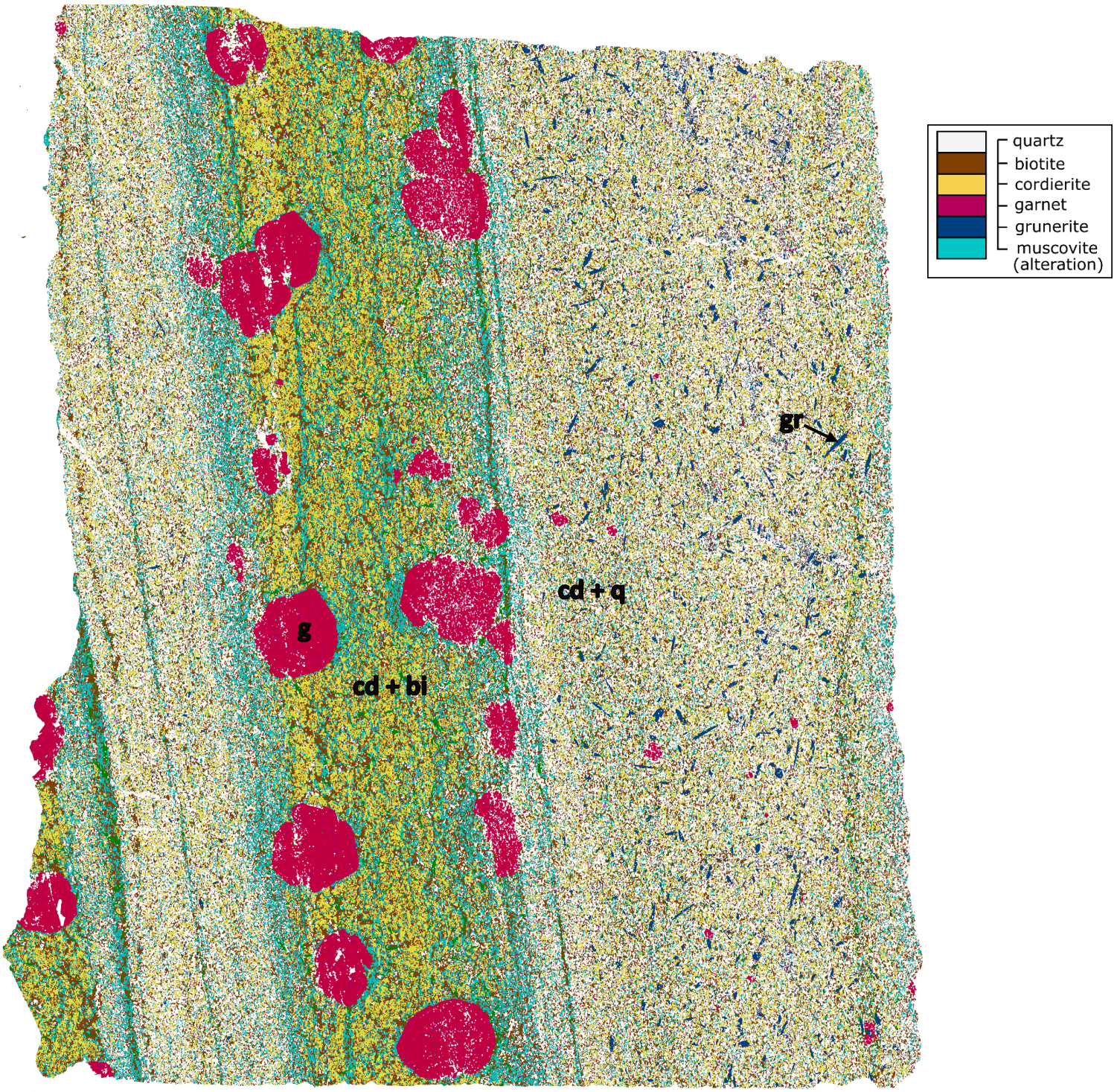

Figure 3.6. SEM-MLA false coloured map of sample 229120 showing compositional layering, with the first layer displaying blue grunerite porphyroblasts within a matrix of quartz and minor cordierite, and the second layer showing large garnet porphyroblasts within a matrix of cordierite and muscovite alteration. The false coloured map was made of a thin section that is 2.5cm x 2cm in size.

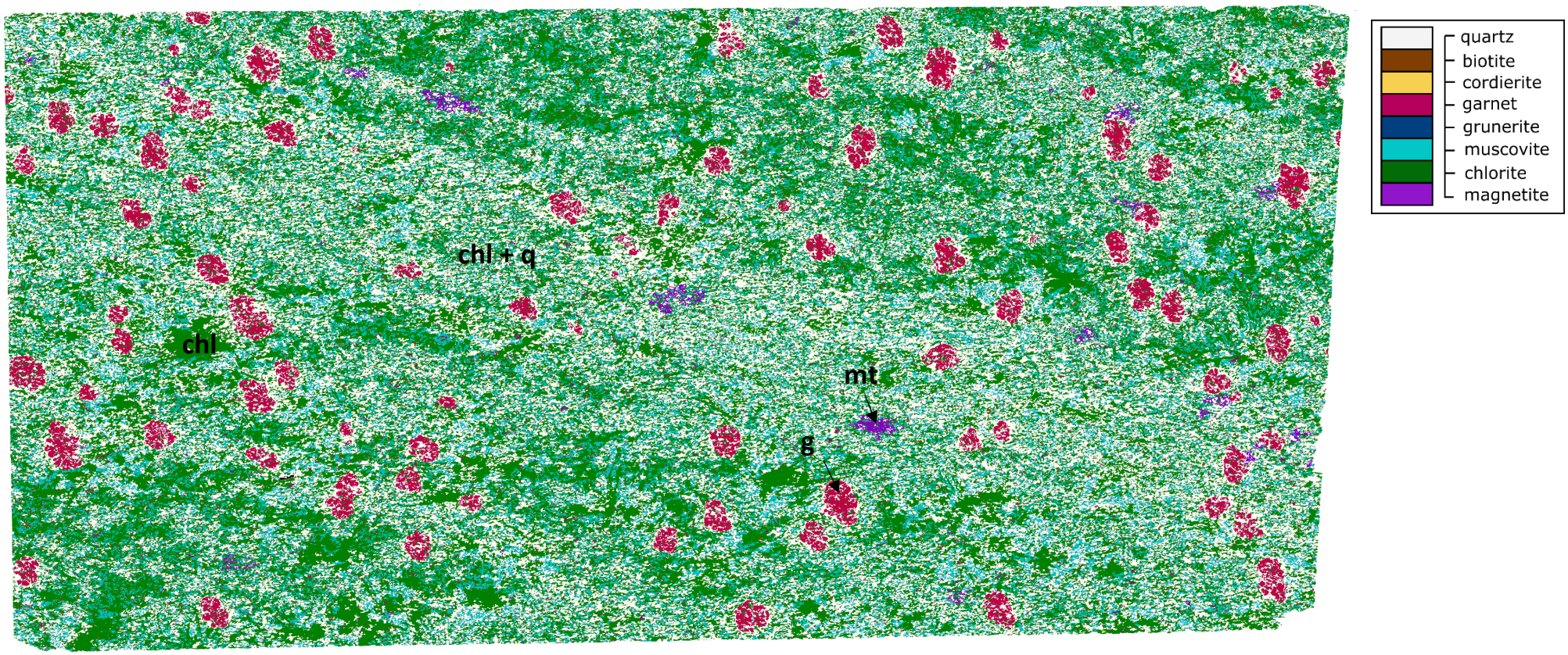

Figure 3.7. SEM-MLA false coloured map of sample 229115 showing pink garnet porphyroblasts and magnetite lenses within a matrix of green chlorite. The false coloured map was made of a thin section that is 4cm x 2cm in size.

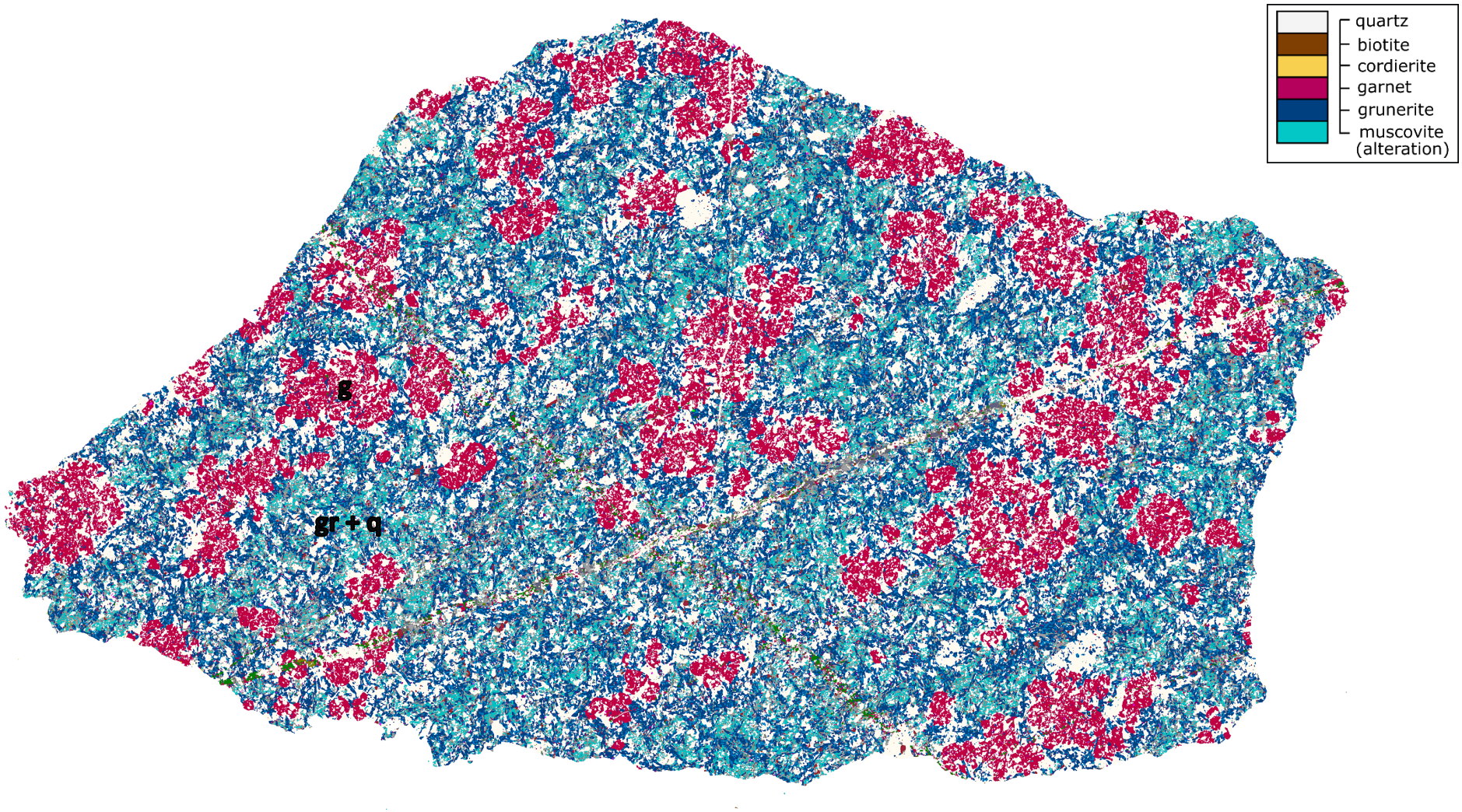

Figure 3.8. SEM-MLA false coloured map of sample 229151 showing garnet porphyroblasts within a matrix of grunerite and plagioclase altered to sericite. The false coloured map was made of a thin section that is 3cm x 2cm in size.

Table 3.2. Compositional ranges of garnet in endmember molar proportions.

Sample	$X_{(Alm)}$	$X_{(Prp)}$	$X_{(Sps)}$	$X_{(Grs)}$	$X_{(Fe)}$
207692 grt 1	0.823-0.847	0.105-0.123	0.009-0.011	0.036-0.053	0.87
grt 2	0.815-0.846	0.110-0.125	0.009-0.011	0.034-0.059	0.87
grt 3	0.824-0.853	0.106-0.119	0.009-0.010	0.031-0.049	0.88
grt 4	0.809-0.846	0.113-0.134	0.009-0.012	0.030-0.046	0.87
229115 grt 1	0.794-0.843	0.075-0.085	0.052-0.079	0.027-0.047	0.91
grt 2	0.817-0.852	0.073-0.084	0.049-0.055	0.025-0.048	0.91
229119 grt 1	0.795-0.814	0.111-0.144	0.008-0.018	0.048-0.062	0.87
grt 2	0.793-0.818	0.101-0.148	0.010-0.025	0.049-0.066	0.87
229111 grt 1	0.799-0.825	0.120-0.139	0.009-0.022	0.035-0.059	0.87
229120 grt 1	0.793-0.823	0.101-0.147	0.011-0.026	0.049-0.063	0.87
229151 grt 1	0.812-0.838	0.083-0.093	0.016-0.018	0.069-0.088	0.91
207693 grt 1	0.858-0.888	0.069-0.096	0.011-0.014	0.021-0.041	0.91
grt 2	0.877-0.901	0.063-0.106	0.010-0.016	0.015-0.033	0.92

Alm – Almandine; **Prp** – Pyrope; **Sps** – Spessartine; **Grs** – Grossular; $X_{(Fe)}$ – Fe/(Fe+Mg)

Table 3.3. Compositional ranges of biotite in apfu.

Sample	Location	$Al_{(VI)}$	$X_{(Fe)}$	Ti(apfu)
207692	**Within grt**	**0.52**	**0.43**	**0.04**
	In contact	**0.42-0.50**	**0.53-0.57**	**0.08-0.09**
	Matrix	**0.39-0.43**	**0.54-0.57**	**0.09-0.10**
229111	**Within grt**	**0.30**	**0.44**	**0.06**
	Matrix	**0.38-0.46**	**0.52-0.54**	**0.08-0.09**
229119	**Within grt**	**0.30**	**0.44**	**0.06**
	Matrix	**0.38-0.46**	**0.52-0.54**	**0.08-0.09**
229120	**Within grt**	**0.45**	**0.54**	**0.07**
	Matrix	**0.34-0.46**	**0.52-0.58**	**0.08-0.10**

$X_{(Fe)}$ – Fe/(Fe+Mg); **apfu** – atom per formula unit

Table 3.4. Representative EPMA analyses of cordierite, amphibole, chlorite, feldspar, and muscovite.

Mineral:	**Cordierite**				**Amphibole**					**Chlorite**				**Feldspar**		**Muscovite**
Sample:	**207692**	**229111**	**229119**	**229120**	**207692**	**207693**	**229111**	**229120**	**229151**	**229111**	**229115**	**229119**	**229120**	**229120**	**229151**	**229115**
Wt%																
SiO_2	**47.64**	**47.48**	**47.43**	**48.56**	**52.61**	**52.03**	**52.65**	**51.42**	**52.28**	**23.66**	**22.90**	**24.03**	**25.24**	**47.12**	**55.20**	**48.49**
TiO_2	**0.02**	**0.00**	**0.01**	**0.00**	**0.08**	**0.04**	**0.02**	**0.11**	**0.03**	**0.12**	**0.12**	**0.32**	**0.07**	**0.00**	**0.00**	**0.11**
Al_2O_3	**32.90**	**32.84**	**32.50**	**33.48**	**2.11**	**2.04**	**1.53**	**2.74**	**0.96**	**22.46**	**22.59**	**22.28**	**22.95**	**34.29**	**29.27**	**39.12**
FeO	**9.03**	**8.69**	**8.60**	**8.69**	**29.79**	**29.38**	**27.37**	**31.36**	**32.76**	**25.31**	**28.88**	**25.09**	**24.61**	**0.00**	**0.00**	**0.88**
MnO	**0.05**	**0.01**	**0.03**	**0.02**	**0.07**	**0.04**	**0.12**	**0.11**	**0.18**	**0.02**	**0.17**	**0.02**	**0.01**	**0.00**	**0.00**	**0.00**
MgO	**7.95**	**8.00**	**8.10**	**7.80**	**13.00**	**13.31**	**14.96**	**11.68**	**10.82**	**14.49**	**11.04**	**14.25**	**13.75**	**0.00**	**0.00**	**0.37**
CaO	**0.01**	**0.01**	**0.01**	**0.01**	**0.22**	**0.19**	**0.39**	**0.29**	**0.54**	**0.01**	**0.02**	**0.02**	**0.02**	**16.25**	**0.93**	**0.00**
Na_2O	**0.00**	**0.00**	**0.00**	**0.00**	**0.13**	**0.07**	**0.06**	**0.17**	**0.08**	**0.00**	**0.00**	**0.00**	**0.04**	**1.86**	**4.67**	**0.89**
K_2O	**0.00**	**0.01**	**0.02**	**0.01**	**0.00**	**0.00**	**0.00**	**0.00**	**0.00**	**0.00**	**0.01**	**0.00**	**0.39**	**0.05**	**6.11**	**9.87**
Total	**97.60**	**97.03**	**96.70**	**98.57**	**98.03**	**97.08**	**97.10**	**97.88**	**97.65**	**86.08**	**85.73**	**86.01**	**87.08**	**99.57**	**96.17**	**99.73**
cations																
Si	**4.96**	**4.96**	**4.97**	**4.99**	**7.87**	**7.85**	**7.87**	**7.78**	**7.98**	**5.10**	**5.07**	**5.17**	**5.33**	**2.16**	**2.57**	**6.10**
Ti	**0.00**	**0.00**	**0.00**	**0.00**	**0.01**	**0.00**	**0.00**	**0.01**	**0.00**	**0.02**	**0.02**	**0.05**	**0.01**	**0.00**	**0.00**	**0.01**
Al	**4.04**	**4.05**	**4.02**	**4.05**	**0.37**	**0.36**	**0.27**	**0.49**	**0.17**	**5.70**	**5.89**	**5.65**	**5.72**	**1.86**	**1.61**	**5.81**
Fe	**0.79**	**0.76**	**0.75**	**0.75**	**3.73**	**3.71**	**3.42**	**3.97**	**4.18**	**4.56**	**5.34**	**4.52**	**4.35**	**0.00**	**0.00**	**0.09**
Mn	**0.00**	**0.00**	**0.00**	**0.00**	**0.01**	**0.01**	**0.02**	**0.01**	**0.02**	**0.01**	**0.04**	**0.00**	**0.00**	**0.00**	**0.00**	**0.00**
Mg	**1.23**	**1.25**	**1.27**	**1.19**	**2.90**	**2.99**	**3.33**	**2.63**	**2.46**	**4.65**	**3.64**	**4.57**	**4.33**	**0.00**	**0.00**	**0.07**
Ca	**0.00**	**0.00**	**0.00**	**0.00**	**0.04**	**0.03**	**0.06**	**0.05**	**0.09**	**0.00**	**0.00**	**0.01**	**0.00**	**0.80**	**0.05**	**0.00**
Na	**0.00**	**0.00**	**0.00**	**0.00**	**0.04**	**0.02**	**0.02**	**0.05**	**0.02**	**0.00**	**0.00**	**0.00**	**0.02**	**0.17**	**0.42**	**0.22**
K	**0.00**	**0.00**	**0.00**	**0.00**	**0.00**	**0.00**	**0.00**	**0.00**	**0.00**	**0.00**	**0.00**	**0.00**	**0.12**	**0.00**	**0.36**	**1.58**
Total	**11.02**	**11.02**	**11.01**	**10.99**	**14.96**	**14.97**	**15.00**	**14.99**	**14.94**	**20.04**	**20.00**	**19.97**	**19.88**	**4.99**	**5.01**	**13.88**
$X_{(Mg)}$	**0.61**	**0.62**	**0.63**	**0.63**						**0.51**	**0.41**	**0.50**	**0.50**			
O value	**18**	**18**	**18**	**18**	**23**	**23**	**23**	**23**	**23**	**28**	**28**	**28**	**28**	**8**	**8**	**22**

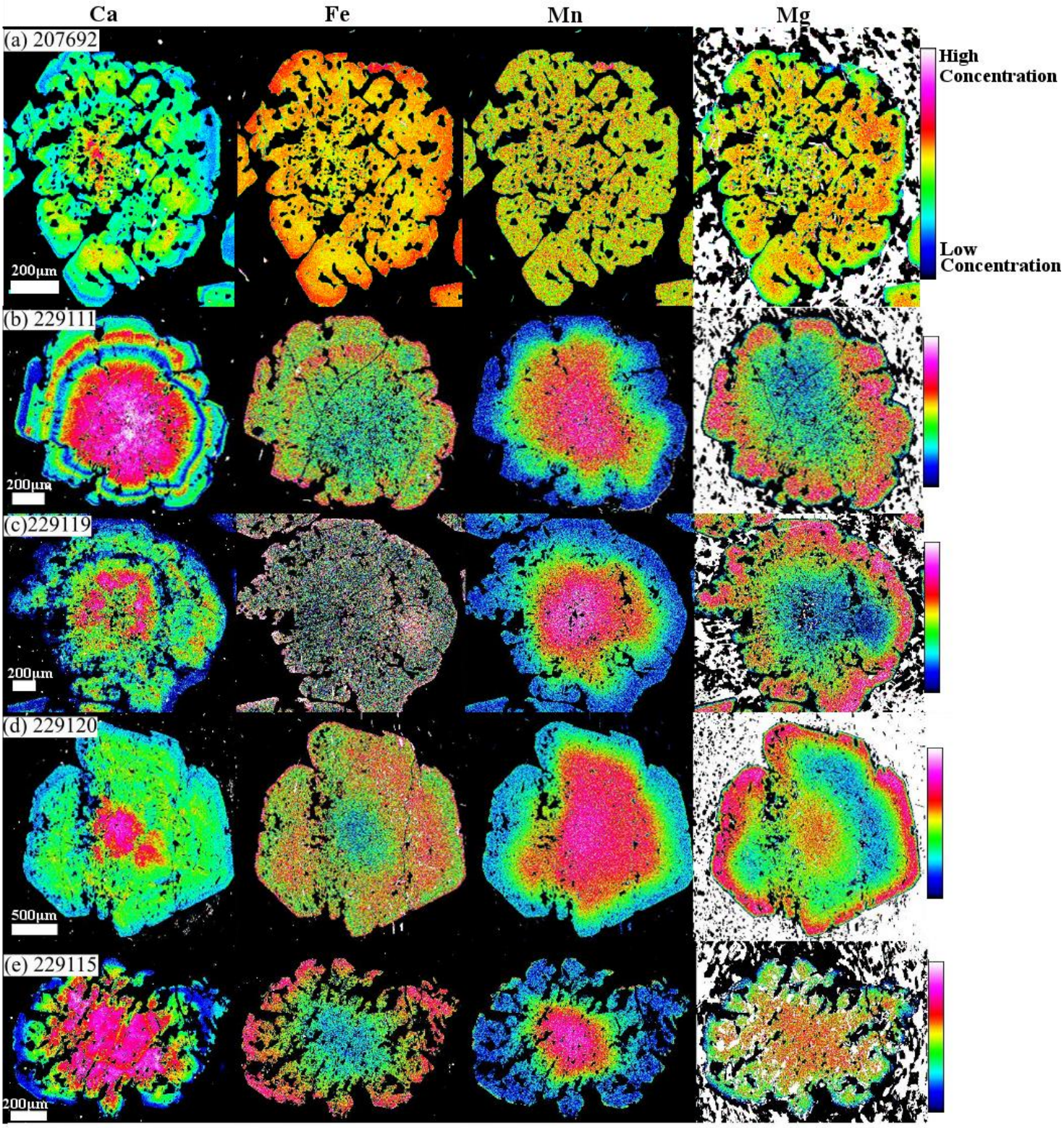

Figure 3.9. X-ray maps showing major element compositional zoning of garnet porphyroblasts from samples (a) 207692, (b) 229111, (c) 229119, (d) 229120, and (e) 229115.

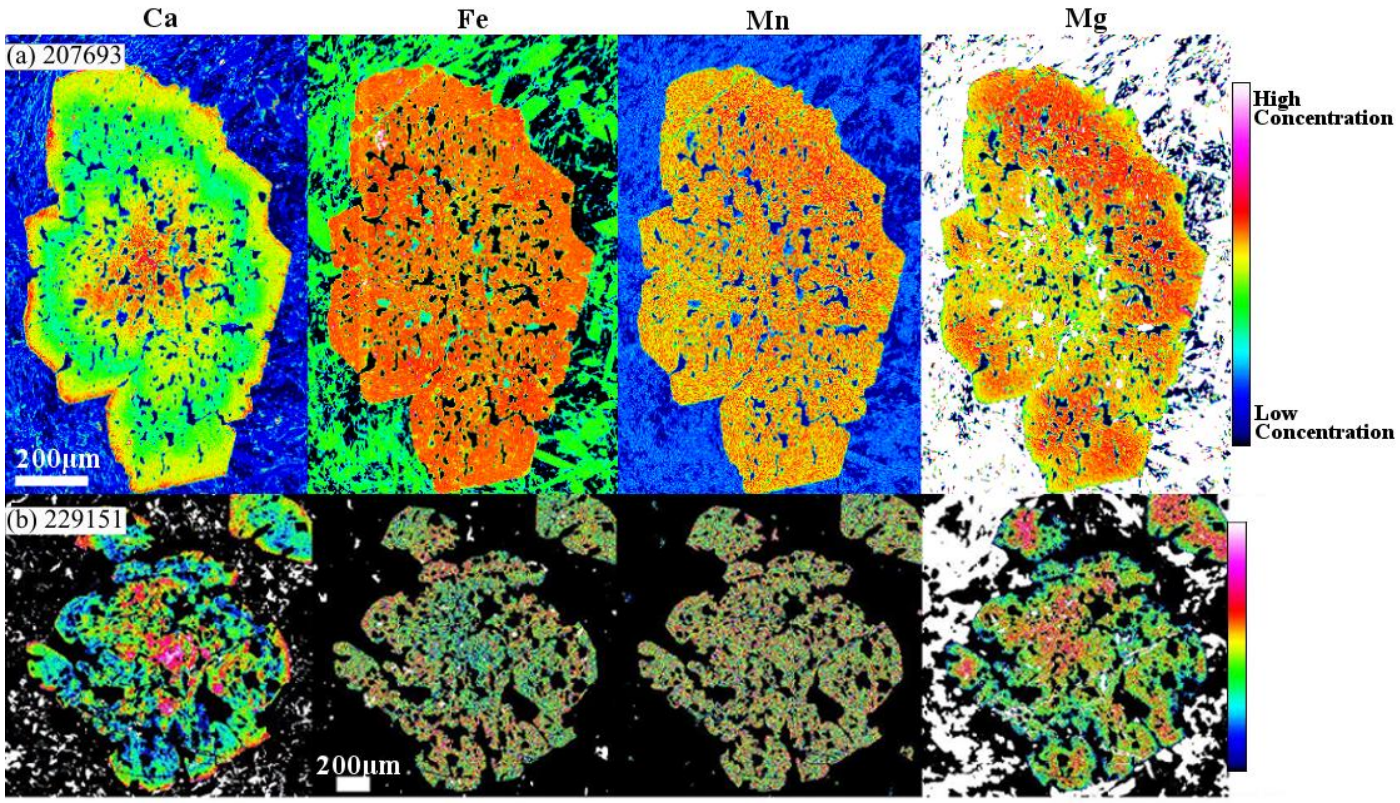

Figure 3.10. X-ray maps showing major element compositional zoning of garnet porphyroblasts from samples (a) 207693, (b) 229151.

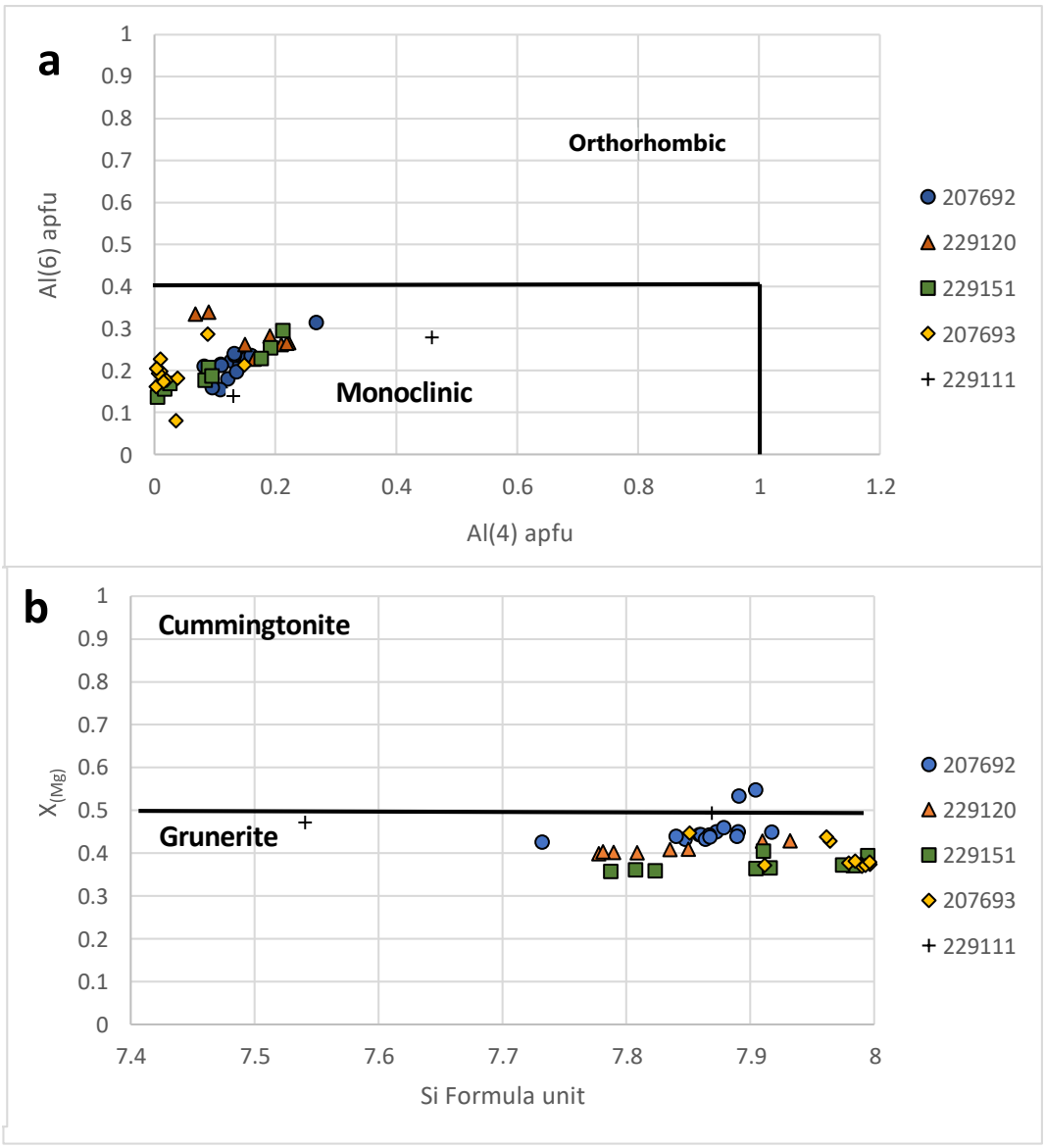

Figure 3.11. Compositional ranges of amphibole based on Al distribution (a) and $X_{(Mg)}$ and Si apfu (b); $X_{(Mg)}$ – Mg/(Mg+Fe).

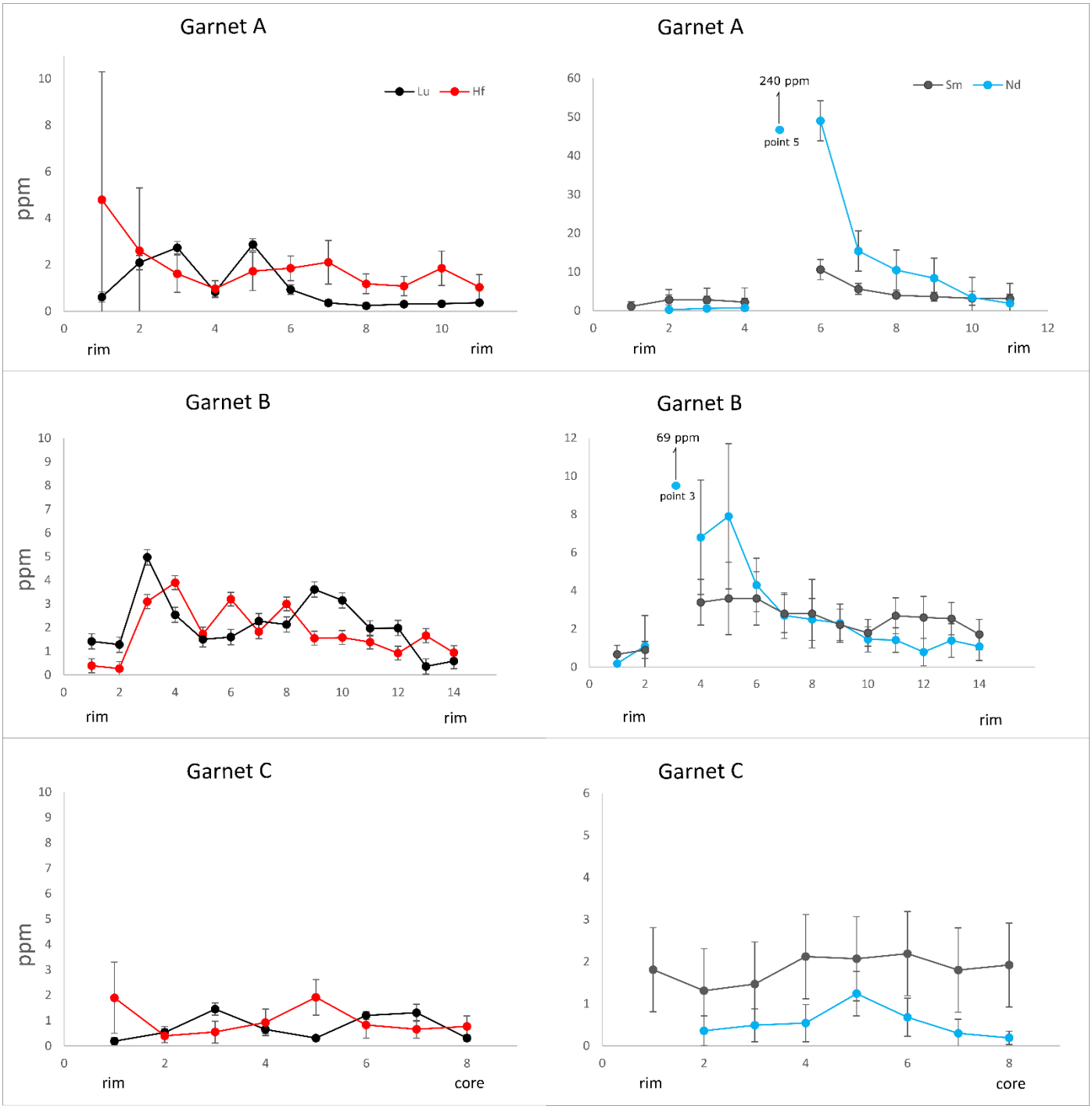

Figure 3.12. Lu-Hf and Sm-Nd profiles for garnet grains from sample 207692.

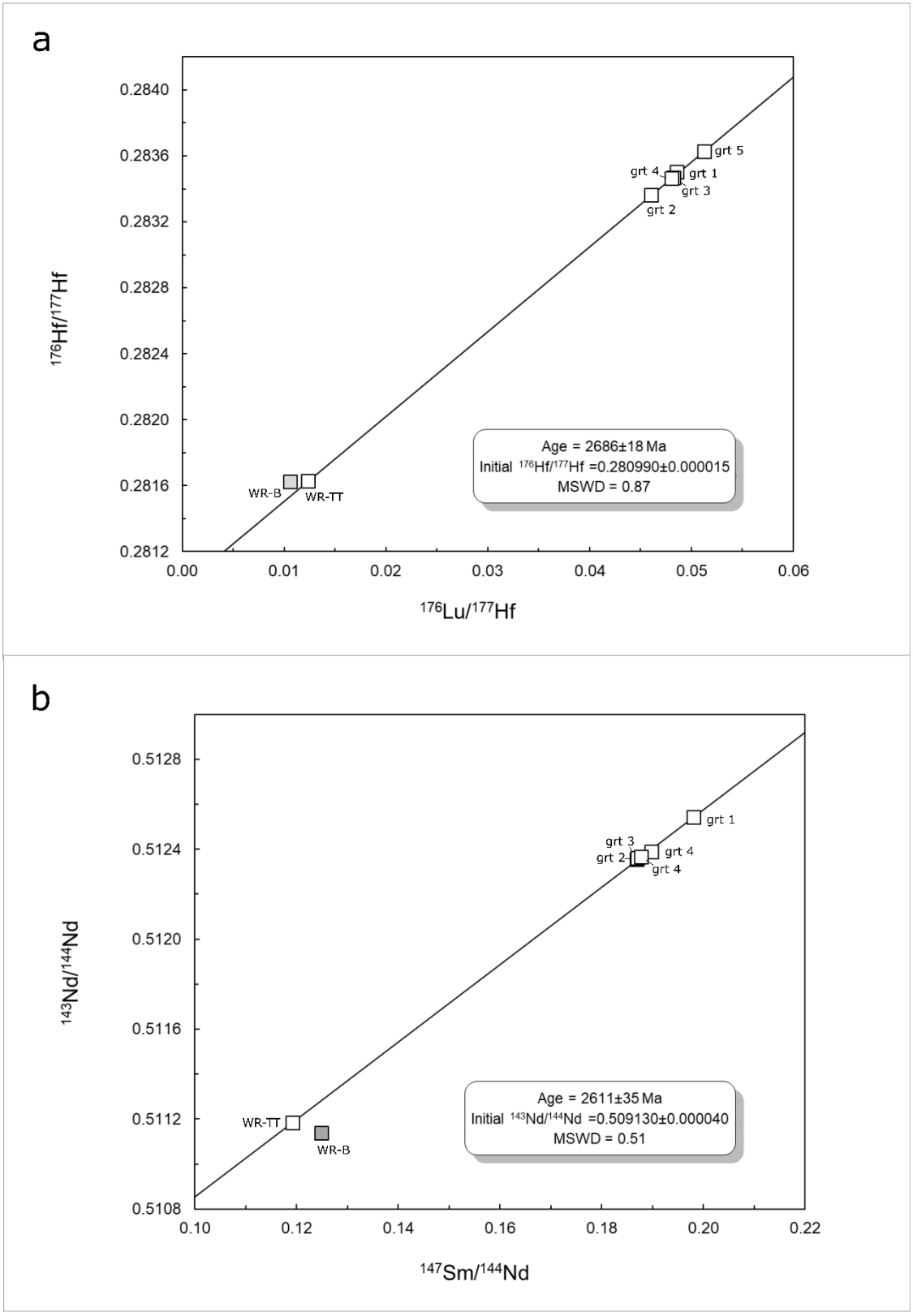

Figure 3.13. Garnet Lu-Hf (a) and Sm-Nd (b) isochron diagrams for sample 207692. Dark grey point is the whole-rock bomb sample which is not in equilibrium with the system and was not included in the age calculation, but is shown here for reference. Uncertainties are 2σ. (**WR-TT**: whole-rock table top; **WR-B**: whole-rock bomb).

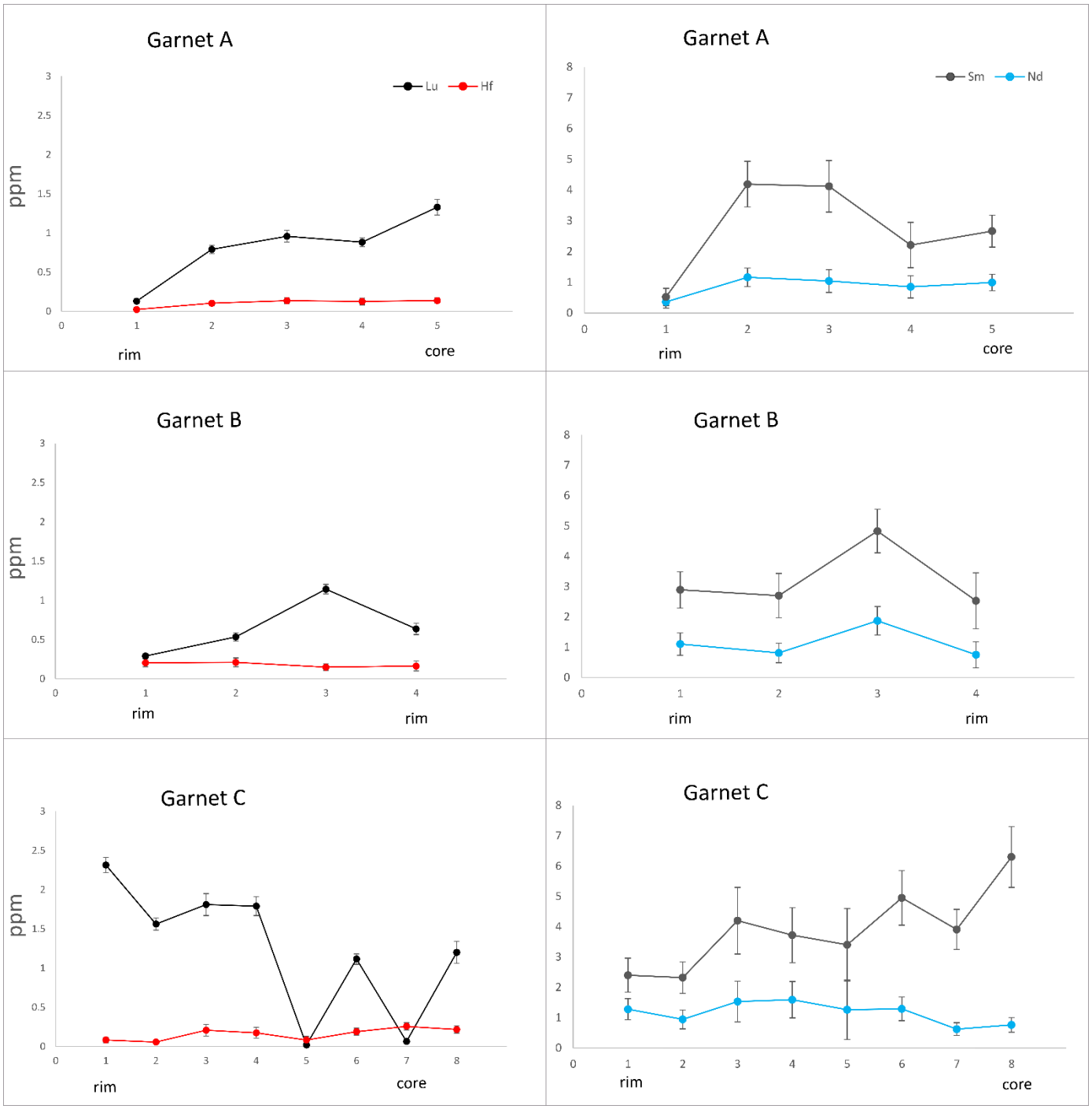

Figure 3.14. Lu-Hf and Sm-Nd profiles for garnet grains from sample 229151.

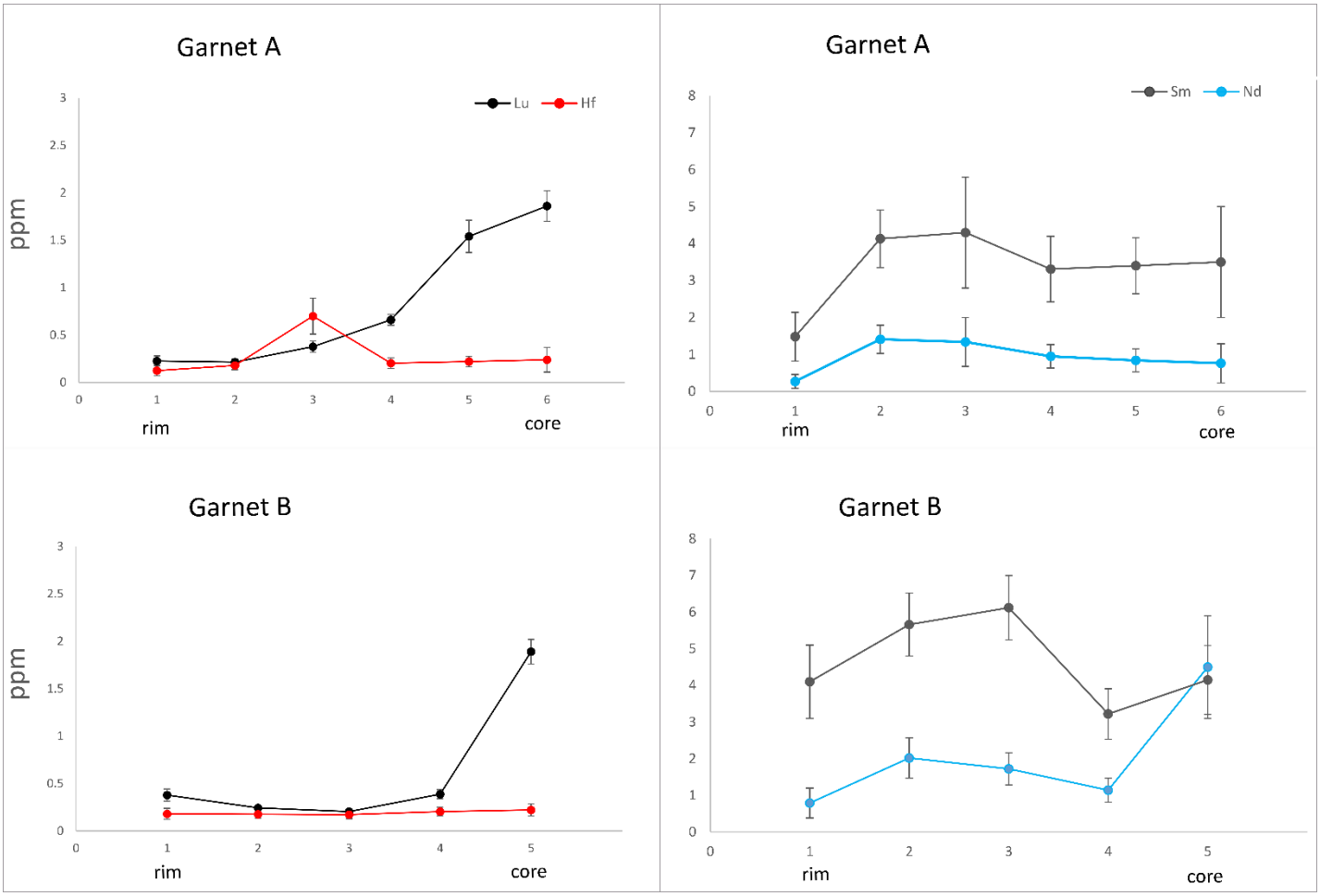

Figure 3.15. Lu-Hf and Sm-Nd profiles for garnet grains of sample 207690.

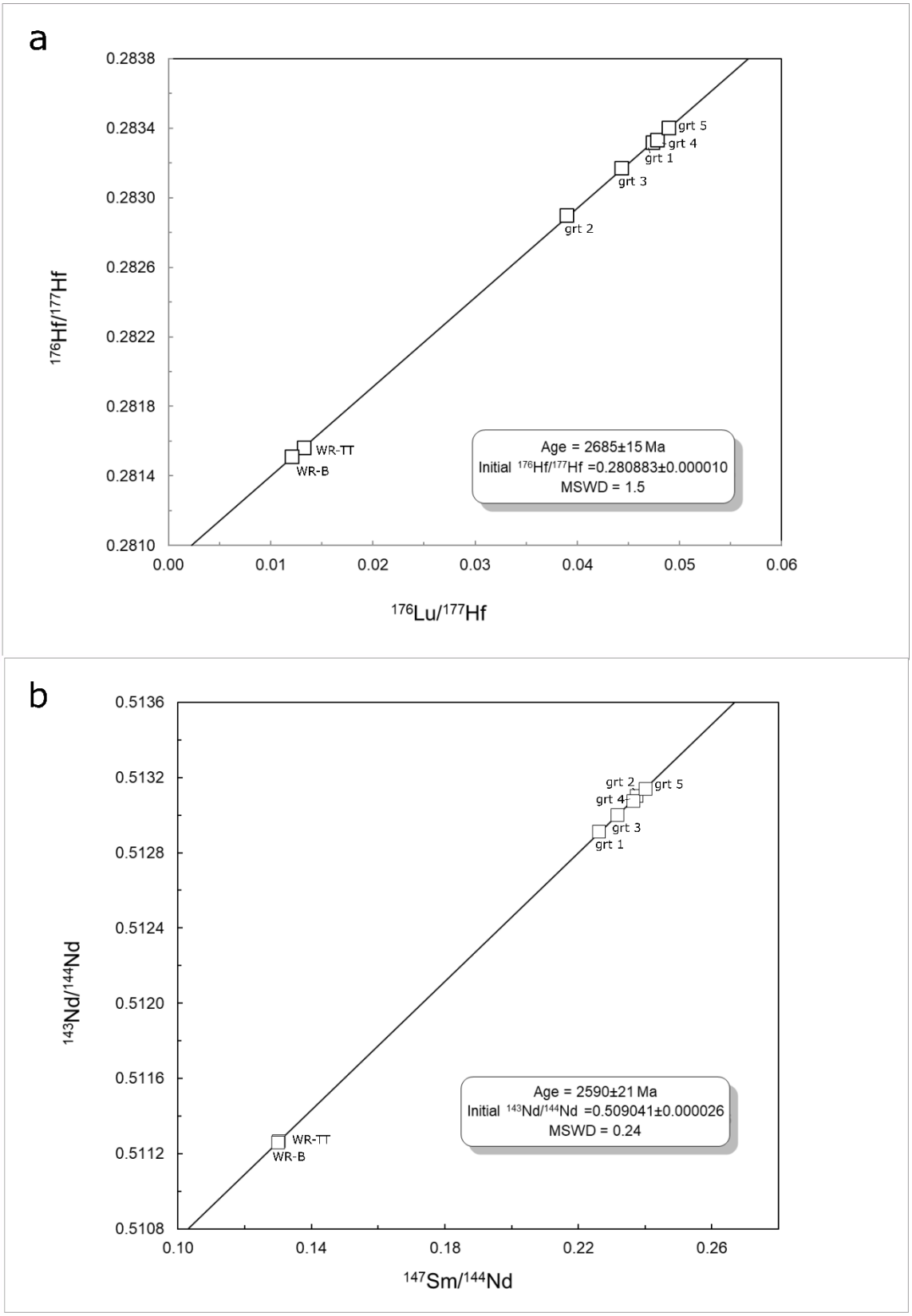

Figure 3.16. Garnet Lu-Hf (a) and Sm-Nd (b) isochron diagrams for sample 229151. Uncertainties are 2σ. (**WR-TT**: whole-rock table top; **WR-B**: whole-rock bomb).

Chapter 4: Pressure-Temperature Estimates

Metamorphic pressure (*P)* and temperature (*T*) estimates for rocks of the Mougooderra Formation were obtained through conventional thermobarometry and isochemical pseudosections. Cummingtonite (Cu) is used during the calculation of the phase equilibrium diagrams to represent the cummingtonite-grunerite solid solution. Diagrams were completed over a range of 450–725°C and <2–6 kbar for rocks of the Mougooderra Formation. Modelled bulk compositions are shown in Table 4.1.

4.1 Garnet-biotite geothermometer and garnet-biotite-Al_2SiO_5-quartz geobarometer

Estimated temperature ranges from the seven calibrations of the garnet-biotite thermometer are listed in Table 4.2. Garnet compositions used during the thermometry calculations were determined by averaging several points from the rim of each individual garnet, which is interpreted to represent the closest approximation to garnet that grew near the peak of metamorphism. If garnet rims show compositional evidence for resorption (e.g. enrichment of Mn at the rim), then points were taken just inside this zone towards the core to avoid possible diffusional re-equilibration during cooling. Biotite compositions were determined by averaging the compositions of biotite grains within matrix. In general, the estimates below are usually assigned an uncertainty of 50°C and 1 kbar based on the propagation of uncertainties in the calibrations and raw experimental data (e.g. Powell and Holland, 2008).

The temperature estimates for sample 207692 between the different calibrations are generally in agreement, the results of which range between 489°C and 591°C. However, the calibration of Dasgupta et al. (1991) consistently estimate much lower temperatures than the other calibrations, while that of Bhattacharya et al. (1992) consistently estimate higher

temperatures. The other five calibrations give a smaller and more consistent temperature range of 555°C to 570°C.

Samples 229111 and 229120 gave similar results to that of sample 207692. Sample 229111 has an overall temperature range of 511–597°C and a range of 551–583°C for the five most consistent calibrations. Overall temperature estimates for sample 229120 range between 508°C and 596°C and range from 566°C to 573°C for the five most consistent calibrations. Sample 229120 also contains minor amounts of aluminosilicate material (inferred to be andalusite) within the garnet and cordierite-rich layer. The garnet-biotite-Al_2SiO_5-quartz barometer calibration of Wu (2017) returned a pressure estimate of 3.3 kbar for this sample.

4.2 Phase equilibrium modelling

207692

In addition to the calculation of the pressure-temperature diagram discussed below, a temperature-Fe_2O_3 diagram was initially calculated over a range of 530°C to 580°C and at a pressure of 2.9 kbar in order to evaluate if the measured ratio of ferric to ferrous iron can reproduce the observed mineral assemblage (c.f. Boger et al., 2012). A pressure of 2.9 kbar was used during this calculation as the model predicts that staurolite will be stable throughout the diagram at higher pressures, however, no staurolite was observed within the sample.

The *T*–Fe_2O_3 pseudosection for sample 207692 is presented in Figure 4.1. The Fe_2O_3 concentrations ranges from 0.0 to 1.047mol% (the Fe_2O_3 value determined for this sample through titration). The major effect of ferric iron on the calculated mineral assemblage of this sample is on the stability of minerals such as magnetite and ilmenite. Below a value of 0.075-0.1 mol% magnetite is unstable within the mineral assemblage. Similarly, at temperatures above

550°C and between Fe_2O_3 values of 0.7 and 1, ilmenite is no longer stable within the mineral assemblage. Another effect that ferric iron has on the mineral assemblages of sample 207692 is on the stability fields of cummingtonite. Cummingtonite becomes stable at temperatures above 564°C at a value of 0.0 mol% Fe_2O_3. As the Fe_2O_3 value increases, the temperature for the cummingtonite-in line becomes increasingly higher. At Fe_2O_3 values of 0.92, cummingtonite is no longer stable within the mineral assemblage, indicating that the stability of a cummingtonite-grunerite phase is limited by the amount of ferric iron within the system.

Grunerite, ilmenite, and magnetite have all been observed within sample 207692. However, at the measured titration Fe_2O_3 value of 1.047 mol%, both ilmenite and grunerite would not be stable within the mineral assemblage of this sample. Due to this, the Fe_2O_3 value has been reduced to 0.5 mol.% during the calculation of the pressure-temperature diagram to ensure that the predicted mineral assemblages of the model are consistent with the observed mineral assemblage of sample 207692. The higher measured concentration of Fe_2O_3 may be due to oxidative weathering at the Earth's surface or during sample processing (e.g. Diener and Powell, 2010).

The mineral assemblage observed within sample 207692 (representative of the high Fe-Mg group, Fig. 3.2) includes garnet + cordierite + biotite + grunerite + ilmenite + magnetite + quartz + minor chlorite, and while no plagioclase was observed within the sample using a petrographic microscope, the results of the SEM-MLA (section 3.3) analysis indicates that plagioclase makes up about 1% of the area for this thin section. The phase equilibrium diagram for sample 207692 (Fig. 4.2) is generally defined by a low-T region that is defined by the presence of greenschist-facies minerals such as epidote, muscovite, chlorite, and andalusite, and a higher temperature region that is defined by the presence of minerals such as garnet, cordierite,

and cummingtonite. Modal proportions of the minerals within this sample at 2.9 kbar and across a temperature range of 540°C to 600°C are presented in Figure 4.3. The modal proportions were determined across a constant pressure to illustrate the reaction sequence along a simplified isobaric heating path. The textures of chlorite grains observed in thin section, and the numerous chlorite inclusions found within other peak minerals indicate that many of those peak minerals grew in the presence of chlorite. If substantial decompression had occurred in these rocks cummingtonite and cordierite would have grown independently of chlorite (Fig. 4.2). On the phase diagram, the breakdown of chlorite from 550–570°C is closely associated with the growth of cummingtonite, garnet, and cordierite, and the formation of cordierite is also associated with the breakdown of andalusite (Fig. 4.3). Cordierite grains with inclusions of aluminosilicate material (Fig. 3.2b), and garnet grains with minor chlorite inclusions and with inclusion patterns similar to that of chlorite grains within the matrix (Fig 3.2e) are observed within samples from the high Fe-Mg group, indicating that the predicated results of the model are generally consistent with the petrographic observations from samples of the high Fe-Mg group.

The model also predicts that cummingtonite becomes a stable mineral within the assemblage of sample 207692 at roughly 545°C (Fig. 4.2). Cummingtonite is predicted to be stable up to the solidus at 723°C and is stable over a pressure range of <2 to 3.35kbar. The mineral assemblage observed within the sample corresponds to a stability field that exists over a temperature range of 545–570°C and pressures of 2.2 to 3.4 kbar. These temperatures are similar to those obtained from garnet-biotite thermometry (section 4.1). The predicted mineral modes calculated by the model for sample 207692 (Fig. 4.3) are generally in agreement with the results of the SEM-MLA for minerals such as biotite, chlorite, ilmenite, magnetite, and grunerite. The mineral modal proportions from the SEM-MLA are given as area %, however, they can be

approximated as volume % so that the modal proportions of the SEM-MLA results are comparable to those of the model. The model predicts garnet modes of 4% and cordierite modes of 24–28% over a temperature range of 550-570°C, while the SEM-MLA indicates 11 % garnet and 18 % cordierite for the analysed thin section. In addition, the model predicts modes of 34% for quartz and 5% for plagioclase, while the SEM-MLA indicates 41% and <1%, respectively. The differences in the predicted mineral modes of the model and those of the SEM-MLA results may be to due to the slightly biased results of the MLA towards the thin section being analysed, which does not take into account variation throughout the rock, while the predicted mineral modes of the model are based on the measured whole-rock bulk composition.

229111

The mineral assemblage in sample 229111 is similar to that of the previous sample and includes garnet + cordierite + biotite + ilmenite + quartz + minor chlorite and grunerite. The modal compositions of this sample as predicted by model are presented in Figure 4.4. The predicted mineral assemblages and proportions are similar to those of sample 207692 for cordierite, biotite, plagioclase, and ilmenite. However, the proportions of cummingtonite, chlorite, and garnet are estimated at higher proportions, while staurolite is the aluminous phase present at lower temperatures. The model appears to underestimate the proportions of garnet and cordierite, while overestimating the amount of amphibole within the sample.

The phase equilibrium diagram for this sample (Fig. 4.5) is defined by the same low-T and high-T regions predicted by the model for sample 207692, with similar stability fields. The model predicts that the formation of cummingtonite is closely associated with the disappearance of chlorite and becomes a stable part of the mineral assemblage at 542°C and 2 kbar.

Cummingtonite continues to be a stable part of the mineral assemblage over several stability fields leading up to the solidus at 698℃. The mineral assemblage observed within sample 229111 corresponds to a stability field with a temperature range of 542°C to 595℃, generally consistent with temperature estimates from the previous sample and with temperature estimates obtained through garnet-biotite thermometry that predicted temperatures between 551℃ and 583℃. For this sample, the model predicts a larger pressure range for the stability fields that include cummingtonite, which exist over pressures from 2 kbar to 4.05 kbar. This larger stability field may be the result of a higher FeO concentrations (13mol% for sample 207692 vs. 19mol% in this sample).

229151

Sample 229151 was collected from the greenstone material of the Polelle Group near the smaller Mt Mulgine granitic intrusion. The mineral assemblage observed within the sample includes garnet + grunerite + K-feldspar + ilmenite + quartz. SEM-MLA results of sample 229151 also indicate the presence of chlorite, however, this chlorite is concentrated along a crack and is interpreted to represent retrograde alteration and is not considered part of the peak assemblage. The *P–T* diagram for this sample was calculated over a temperature range of 500°C to 690℃, and over a pressure range of 2 to 8 kbar, with the O value adjusted to 0.5 mol% to allow for the stabilization of ilmenite within the model (similar to sample 207692).

The phase equilibrium diagram for this sample is presented in Figure 4.6 and shows a lower temperature region defined by stability fields that contain chlorite, epidote, garnet, K-feldspar, and hornblende. Moderate to high temperature regions of the diagram are predicted to

contain cummingtonite, garnet, K-feldspar, and cordierite, with chlorite and hornblende unstable at higher temperatures. The observed mineral assemblage corresponds to a stability field with temperature range from 612℃ to 649℃, and over a large pressure range from 4–7.2 kbar.

Summary of *P–T* conditions

A summary of the *P–T* conditions for the Mougooderra Formation and Polelle greenstone sample from both garnet-biotite geothermometry and through forward modelling using phase equilibrium modelling is presented in Figure 4.7a, b. Garnet-biotite geothermometry results have temperature ranges for sample 207692 of 555–567°C for garnet 1, 559– 567°C for garnet 2, 559–570℃ for garnet 4, and an overlapping temperature range from the three garnets for this sample giving a range of 559 to 567℃ (Fig. 4.7b). The estimated temperatures are consistent with those determined from the isochemical phase diagram (Fig. 4.2), which predict a stability field with a temperature range of 545–579℃. Garnet and biotite compositions obtained from sample 229111 gave an overall range of 511–597℃, with the majority of the garnet-biotite calibrations giving a range of 551–567℃, again consistent with the previous sample and the temperature range determined through modelling which estimated a stability field with temperatures of 542°C to 595℃ (Fig. 4.5). Pressures at peak temperatures of the Mougooderra Formation are restricted from 2.2 to 3.4 kbar for sample 207692, and from <2 to 4 kbar for sample 229111, with the stability fields of both samples overlapping at 2.5-3.1 kbar (Fig. 4.7a). While samples from the high Al group do not have assemblages with useful metamorphic minerals to constrain the *P–T* conditions of these rocks using ferromagnesian minerals, the presence of andalusite throughout the samples of this group is consistent with pressures <4.2 kbar and pressures within the stability fields of samples 207692 and 229111 (Fig. 4.7a).

In summary, the *P–T* conditions of the Mougooderra Formation are estimated to be 550-570°C and between 2.5 and 3.3 kbar as determined using samples 207692 and 229111 from the high Fe-Mg group. Samples from the greenstone material give higher temperature conditions with a range between 610°C and 650°C and pressures estimated from one sample ranging from 4 to 7.2 kbar, which are higher than estimates from the Mougooderra Formation.

Relationship between the high Fe-Mg, average pelitic, and high Al groups

The different compositional groups have different mineral assemblages, but generally have similar estimated *P–T* conditions of peak metamorphism. The main changes in bulk composition include the depletion of MgO, FeO, K_2O, and the enrichment of SiO_2 as the bulk composition transitions from that of the high Fe-Mg group towards that of the high Al group (Fig. 3.1). To investigate the changes in mineral assemblage as a function of composition and temperature, a *T-X* phase diagram (Fig. 4.8) was calculated across a temperature range of 530°C to 580°C and at a pressure of 2.75 kbar (this pressure was chosen to ensure that the predicted mineral assemblages were consistent with the observed mineral assemblages of all three geochemical groups). $X = 0$ represents the bulk composition of sample 207692 from the high Fe-Mg group (Fig. 4.2, 4.3), and $X = 1$ represents the bulk composition of sample 229135 from the high Al group.

Over a range of temperatures from 552°C to 580°C and a range of X values from 0.0 to 0.26 the model predicts that several different mineral assemblages will be stable that include garnet + biotite + ilmenite + magnetite ± chlorite ± cordierite ± cummingtonite, all of which are consistent with the main mineral assemblages observed within the rocks of the high Fe-Mg

group. At elevated temperatures, the depletion of FeO and MgO affect the predicted mineral assemblages by destabilizing cummingtonite and garnet, while the enrichment of SiO_2 stabilizes andalusite. This leads to the predicted mineral assemblages of cordierite + biotite + plagioclase + ilmenite + magnetite ± andalusite. These predicted assemblages are consistent with the observed assemblages from the average pelitic group (section 3.2). As the modelled bulk composition continues to transition from intermediate (i.e. average pelitic) compositions, the continued depletion of FeO and MgO causes the destabilization of cordierite. The resulting mineral assemblages include biotite + plagioclase + ilmenite + magnetite + andalusite ± muscovite, consistent with petrographic observations of the rocks from the high Al group. In summary, the various metamorphic mineral assemblages observed in the Mougooderra Formation are compatible with variations in bulk compositions at similar pressure and temperature conditions.

Table 4.1. Bulk compositions used in the calculation of phase equilibrium diagrams (mol%).

Sample	SiO_2	Al_2O_3	CaO	MgO	FeO	K2O	Na_2O	TiO_2	MnO	O
207692 (X=0)	62.82	11.48	0.6	8.7	13.38	1.98	0.41	0.57	0.08	0.0
207692 (X=1)	62.16	11.36	0.59	8.6	13.24	1.96	0.40	0.57	0.08	1.04
229111	54.24	12.78	0.605	9.75	19.31	1.72	0.318	0.654	0.096	0.53
229135	86.75	8.87	0.191	0.199	1.758	0.86	0.108	0.510	0.009	0.74
229151	62.68	8.04	2.09	6.16	17.76	1.09	0.89	0.65	0.13	0.5

Table 4.2. Temperature estimates in °C based on garnet-biotite thermometry calibrations.

Sample	Thompson 1975	Holdaway and Lee, 1977	Ferry and Spear, 1978	Perchuk 1983	Dasgupta et al., 1991	Bhattachary et al., 1992	Holdaway 2000
207692 grt 1	557	559	555	567	489	588	565
207692 grt 2	559	561	557	567	493	590	567
207692 grt 4	560	562	559	570	492	591	567
229111	567	559	551	567	511	597	583
229120	566	567	566	573	508	596	578

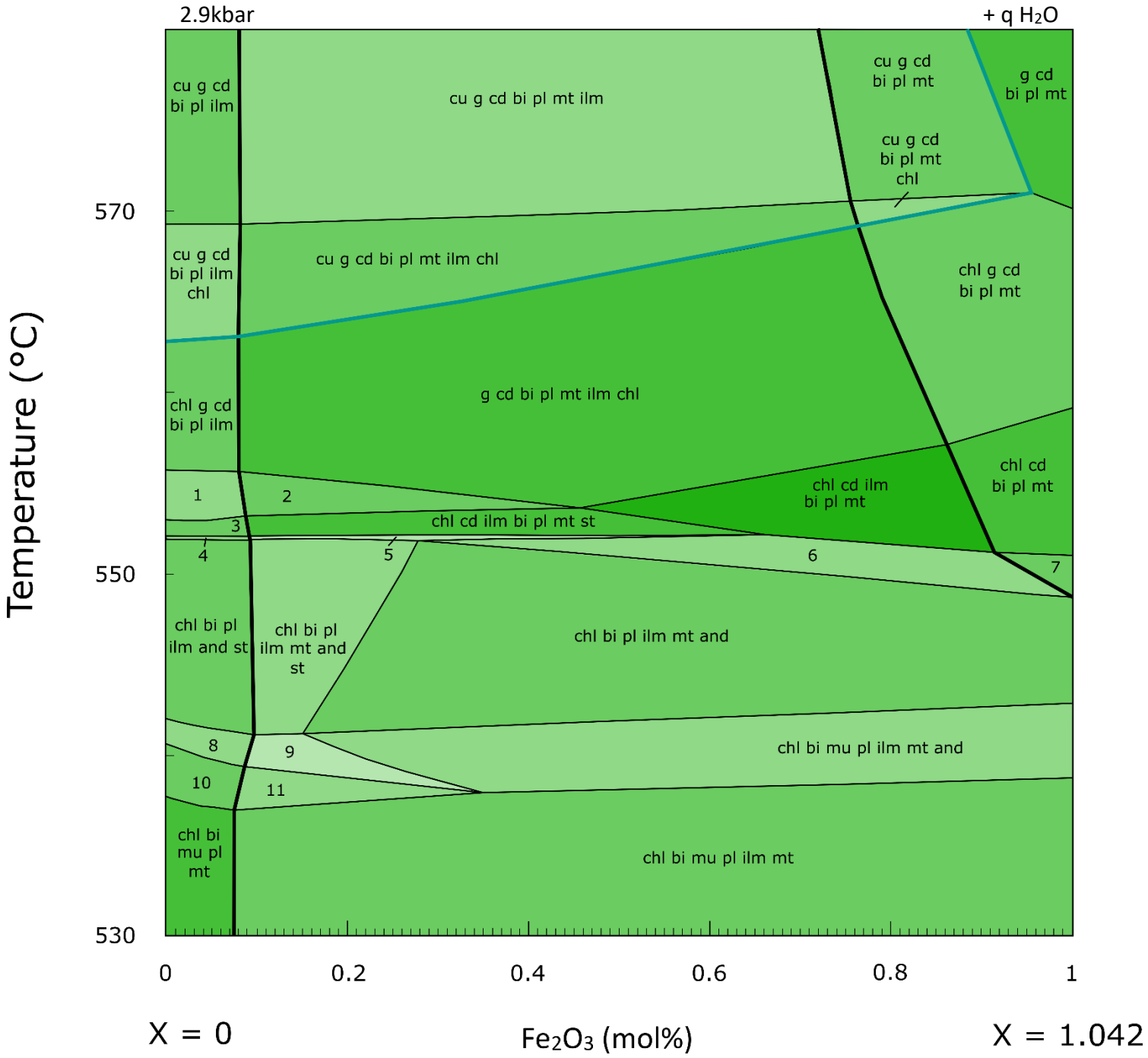

1. cd st chl bi pl ilm g
2. cd st chl bi pl mt ilm g
3. cd st chl bi pl ilm
4. cd st chl bi pl ilm and
5. cd st chl bi pl mt ilm and
6. cd chl bi pl mt ilm and
7. cd chl bi pl mt and
8. st chl bi mu pl ilm and
9. st chl bi mu pl mt ilm and
10. st chl bi mu pl ilm
11. st chl bi mu pl mt ilm

Figure 4.1. Temperature-Fe_2O_3 diagram for sample 207692 at a pressure of 2.9 kbar. Bold lines represent the magnetite and ilmenite-out lines, while the blue line represents the cummingtonite-in line.

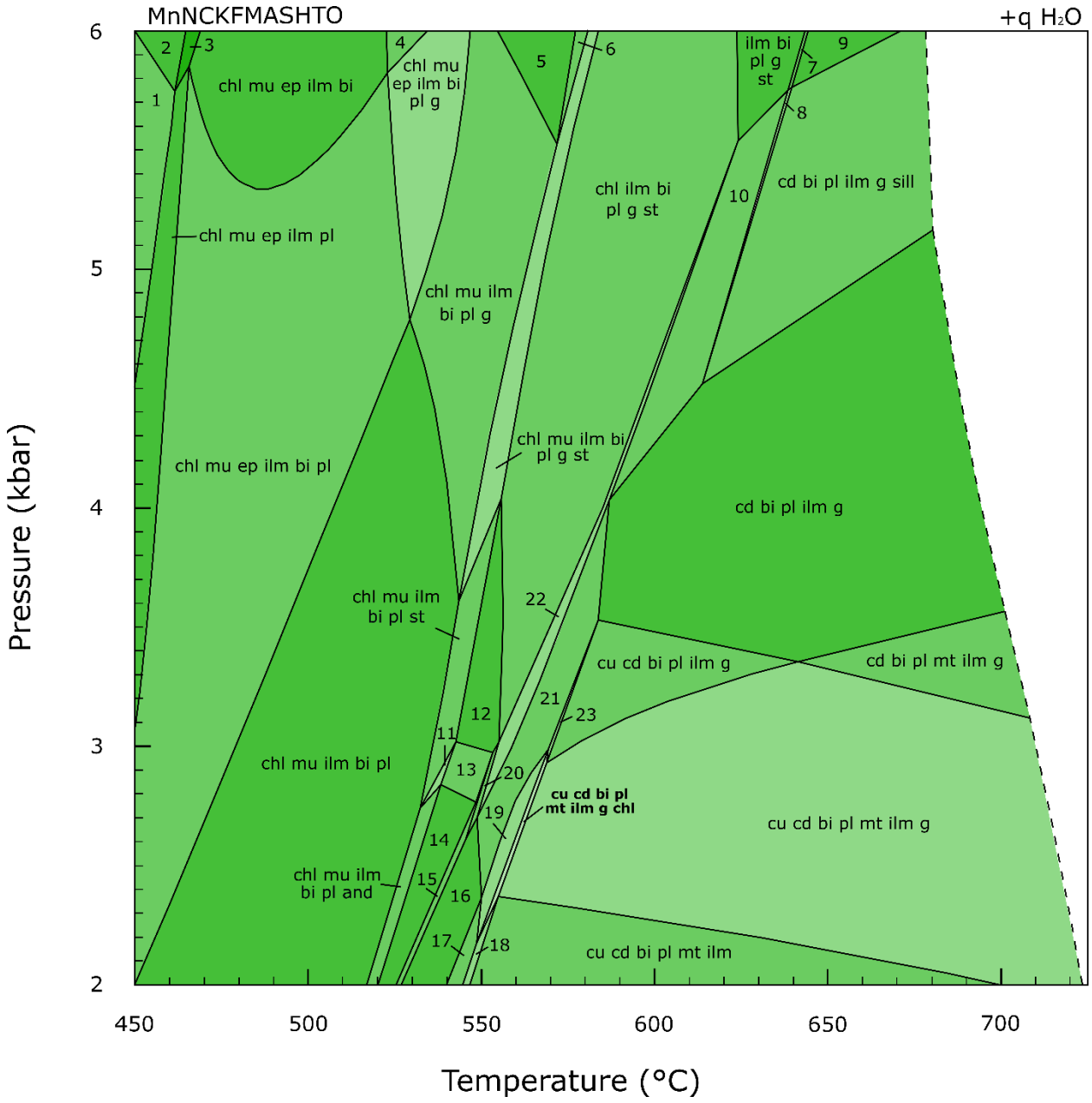

1. chl mu pl ilm ep ru
2. chl mu ilm ep ru
3. chl mu pl ilm ep
4. chl mu pl ilm ep bi g
5. chl mu ilm bi g
6. chl mu ilm bi g st
7. pl ilm bi g st sill
8. pl ilm bi g st sill cd
9. pl ilm bi g st sill
10. pl ilm bi g st cd
11. chl mu ilm bi pl st and
12. chl ilm bi pl st
13. chl ilm bi pl st and
14. chl ilm bi pl and
15. chl ilm bi pl and cd
16. chl ilm bi pl cd
17. chl ilm bi pl cd mt
18. chl ilm bi pl cd mt cu
19. chl ilm bi pl cd mt g
20. chl ilm bi pl cd st
21. chl ilm bi pl cd g
22. chl ilm bi pl cd g st
23. chl ilm bi pl cd g cu

Figure 4.2. Temperature-Pressure diagram of sample 207692. The dashed line represents the solidus, while the field labeled in bold text represents the observed mineral assemblage for this sample.

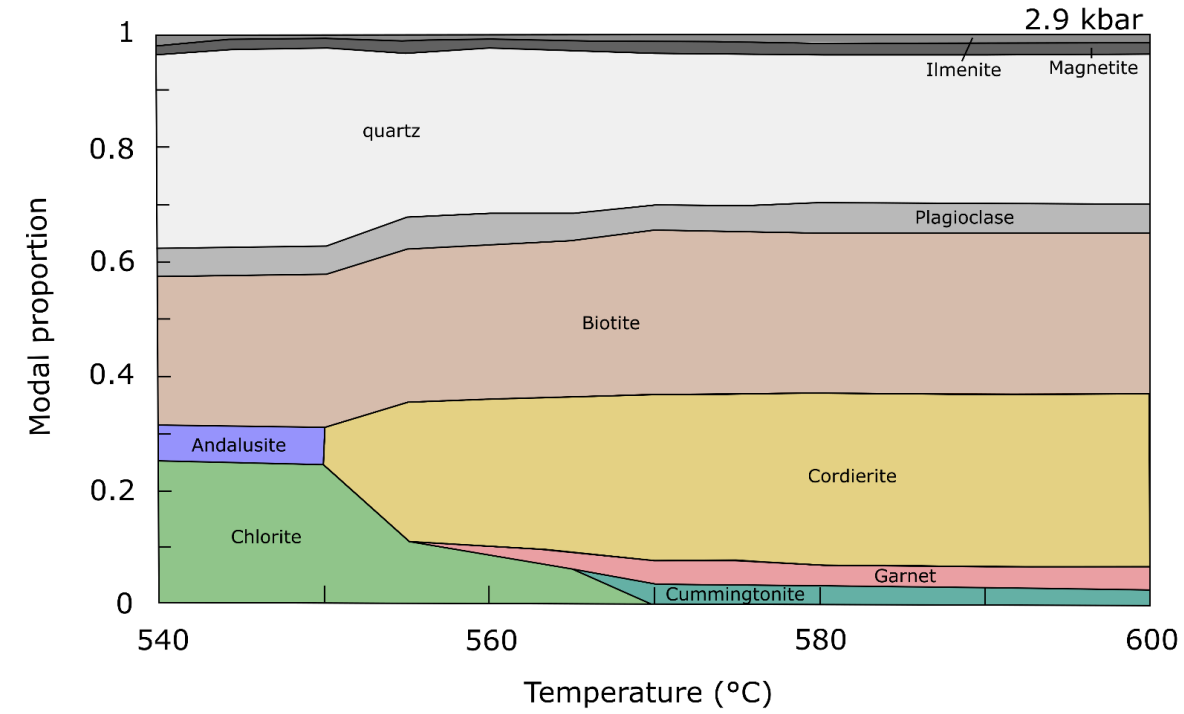

Figure 4.3. Modal proportions of minerals within sample 207692 at 2.9 kbar over a range of 540 to 600°C.

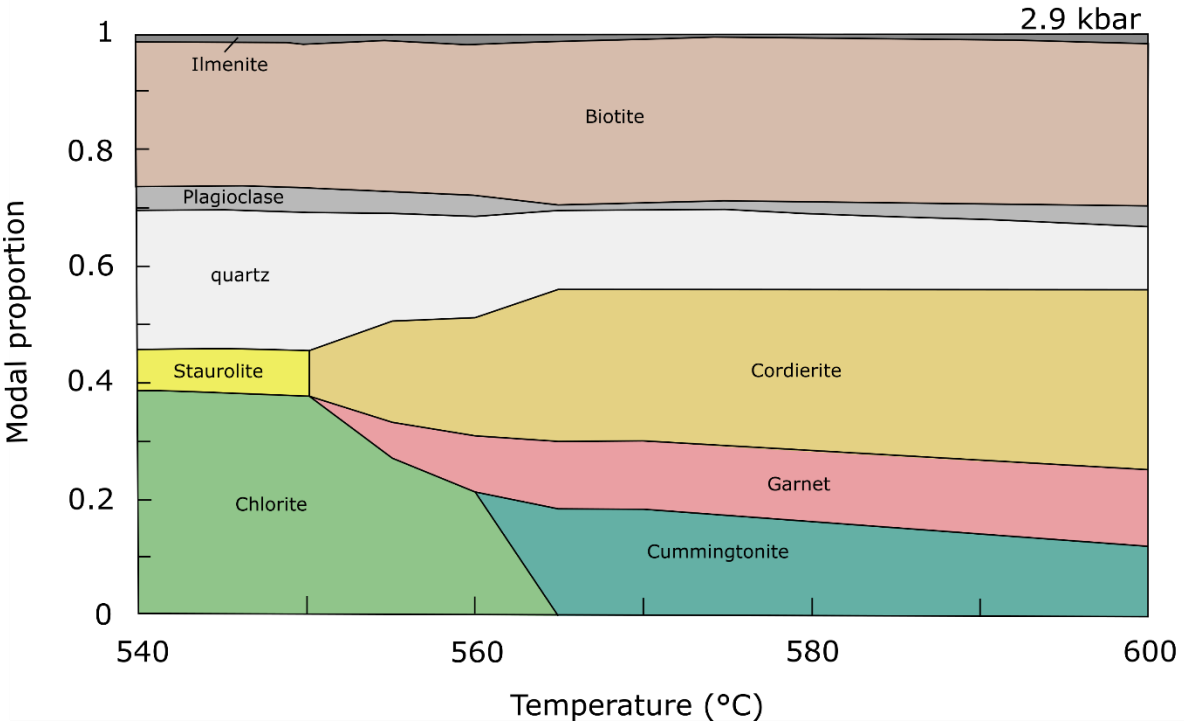

Figure 4.4. Modal proportions of minerals within sample 207111 at 2.9 kbar over a range of 540 to 600°C.

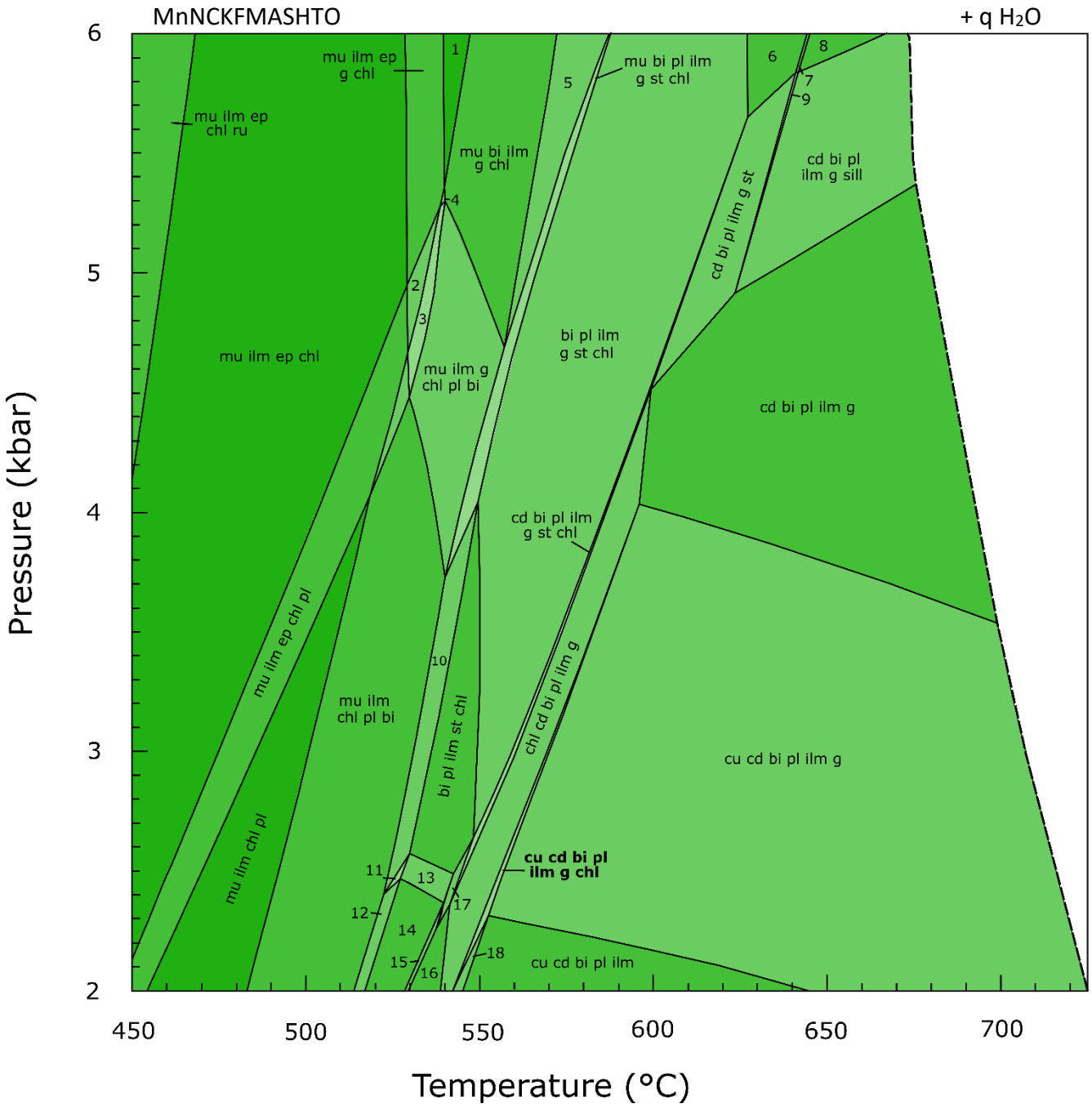

1. mu ilm g chl
2. mu ilm g chl pl
3. mu bi ilm g chl pl
4. mu bi ilm g chl ep
5. mu bi ilm g chl st
6. bi pl ilm g st
7. bi pl ilm g st sill
8. bi pl ilm g sill
9. cd bi pl ilm g st sill
10. mu ilm chl bi pl st
11. mu ilm chl bi pl st and
12. mu ilm chl bi pl and
13. ilm chl bi pl st and
14. ilm chl bi pl and
15. cd ilm chl bi pl and
16. cd ilm chl bi pl
17. cd ilm chl bi pl st
18. cu chl cd bi pl ilm

Figure 4.5. Temperature-Pressure diagram of sample 229111. The dashed line represents the solidus, while the field labeled in bold text represents the observed mineral assemblage for this sample.

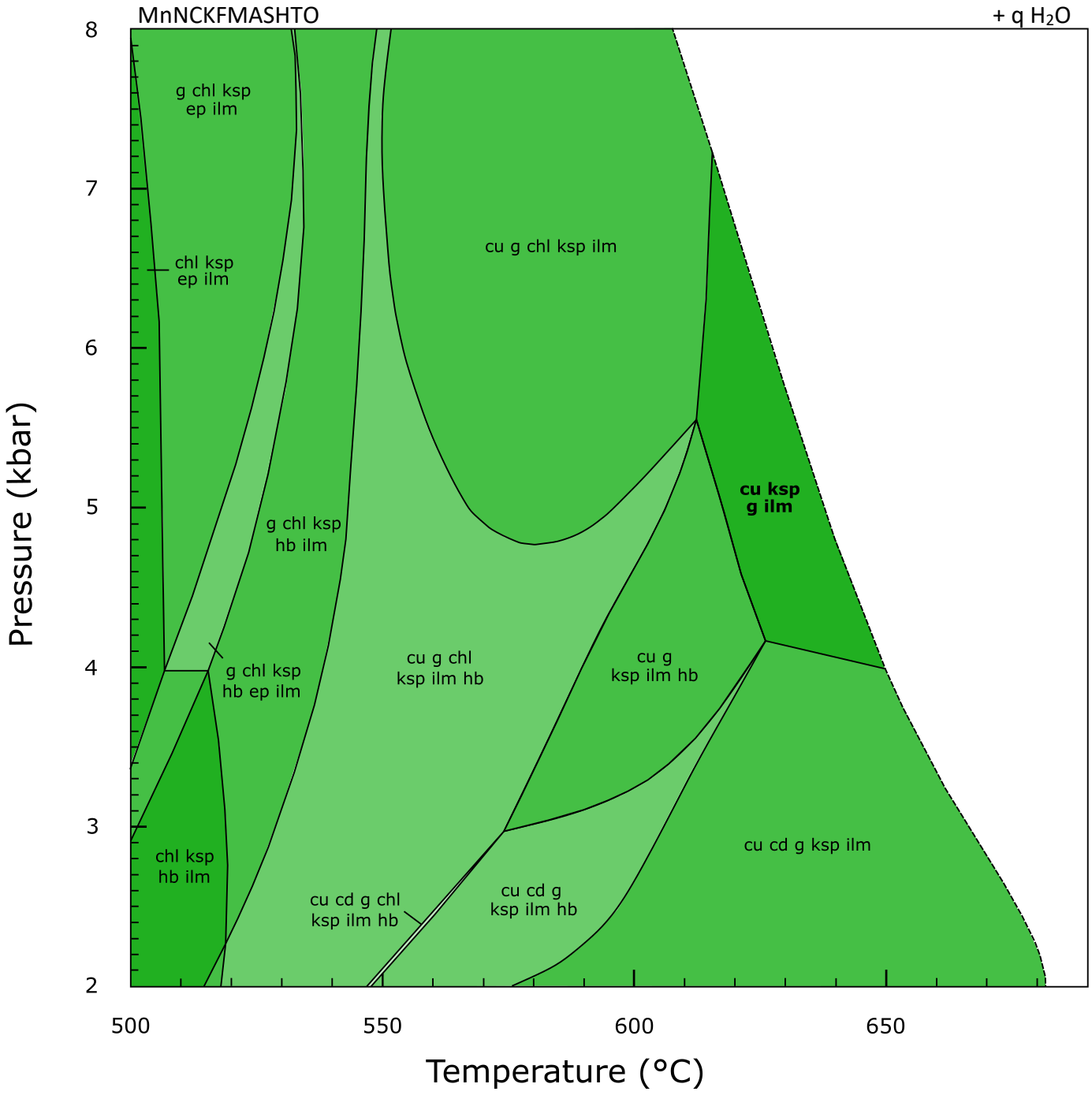

Figure 4.6. Temperature-Pressure diagram of sample 229151. The dashed line represents the solidus, while the field labeled in bold text represents the observed mineral assemblage for this sample.

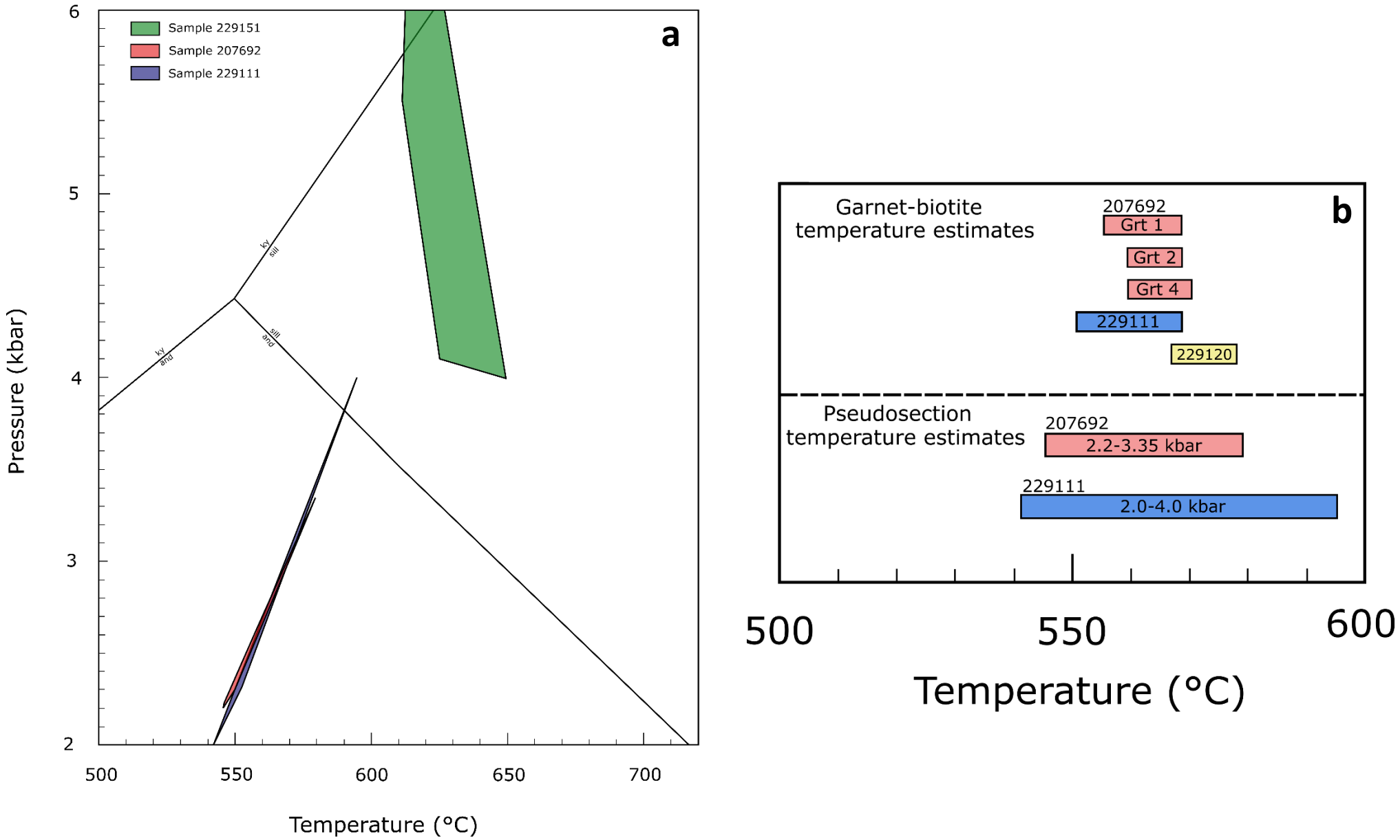

Figure 4.7. (a) Summary of *P–T* conditions for rocks of the Mougooderra Formation (207692 and 229111) and greenstone samples (229151), **(b)** Comparison of temperatures determined through forward modelling and garnet-biotite geothermometry for samples 207692, 229111, and 229120.

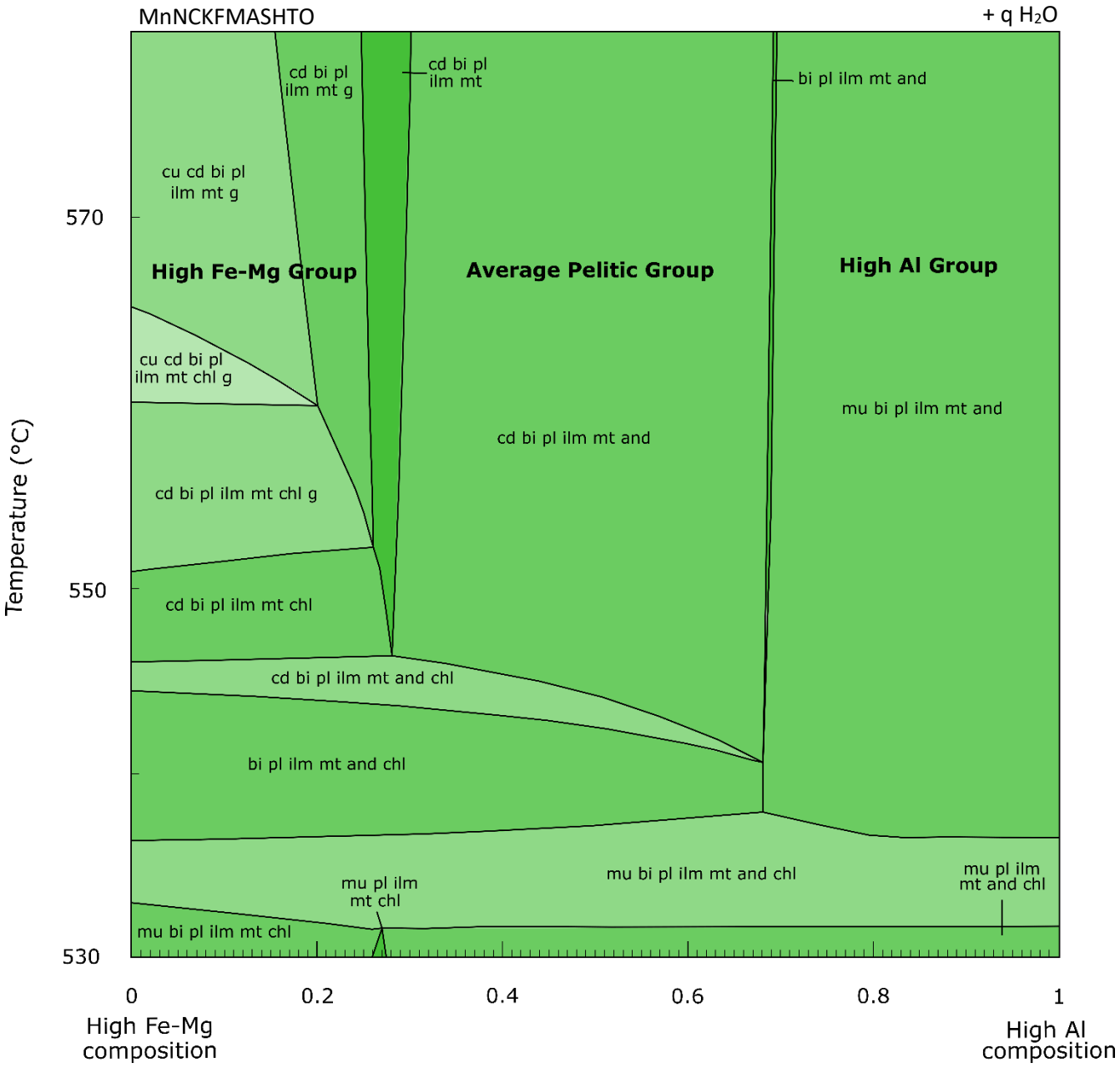

Figure 4.8. *T-X* diagram calculated for bulk compositions between sample 207692 of the high Fe-Mg group and sample 229135 of the high Al group at 2.75 kbar.

Chapter 5: Discussion

5.1 Conditions of Metamorphism

Within the Ninghan area, rocks of the Mougooderra Formation preserve rare *P–T*-sensitive metamorphic mineral assemblages (e.g. garnet, cordierite, and grunerite) that can be used to infer the *P–T* conditions and timing of metamorphism as well as the associated geodynamic environment. These rocks, as well as samples from greenstone material of the Polelle Group, were used to determine peak metamorphic conditions. Phase equilibria modelling and thermobarometry suggest that the Mougooderra Formation experienced relatively low pressures (2.5–3.3 kbar) and high temperatures (550–570°C) at peak metamorphism, while pressures and temperatures experienced by the greenstone at this time were higher (4.0–7.2 kbar and 610–650°C).

5.2 Timing of Metamorphism

The timing of metamorphism is similar for both samples with a sample from the Mougooderra Formation returning a Lu-Hf age of 2686±18 Ma and a Sm-Nd age of 2611±35 Ma, while a sample from the Polelle Group returned a Lu-Hf age of 2685±15 Ma and a Sm-Nd age of 2590±21 Ma. The significant age differences between the garnet Lu-Hf and Sm-Nd systems may be the result of resetting of the Sm-Nd system during contact metamorphism, however, it may also represent either a prolonged period of prograde metamorphism or a slowly cooling terrane depending on the zoning of the parent isotopes within the garnet grains and the factors taken into consideration for the closure temperature of the Sm-Nd system. In the contact metamorphic model, the garnet Lu-Hf system would be recording an older metamorphic event, while the Sm-Nd system is recording a resetting of the system due to a rejuvenated heat source

such as the ascent and crystallization of post-tectonic magma from the middle crust and a contact metamorphic overprint. For example, the Sm–Nd garnet age from sample 207692 is within uncertainty of the age of the nearby Seeligson monzogranite (Fig. 5.1). However, the Sm-Nd garnet age of sample 229151 is not within uncertainty of the Seeligson monzogranite and the Lu-Hf garnet ages still require an earlier, regional metamorphic event that resulted in initial growth of the garnet grains. Therefore, other explanations for the large age differences must be considered.

The growth of garnet grains within a metamorphic rock is a protracted process that commonly results in the zoning of major and trace elements. As a result, Lu-Hf and Sm-Nd ages may be biased towards the zones of the grain that contain elevated amounts of the parent isotope (Baxter et al., 2017). In low-temperature garnets with well-preserved prograde zoning, Lu will typically be concentrated within the core of the grain as it partitions strongly into garnet (Baxter and Scherer, 2013). In this case the age will be biased towards the core of the garnet and the first increment of garnet growth along the prograde path. In some studies, the significant age differences observed between the Sm-Nd and Lu-Hf chronometers is related to parent isotope zonation within the garnet grains (Skora et al., 2009). For example, if Lu was strongly concentrated within the core of a grain whereas Sm was distributed equally throughout, then the Lu-Hf age would be biased towards the early part of the garnet growth and the Sm-Nd age would represent an integrated, likely younger age (i.e. recording later parts of the prograde path). Taken into consideration the slight zoning of the parent isotopes of sample 207690 (Fig. 3.16), the difference in the Lu-Hf and Sm-Nd ages may be interpreted to represent different parts of the prograde path. However, it is unlikely that zoning of Sm within the garnet grains can alone explain the large age discrepancy between the two systems given the lack of substantial Lu and

Sm zoning observed within the garnet grains of samples 207692 and 229151 (Fig 3.14; 3.15). The difference in age is not likely related solely to different zoning patterns in the two parent isotopes.

The closure temperature of an isotopic system within a given mineral depends on a number of factors including the duration of the thermal event, the size, shape, and composition of the mineral, and the diffusivity of the element (Scherer et al., 2000). Estimates of the closure temperature for the Sm-Nd system within garnet have resulted in a wide range of temperatures and varies from <500°C to over 800°C, with many studies suggesting roughly 700°C as a general estimate (Humphries and Cliff, 1982; Cohen et al., 1988; Jagoutz, 1988; Mezger et al., 1992; Hensen and Zhou, 1995; Burton et al., 1995; Ganguly et al., 1998; Scherer et al., 2000; Dutch and Hand, 2009; Pollington and Baxter, 2011). A plot of closure temperature for Nd and Hf as a function of cooling rate, temperature, and garnet radius along with information relevant to the two samples investigated here is shown in Figure 5.2 (Smit et al., 2013). Considering the metamorphic temperatures of ~570°C for the Mougooderra Formation, either very slow cooling or very small garnet radii are required to result in significant difference in the closure temperatures of Nd and Hf in garnet. Considering that garnet grains of the sample from the Mougooderra Formation have radii of ≤0.5mm, cooling rates of <2°C/Ma are required to explain the difference in ages from the Lu-Hf and Sm-Nd isochrons. For example, given an activation energy of 250 kJ/mol, a cooling rate of 2°C/Ma, and an assumed garnet radius of 0.5mm, closure temperature for the Lu-Hf system would roughly be 800°C, while that of the Sm-Nd system would be roughly 650°C (Fig. 5.2). Given that some garnet grains within the analysed sample have radii less than 0.5mm, plus the uncertainties associated with *P–T* estimates (e.g. Palin et al., 2016) and isotopic closure temperatures of garnet (e.g. Smit et al., 2013), peak metamorphic

temperatures overlap closely with the closure temperature of the Sm-Nd system. In this case the peak metamorphic temperature would be below the closure temperatures of both the Lu-Hf and Sm-Nd systems, and the ages would both represent similar prograde garnet ages, which is not the case for these samples. However, reported Sm-Nd closure temperatures for garnet grains of smaller radii from other studies (e.g. T_c = 485°C and 500°C for respective garnet radii of 0.16 and 0.24mm of Scherer et al. (2000); Fig. 5.2) are inconsistent with those of Smit et al. (2013), which estimate a much higher closure temperature of >600°C. This indicates that a lower Nd closure temperature is possible, and also demonstrates that obtaining a closure temperature for the Sm-Nd system depends on numerous factors and is often difficult to constrain and as a result the Sm-Nd dates of this study remain somewhat ambiguous.

In summary, the Sm–Nd dates of this study are ambiguous, they may represent slow cooling, a prolonged period of prograde metamorphism, or resetting during a contact metamorphic event. However, taking into consideration the similar ages from both isotope systems between the two samples and the higher temperatures recorded by the samples of the Mt Mulgine area, which are further away from the Seeligson monzogranite than those of the Mougooderra Formation, it is suggested that these dates represent a slowly cooling (<2°C/Ma) terrane, as the *P*–*T* conditions are inconsistent with the architecture and rapid cooling rates (>1000°C/Ma) expected in contact aureoles around granite plutons (Nabelek et al., 2012), and such a significant age difference is unlikely to be attributed solely to zoning of the parent isotopes.

5.3 Processes Driving Metamorphism

The relatively low *P* and high *T* metamorphic conditions recorded by the Mougooderra Formation are compatible with two contrasting tectonic settings: (1) contact metamorphism as a result of the emplacement of a large syn to post-tectonic granitic body into supracrustal rocks, and (2) regional metamorphism resulting from a large-scale mantle plume event and associated crustal instabilities (Van Kranendonk et al., 2013), or through an orogenic event in the Neoarchean (Zibra et al., 2017a).

In the case of the contact metamorphic model, metamorphism of the Mougooderra Formation would most likely be driven by the emplacement of the nearby Seeligson monzogranite. The Seeligson monzogranite crosscuts the main body of the Mougooderra Formation within the Ninghan area (Fig. 1.2). Contact metamorphism of the Mougooderra Formation adjacent to the Seeligson monzogranite would result in the high temperatures, while the relatively low pressures would be the result of the stratigraphic placement of the Mougooderra Formation at the time of granite emplacement. In this scenario, the higher pressures and temperatures observed in the samples from the greenstones are the result of being at a stratigraphically lower position within the region. For example, assuming a crustal density of 2,700 kg/m^3, given the pressure ranges determined for the Mougooderra Formation and underlying greenstones, the difference of 1.3 to 5 kbar in pressure would result in a structural separation between 5 and 18 km.

However, several problems exist with the contact metamorphism model. First, the garnet Lu-Hf ages from the Mougooderra Formation do not overlap in time with any nearby granitoids and suggest that garnet growth began at a minimum of 36 Ma (considering the maximum uncertainty) prior to the crystallization of the Seeligson monzogranite at 2626±6 Ma (Wingate et

al., 2014), and is significantly younger than the granitoids of Mt Mulgine which have been dated at 2756±20 Ma (Fletcher and McNaughton, 2002) and 2752±8 Ma (Wingate et al., 2018). Second, studies of contact aureoles around other large granitoid intrusions have shown that the thermal effect on the surrounding bedrock generally ranges from 0.5 to 3 km from the intrusive body with temperatures decreasing away from the intrusion (Symmes and Ferry, 1995; Pattison and Vogl, 2005; Jamieson et al., 2012). The Lu-Hf ages of the greenstone indicates nearly contemporaneous metamorphism >3 km northwest of the Seeligson monzogranite. In addition, the estimated peak temperatures near Mt Mulgine are higher than those of the Mougooderra Formation, which is inconsistent with the architecture of a local contact aureole. Finally, samples collected outside the Ninghan area, located 5–10 km away from any granitic intrusion, still contain metamorphic minerals such as andalusite, indicating that there was low-*P* metamorphism at a regional scale.

Considering that a contact metamorphic scenario is incompatible with the garnet geochronology and metamorphic temperatures away from nearby plutons, a regional metamorphic model that predates the emplacement of the granitoids is needed. Two general scenarios have been proposed for the thermotectonic history of the Yilgarn craton that could generate regional metamorphism, including (1) an accretion–orogenesis model dominated by modern-style plate-tectonic processes (e.g. Myers, 1993; 1995; Wilde, 1996; Krapez and Barley et al., 2008; Standing, 2008), and (2) a vertical-tectonic model involving the ascent of granitic diapirs and sinking of greenstone material (e.g. Van Kranendonk, 2013).

Orogenesis due to the accretion of exotic terranes has been proposed for the tectonic evolution of the Yilgarn Craton (Myers, 1993; Cassidy et al., 2006; Champion and Cassidy, 2007). Recent structural work within the Murchison Domain has indicated the presence of a

north-trending foliation within syntectonic plutons (2700-2660 Ma) that overprints older doming fabrics (Zibra et al., 2017a; 2018). These structures are subparallel-to-parallel to other shear zones throughout the Yilgarn Craton, including the large-scale east dipping shear zones that separate the terranes of the Yilgarn craton (Zibra et al., 2017a; 2018). Zibra et al. (2017a) suggest that this structural data in conjunction with the quick change in depositional environments from a low energy, deep marine environment to a high energy, shallow marine environment marks a geodynamic transition within the Yilgarn Craton from granitic doming to crustal shortening as a result of orogenesis. Sub-horizonal fabrics in the middle to deep crust of the Youanmi Terrane inferred from seismic imaging are also consistent with a terrane-accretion model (Calvert and Doublier, 2018). The metamorphic signature of a terrane–accretion model should include syn-tectonic metamorphic mineral assemblages and apparent thermal gradients indicative of intermediate d*T*/d*P* metamorphism (e.g. Brown and Johnson, 2018). These two features are observed in the Southern Cross Domain to the east of the Murchison Domain (Zibra et al., 2017b). However, in the Mougooderra Formation, post-kinematic garnet (section 3.2) and apparent thermal gradients of >1500°C/GPa (section 5.3) are both incompatible with metamorphism accompanying terrane accretion.

An alternative tectonic model that could have generated regional metamorphism is upwelling asthenosphere and melting of the mantle and crust as the result of mantle-crust interactions either in the form of mantle plumes (e.g. Van Kranendonk et al., 2013), or through mantle overturn as suggested by Bédard (2018). The different terranes of the Yilgarn Craton share a similar tectonic history between 2820 and 2600 Ma and include events such as widespread ultramafic-to-mafic volcanism near 2720 Ma, the emplacement of granitic rocks with similar compositions from 2690 to 2640 Ma, shearing and gold emplacement from 2660 to 2630

Ma, followed by the emplacement of post-tectonic intrusions from 2630-2600 Ma (Van Kranendonk et al., 2013). The cause of widespread magmatism is inferred by Van Kranendonk et al. (2013) to be mantle plume overturn events, which caused partial melting in the mid-crust and partial convective overturn of greenstone material. Lithospheric extension and the onset of a new mantle plume event across the Yilgarn Craton at ~2735–2711 Ma is consistent with the crystallization of komatiitic basalt of the Glen Group and the emplacement of gabbroic sills with a pyroxenite to peridotite cumulate base of the Yalgowra Suite, as well as the similar ages of ultramafic intrusions within the Eastern Goldfields Superterrane (Van Kranendonk et al., 2013). Subsequent thermal blanketing and crustal overturn, followed by partial melting of the mid-crust, and the formation of an eclogitic-granulitic crustal residue that delaminated may have caused the formation and emplacement of the post-tectonic granites at 2640-2630 Ma in the craton (Van Kranendonk et al., 2013).

This plume-driven model is supported by structural data that indicates that the Yalgoo Dome (a large granitoid body just north of the Ninghan map sheet) and smaller associated granitic bodies (such as Mt. Mulgine; Fig. 1.1) were likely emplaced during a period of magmatic doming (Zibra et al., 2018). In addition to this, detrital zircon analyses have shown that the main detrital zircon population from the Mougooderra Formation near the Yalgoo Dome have similar Th/U ratios and ages to that of the main zircon populations from the nearby Kynea Tonalite (2950 Ma) and the granitic rocks of the Rothsay Suite (2760-2750 Ma; Zibra et al., 2018). This combined with the similarity of clasts within conglomerate beds of the Mougooderra Formation to that of the underlying greenstone material (Watkins and Hickman, 1990) suggests that the sediment which formed the Mougooderra Formation may have been deposited as a result of rising granitic domes that caused the uplift and erosion of greenstone and granitic material

(Zibra et al., 2018). A similar model has been proposed for the Superior Province where diapirism and sagduction resulted in the erosion of the greenstone material followed by erosion of rising granitic domes (e.g. Lin et al., 2013). In these models, the upwelling mantle and rising granitic domes during crustal overturn would be an important source of the heat responsible for metamorphism of the Mougooderra Formation.

The metamorphic signature of a model driven by heat from the mantle would include mafic to ultramafic magmatism followed by high temperature metamorphism as the overlying crust experiences high heat flow (Owada et al., 2016; Bédard, 2018) and high apparent thermal gradients (Brown and Johnson, 2018). Within the Murchison Domain ultramafic rocks of the Yalgowra Suite and Glen group are at a minimum of 7 Ma older than the timing of metamorphism indicated by the Lu-Hf garnet geochronology, which is consistent with a mantle-driven model. In addition, rocks with apparent thermal gradients greater than 1000°C/GPa have been observed for the Mougooderra Formation and from several other localities throughout the western Yilgarn Craton (Section 5.3; Barnicoat et al., 1991; Nemchin et al., 1994; Mueller et al., 2004; Brown and Johnson, 2018), indicating high heat flow at this time. Therefore, the garnet geochronology and *P–T* estimates are generally compatible with metamorphism generated through a plume-driven tectonic model.

5.4 Apparent Thermal Gradient and Tectonic Implications

Apparent thermal gradients derived from metamorphic rocks provide important constraints on the geodynamic processes in the modern and early Earth (Brown and Johnson, 2018). For example, high pressures and low temperatures together are a signature of subduction on modern earth whereas low temperatures or high pressures alone can occur in many

geodynamic environments. Brown and Johnson (2018) categorize metamorphism into three groups including low d*T*/d*P* metamorphism, intermediate d*T*/d*P* metamorphism, and high d*T*/d*P* – these regimes are inferred to represent different geodynamic processes. The compilation of Brown and Johnson (2018) along with *P–T* data from this thesis are plotted in Figure 5.3. Note that Brown and Johnson (2018) summarized the *P/T* values from individual locations around the world as single points calculated from the temperature of peak metamorphism and the pressure at this temperature. In reality, uncertainties exist when estimating peak metamorphic conditions which are typically presented as a range (e.g. 2–4 kbar) and will therefore also give a range of calculated apparent thermal gradients (Fig. 5.3).

The apparent thermal gradient of the Mougooderra Formation was calculated at a temperature of 570°C over a range of pressures from 2.5 to 3.3 kbar and has an apparent thermal gradient ranging between 1727 and 2280 °C/GPa. The apparent thermal gradient of the underlying greenstone material was calculated at a temperature of 650°C over a pressure range of 4 to 7 kbar and has an apparent thermal gradient ranging from 928 to 1625°C/GPa. These values are among the highest recorded at this time in the Neoarchean. A similar gradient was inferred from rocks in the Southern Cross Domain to the east of the study area (Fig. 1.1), which has similar peak *P–T* conditions to that of the Mougooderra Formation (Mueller et al., 2004). Estimated temperatures for rocks in the Southern Cross Domain range between ~520 and 590°C with pressures ranging between 2.9 and 4.2 kbar and an apparent thermal gradient of 1685°C/GPa at 590°C and 3.5kbar (Mueller et al., 2004). These calculated apparent thermal gradients are also within range of two other locations within the southwestern Yilgarn Craton (Barnicoat et al., 1991; Nemchin et al., 1994), both of which have apparent thermal gradients near 1250°C/GPa.

The *P–T* conditions and apparent thermal gradient obtained for the Mougooderra Formation and underlying rocks coupled with the slow cooling rate inferred from the garnet geochronology indicate the presence of a large and long-lived heat source within this region of the Murchison Domain. Heating due to thickening of the crust is ruled out as the pressure conditions recorded by these rocks was not high enough to allow for heating associated with overthickened crust to occur (e.g. England and Thompson, 1984). Extrapolating along the apparent thermal gradients recorded by the Mougooderra samples, temperatures of 1000°C and greater would be reached at pressures of <10kbar. At these *P–T* conditions these rocks would be near the liquidus for most crustal rocks (e.g. Gerya et al., 2008) and unable to support a stable continental crust. Possible heat sources within the Yilgarn Craton at this time include the presence of a large mid-crustal intrusive body or from the heat associated with the mantle in an environment with thin continental lithosphere. As mentioned above, coupled garnet Lu-Hf geochronology indicates that metamorphism of the Mougooderra Formation and underlying greenstone material began prior to the emplacement of any nearby granitoids, suggesting that metamorphism of these rocks was not the result of contact metamorphism with the known granitic rocks from the area. The *P–T* conditions and apparent thermal gradient, therefore, likely indicate a metamorphic event in a tectonic environment with a thin continental lithosphere and high heat flow, while the large age difference between Lu-Hf and Sm-Nd systems is due to very slow cooling rates. An environment with a thin continental lithosphere is supported by the presence of komatiitic basalt of the Glen Group and ultramafic-mafic intrusions of the Yalgowra Suite that were emplaced from 2735 to 2711 Ma (Ivanic et al., 2012).

In summary, the *P–T* conditions and apparent thermal gradient of the Mougooderra Formation and underlying greenstone material suggests metamorphism occurred in an

environment with a thin continental lithosphere and high heat flow from the mantle. This may have been the result of mantle plume interaction, residue delamination (Van Kranendonk et al., 2013), or mantle overturn cycles (Bédard, 2018). It remains unclear if this event is the result of mechanisms often associated with horizontal plate tectonics or if it is the result of vertical tectonics and crustal instabilities. However, as Bédard (2018) suggests, vertical and horizontal movements of the crust within the Archean were likely accommodated by the same process.

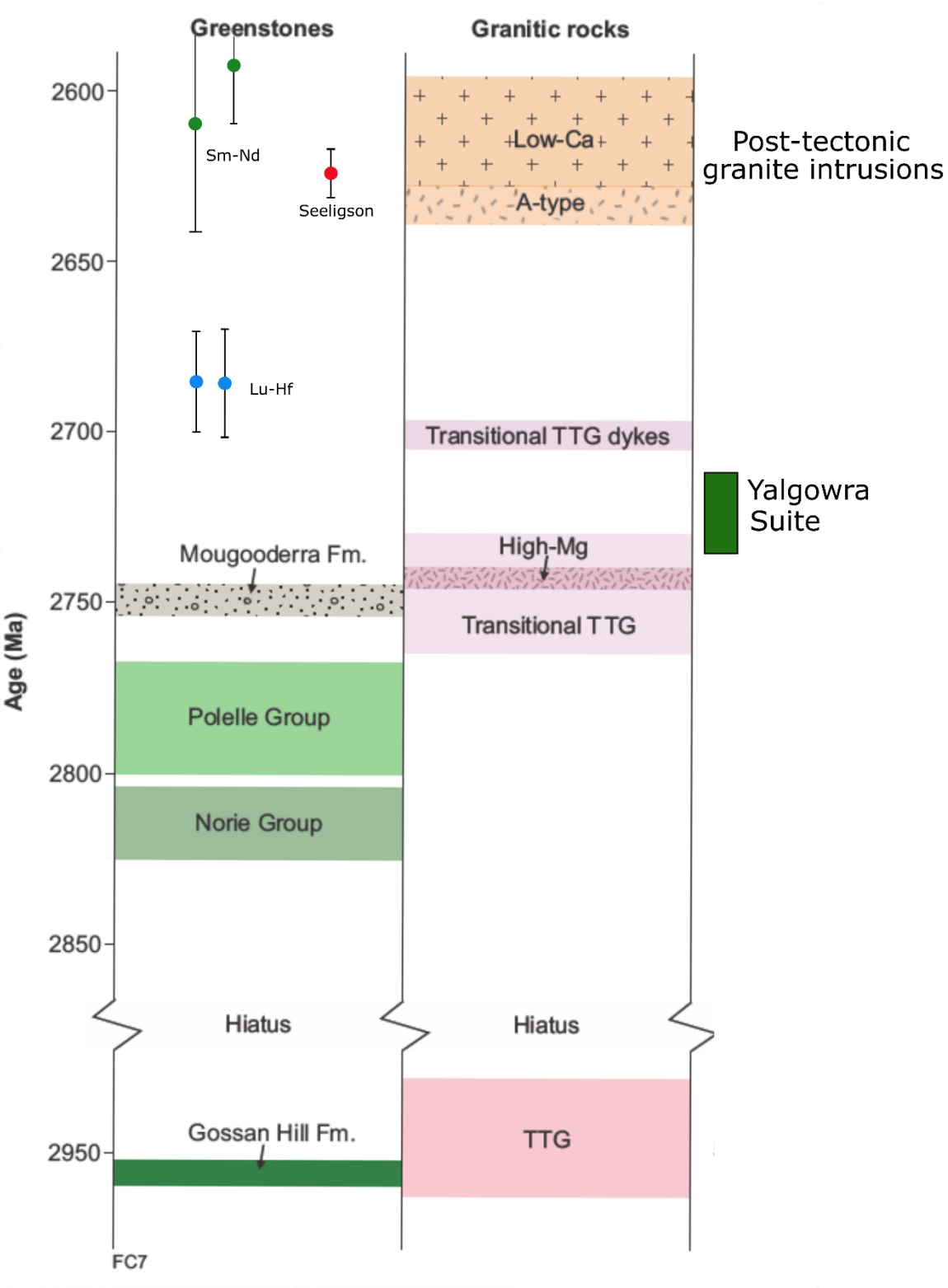

Figure 5.1. Timing of greenstone formation and emplacement of granitic intrusions compared to timing of metamorphism (modified from Clos et al. 2018).

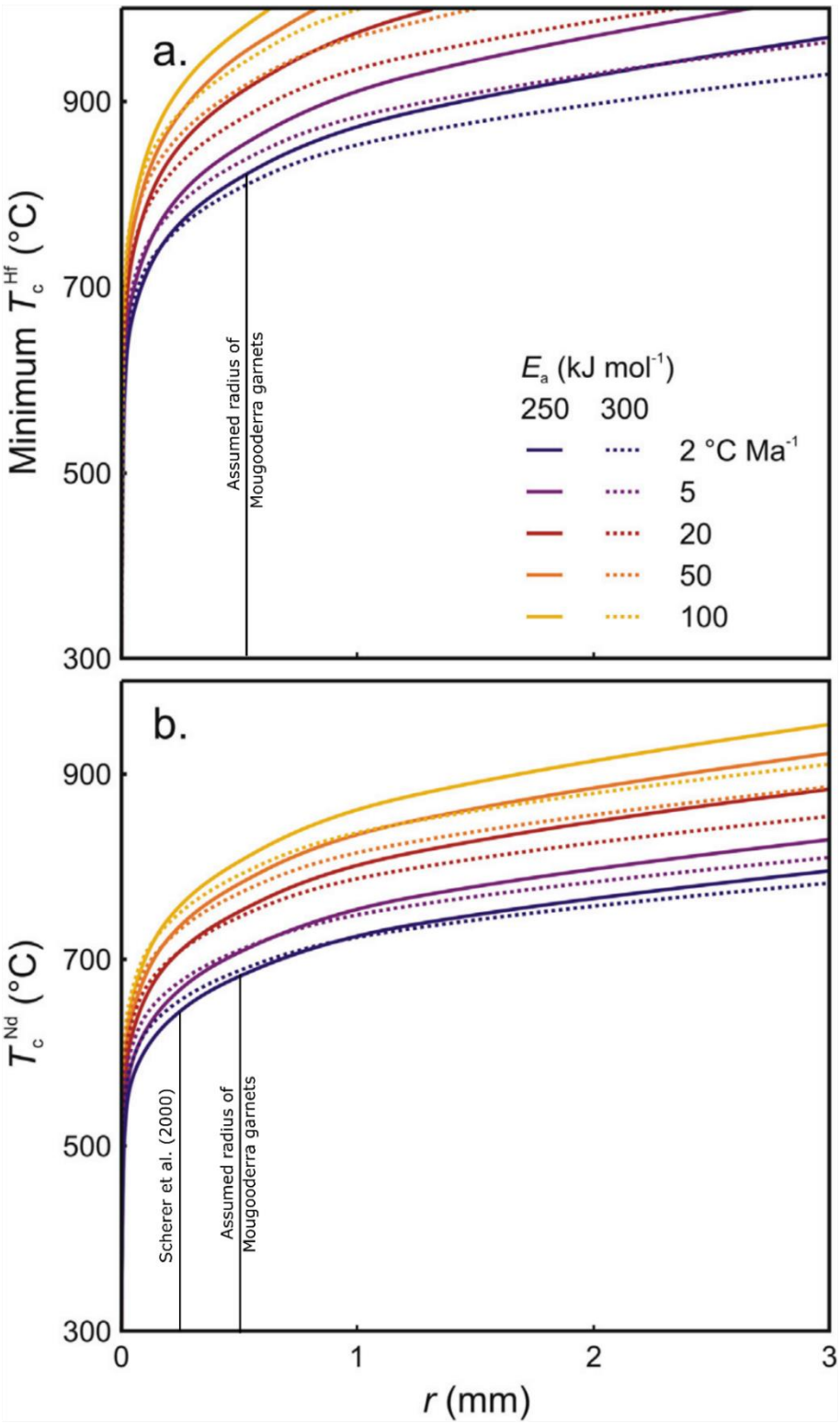

Figure 5.2. Closure temperatures for the Lu-Hf (a) and Sm-Nd (b) systems dependent on activation energy, cooling rate, and radii of a garnet (modified from Smit et al. 2013). The estimated closure temperatures for the garnet grains of Scherer et al. (2000) are also considered in (b).

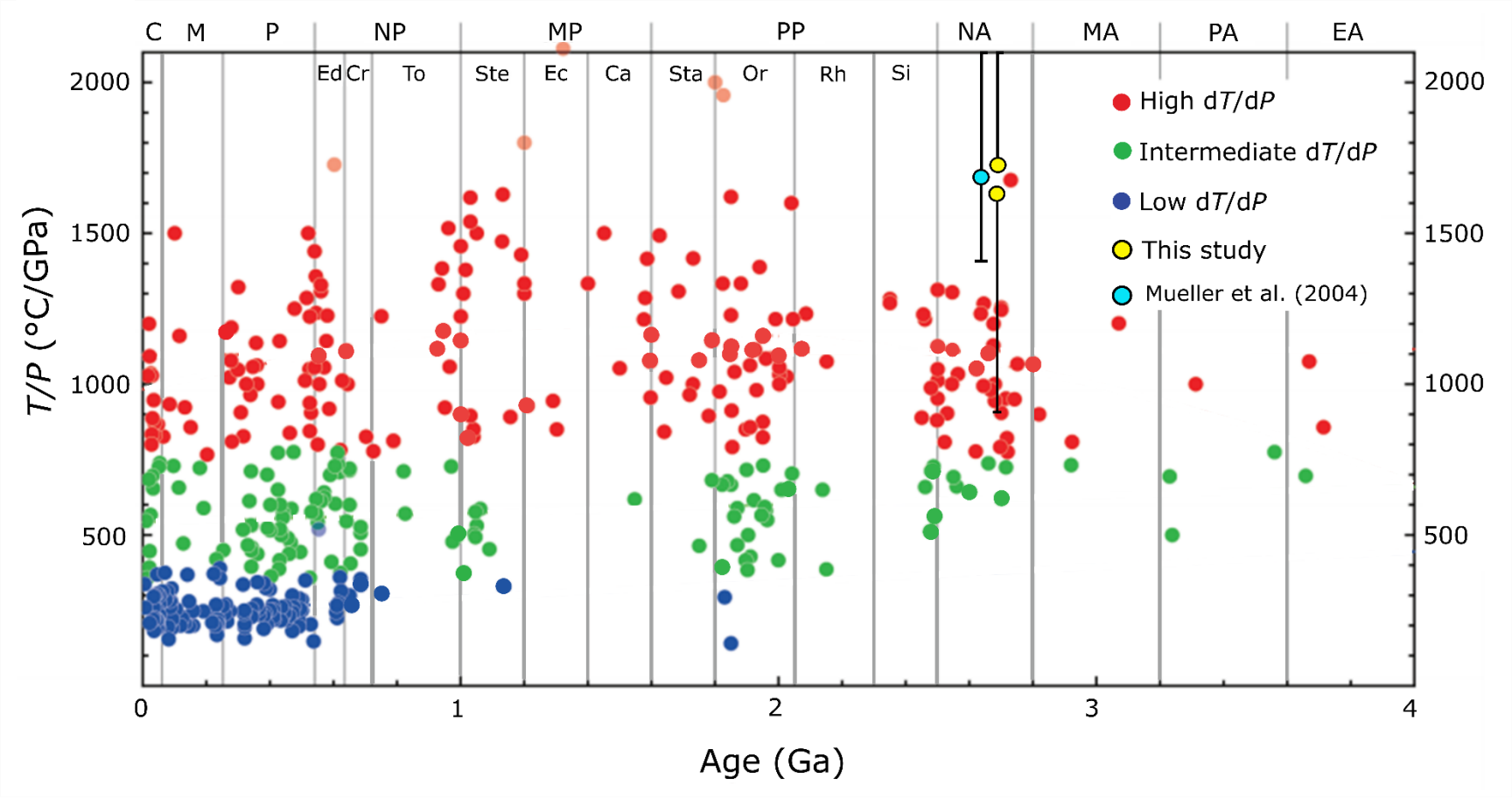

Figure 5.3. Apparent thermal gradients calculated for this study compared to apparent thermal gradients from various geological environments around the world (modified from Brown and Johnson, 2018). The abbreviations at the top of the page represent different eras and periods throughout time.

Chapter 6: Conclusions

6.1 Summary and Conclusions

The Mougooderra Formation is one of several large sedimentary sequences within the Youanmi Terrane, and until recently has received very little attention since the 1990s (Watkins and Hickman, 1990; Zibra et al., 2018). The purpose of this thesis was to investigate the metamorphic history of the Mougooderra Formation through the characterization of the metamorphic mineral assemblages, determination of *P–T* conditions, determination of the timing of metamorphism, and to use those objectives to give insights about the geological environment of this region during the time of metamorphism.

The characterization of the metamorphic mineral assemblages of the rocks from the Mougooderra Formation and underlying greenstone material of the Polelle Group was completed using whole rock geochemistry, identification of mineral assemblages using both petrographic and SEM work, and the determination of mineral compositions for major metamorphic minerals using EPMA (Sections 3.1-3.4). The Mougooderra Formation was found to have a variety of metamorphic mineral assemblages depending on the bulk composition of the sample. Rocks from this Formation were separated into several groups based on variations in major element geochemistry and includes the high Fe-Mg group, the high Al group, and the average pelitic group. Despite the variation in bulk composition and metamorphic mineral assemblages, it was shown that each group likely formed under similar pressure and temperature conditions (Fig 4.8). In addition to the results obtained from this work, garnet-biotite thermobarometry and phase equilibrium modelling (Section 4.1-4.2) allowed the conditions of metamorphism within the Mougooderra and Polelle Group to be constrained. The presence of metamorphic minerals such as garnet, cordierite, and grunerite indicate that the Mougooderra Formation experienced

relatively high-*T* low-*P* metamorphism. Peak metamorphic temperatures of the Mougooderra Formation were estimated to range between 550 and 570°C and a pressure range of 2.5 to 3.3 kbar. Select samples from underlying greenstone units were also considered in this study. These samples fall within the high Fe-Mg group and gave pressure estimates of 4 to 7.2 kbar and temperature conditions of 610°C and 650°C. Phase equilibrium modelling was also used to demonstrate that Fe_2O_3 values obtained through titration methods are slightly overestimated for some rocks within the region (Fig. 4.1). This overestimation of ferric iron is likely the result of the long exposure of these rocks at the Earth's surface in an oxidizing environment.

The timing of metamorphism was constrained using coupled garnet Lu-Hf and Sm-Nd for one sample from the Mougooderra Formation and one sample from the underlying greenstone unit. Both samples returned similar results with Lu-Hf ages of 2686±18 Ma and 2685±15 Ma, whereas the Sm-Nd system returned ages of 2611±35 Ma and 2590±21 Ma. These dates have been found to be considerably different than the ages of nearby granitoids and have been interpreted to represent the timing of regional metamorphism in a slowly cooling terrane.

These results were used in combination with apparent thermal gradients (Section 5.3) to show that the Mougooderra Formation and underlying greenstone unit has similar *P–T* conditions and apparent thermal gradients as other locations within the Yilgarn Craton (Fig 5.3). The work from this thesis suggests that at the time of metamorphism this region of the Murchison Domain experienced high heat flow as a result of a thin continental lithosphere and crust-mantle interactions. This geological environment may have been the result of extension and mantle upwelling, delamination of underplated basaltic crust (van Kranendonk et al., 2013), or a mantle overturn event (Bédard, 2018).

6.2 Future Studies

Until recently many studies within the Murchison Domain have focused on the understanding of geochemical evolution of the granitic intrusions and the structures and stratigraphy of greenstone sequences. Recommendations for future studies include:

(1) Further constraints on the timing of metamorphic events using other isotope systems. Given that the interpretation of a regional metamorphic event in this study is based on coupled garnet Lu-Hf and Sm-Nd ages that do not overlap with any significant geological event observed in the Murchison Domain, it is recommended that these dates be confirmed in future studies, possibly through U–Pb geochronology of accessory minerals.

(2) It is also recommended that detrital zircon work be completed on the Mougooderra Formation in the Ninghan area to compliment the detrital zircon work completed for this formation in the Yalgoo Dome area to assess lateral variations in sediment provenance.

(3) Constraints on *P–T* conditions within the Murchison Domain are limited, it is recommended that future studies should continue to focus on the characterization of metamorphic mineral assemblages and constraining *P–T* conditions when appropriate low variance mineral assemblages are available. This work may focus on overlying cover sequences such as the Mougooderra Formation, but it is also recommended that future studies continue to investigate the metamorphic conditions of underlying greenstone material. The conclusions of this study are based on only a few *P–T* constraints, a larger dataset of *P–T* conditions may be incorporated with other structural, geochemical, isotope, and sedimentary studies to give a better understanding of the geological history of the Murchison Domain.

References

Abbott, D. H., Mooney, W. D., Van Tongeren, J. A. 2013. The character of the Moho and lower crust within Archean cratons and the tectonic implications. Tectonophysics, **609**: 690-705.

Anhaeusser, C. R. 2014. Archean greenstone belts and associated granitic rocks- A review. Journal of African Earth Sciences, **100**: 684-732.

Barley, M.E., Brown, S.J.A., Krapez, B., Kositcin, N. 2008. Physical volcanology and geochemistry of a Late Archaean volcanic arc: Kurnalpi and Gindalbie Terranes, Eastern Goldfields Superterrane, Western Australia. Precambrian Research, **161**: 53–76.

Barnicoat, A. C., Fare, R. J., and Groves, D. I. 1991. Synmetamorphic lode-gold deposits in high-grade Archean settings. Geology, **19**: 921-924.

Baxter, E. F., Caddick, M. J., and Dragovie, B. 2017. Garnet: A Rock-Forming Mineral Petrochronometer. Reviews in Mineralogy & Geochemistry, **83**: 469-533.

Baxter, E. F., and Scherer, E. E. 2013. Garnet Geochronology: Timekeeper of Tectonometamorphic Processes. Elements, **9**: 433-438.

Bédard, J. H. 2018. Stagnant lids and mantle overturns: Implications for Archean tectonics, magmagenesis, crustal growth mantle evolution, and the start of plate tectonics. Geoscience Frontiers, **9**: 19-49.

Bhattacharya, A., Mohanty, L., Maji, A., and Raith, M. 1992. Non-ideal mixing in the phlohopite-annite binary: constraints from experimental data on Mg-Fe partitioning and a reformulation of the biotite-garnet geothermometer. Contributions to Mineralogy and Petrology, **111**: 87-93.

Boger, S.D., White, R.W. and Schulte, B. 2012. The importance of iron speciation (Fe+ 2/Fe+ 3) in determining mineral assemblages: an example from the high-grade aluminous metapelites of southeastern Madagascar. Journal of Metamorphic Geology, **30**(9): 997-1018.

Bouvier, A., Vervoort, J. D. and Patchett, P. J. 2008. The Lu-Hf and Sm-Nd isotopic composition of CHUR: constraints from unequilibrated chondrites and implications for the bulk composition of terrestrial planets. Earth and Planetary Science Letters, **273**: 48-57.

Bouvier, A., Blichert-Toft, J., Boyet, M. and Albarède, F. 2015. 147Sm-143Nd and 176Lu-176Hf systematics of eucrite and angrite meteorites. Meteoritics & Planetary Science, **50**(11): 1896-1911.

Brown, M., and Johnson, T. E. 2018. Secular change in metamorphism and the onset of global plate tectonics. American Mineralogist, **103**(2): 181-196.

Burton, K. W., Kohn, M. J., Cohen, A. S., and O'Nions, R. K. 1995. The relative diffusion of Pb, Nd, Sr and O in garnet. Earth and Planetary Science Letters, **133**: 199-211.

Calvert, A. J. and Doublier, M. P. 2018. Archean continental spreading inferred from seismic images of the Yilgarn Craton. Nature Geoscience, **11**: 526-530.

Cassidy, K.F., Champion, D.C., Krapeˇz, B., Barley, M.E., Brown, S.J.A., Blewett, R.S., Groenewald P.B., Tyler, I.M., 2006. A revised geological framework for the Yilgarn Craton, Western Australia. Western Australia Geological Survey, Record 2006/8, 8 pp.

Champion, D. C., Cassidy, K. F. 2007. An overview of the Yilgarn Craton and its crustal evolution (in Bierlein, F.P., Know-Robinson, C. M., (Eds), 2007. Proceeding of Geoconferences (WA) Inc. Kalgoorlite 07' Conference. Geoscience Australia Record 2007/ 14), p. 13-35.

Chen, S. F., Riganti, A., Wyche, S., Greenfield, J. E., and Nelson, D. R. 2003. Lithostratigraphy and tectonic evolution of contrasting greenstone successions in the central Yilgarn Craton, Western Australia. Precambrian Research, 127: 249-266.

Clos, F., Weinberg, R., and Zibra, I. 2018. Building the Archean continental crust: 300 Ma of felsic magmatism in the Yalgoo Dome (Yilgarn Craton); Geological Report 186: Geological Survey of Western Australia.

Coggon, R., and Holland, T.J.B. 2002. Mixing properties of phengitic micas and revised garnet-phengite thermobarometers. Journal of Metamorphic Geology, **20**: 683-696.

Cohen, A. S., O'Nions, R. K., Siegenthaler, R., and Griffin, W. L. 1988. Chronology and the pressure-temperature history recorded by a granulite terrane. Contributions to Mineralogy and Petrology: **98**, 303-311.

Compston, W. and Pidgeon, R. T. 1986. Jack Hills, evidence of more very old detrital zircons in Western Australia. Nature, **321**: 766-769.

Dasgupta, S., Sengupta, P., Guha, D., and Fukuoka, M. 1991. A refined garnet-biotite Fe-Mg exchange geothermometer and its application in amphibolites and granulites. Contributions to Mineralogy and Petrology, **109**: 130-137.

Diener, J.F.A., Powell, R., White, R.W., and Holland, T.J.B. 2007. A new thermo-dynamic model for clino- and orthoamphiboles in Na2O-CaO-FeO-MgO-Al2O3-SiO2-H2O-O. Journal of Metamorphic Geology, **25**: 631-656.

Diener, J. F. A., and Powell, R. 2010. Influence of ferric iron on the stability of mineral assemblages. Journal of Metamorphic Geology, **28**: 599-613.

Dutch, R. H., and Hand, M. 2009. Retention of Sm–Nd isotopic ages in garnets subjected to high-grade thermal reworking: Implications for diffusion rates of major and rare earth elements and the Sm–Nd closure temperature in garnet. Contributions to Mineralogy and Petrology, **159**: 93-112.

England, P. C., Thompson, A. B. 1984. Pressure-Temperature-Time Paths of Regional Metamorphism I. Heat Transfer during the Evolution of Regions of Thickened Continental Crust. Journal of Petrology, **25**: 894-928.

Ferry, J.M., and Spear, F.S. 1978. Experimental Calibration of the Partitioning of Fe and Mg Between Biotite and Garnet. Contributions to Mineralogy and Petrology, **66**: 113-117.

Fletcher, I.R., and McNaughton, N.J. 2002. Granitoid geochronology: SHRIMP zircon and titanite data, *in* The characterisation and Metallogenic Significance of Archaean Granitoids of the Yilgarn Craton, Western Australia *edited by* KF Cassidy, DC Champion, NJ McNaughton, IR Fletcher, AJ Whitaker, IV Bastrakova and A Budd: Minerals and Energy Research Institute of Western Australia (MERIWA), Project no. M281/AMIRA Project no. 482 (unpublished report no. 222), p. 1–156.

Ganguly, M., Tirone, M., and Hervig, R. 1998. Diffusion kinetics of Samarium and Neodymium in garnet, and a method for determining cooling rates of rocks. Science, **281**: 805-807.

Gerya, T. V., Perchuk, L. L., and Burg, J. P. 2008. Transient hot channels: perpetrating and regurgitating ultrahigh-pressure, high-temperature crust-mantle associations in collision belts. Lithos, **103**: 236-256.

Hensen, B. J., and Zhou, B. 1995. Retention of isotopic memory in garnets partially broken down during an overprinting granulite facies metamorphism: Implications for the Sm–Nd closure temperature. Geology, **23**: 225-228.

Holdaway, M.J. 2000. Application of new experimental and garnet Margules data to the garnet-biotite geothermometer. American Mineralogist, **86**: 1117-1129.

Holdaway, M.J., and Lee, S.M. 1977. Fe-Mg Cordierite stability in High-Grade Pelitic Rocks Based on Experimental, Theoretical, and, Natural Observations. Contributions to Mineralogy and Petrology, **63**: 175-198.

Holland, T.J.B., and Powell, R. 1998. An internally consistent thermodynamic dataset for phases of petrological interest. Journal of Metamorphic Geology: **16**, 309-343.

Holland, T.J.B., and Powell, R. 2003. Activity-composition relations for phases in petrological calculations: an asymmetric multicomponent formulation. Contributions to Mineralogy and Petrology, **145**: 492-501.

Humphries, F. J., and Cliff, R. A. 1982. Sm-Nd dating and cooling of Scourian granulites, Sutherland. Nature: **285**, 515-517.

Ivanic, T. J., Wingate, M. T. D., Kirkland, C. L., Van Kranendonk, M. J., and Wyche, S. 2010. Age and significance of voluminous mafic-ultramafic magmatic events in the Murchison Domain, Yilgarn Craton. Australian Journal of Earth Sciences, **57**: 597-614.

Ivanic, T. J., Van Kranendonk, M. J., Kirkland, C. L., Wyche, S., Wingate, M. T. D., and Belousova, E. A. 2012. Zircon Lu-Hf isotopes and granite geochemistry of the Murchison Domain of the Yilgarn Craton: Evidence for reworking of Eoarchean crust during Meso-Neoarchean plume-driven magmatism. Lithos, **148**: 112-127.

Ivanic, T. J. 2018. Ninghan, WA Sheet 2339: Geological Survey of Western Australia, 1:100 000 Geological Series.

Jagoutz, E. 1988. Nd and Sr systematic in an eclogite xenolith from Tanzania: Evidence for frozen mineral equilibria in the continental lithosphere. Geochimica et Cosmochimica Acta, **52**: 1285-1293.

Jamieson, R. A., Hart, G. G., Chapman, G. G., and Tobey, N. W. 2012. The contact aureole of the South Mountain Batholith in Halifax, Nova Scotia: geology, mineral assemblages, and isograds. Canadian Journal of Earth Science, **49**: 1280-1296.

Jochum, K, P., Weis, U., Schwager, B., Stoll, B., Wilson, S. A., Haug, G, H., Andreae, M, O., and Enzweiler, J. 2016. Reference Values Following ISO Guidelines for Frequently Requested Rock Reference Material. Geostandards and Geoanalytical Research, **40**: 333-350.

Krapez, B., and Barley, M.E. 2008. Late Archaean synorogenic basins of the Eastern Gold-fields Superterrane, Yilgarn Craton, Western Australia. Part III: Signatures of tectonic escape in an arc-continent collision zone. Precambrian Research: **161**, 183–199.

Lin, S., Parks, J., Heaman, L.M., Simonetti, A., and Corkery, M.T. 2013. Diapirism and sagduction as a mechanism for deposition and burial of "Timiskaming-type" sedimentary sequences, Superior Province: Evidence from detrital zircon geochronology and implications for the Borden Lake conglomerate in the exposed middle to lower crust in the Kapuskasing uplift. Precambrian Research, **238**: 148-157.

Ludwig, K. R. 2011. Isoplot/Ex version 4.14. A Geochronological Toolkit for Microsoft Excel., Berkeley Geochronology Center.

Mezger, K., Essene, E. J., and Halliday, A. N. 1992. Closure temperatures of the Sm-Nd system in metamorphic garnets. Earth and Planetary Science Letters, **113**: 391-409.

Mueller, A.G., Nemchin, A.A., Frei, R. 2004. The Nevoria Gold Skarn Deposit, Southern Cross Greenstone Belt, Western Australia: II. Pressure-Temperature-Time Path and Relationship to Postorogenic Granites. Economic Geology: **99**, 453-478.

Myers, J. S. 1993. Precambrian history of the West Australian Craton and adjacent orogens. Annual Review of Earth and Planetary Science, 21: 453-485.

Myers, J. S. 1995. The generation and assembly of an Archean supercontinent evidence from the Yilgarn craton, Western Australia: In: Coward, M. P., Reis, A. C. (Eds), Early Precambrian Processes, vol. 95. Geological Society of London, Special Publication, p. 143-154.

Nabelek, P. I., Hofmeister, A. M. and Whittington, A. G. 2012. The influence of temperature-dependent thermal diffusivity on the conductive cooling rates of plutons and temperature-time paths in contact aureoles. Earth and Planetary Science Letters, 317: 157-164.

Nelson, D. R., Robinson, B. W., and Myers, J. S. 2000. Complex geological histories extending for >4.0 Ga deciphered from xenocryst zircon microstructures. Earth and Planetary Science Letters, 181: 89-102.

Nemchin, A. A., Pidgeon, R. T., and Wilde, S. A. 1994. Timing of Late Archean granulite facies metamorphism in the southwestern Yilgarn Craton of Western Australia: evidence from U-Pb ages of zircon from mafic granulites. Precambrian Research, **69**: 307-321.

Owada, M., Osanai, Y., Nakano, N., Adachi, T., Kitano, I., Van Tri, T., and Kagami, H. 2016. Late Permian plume-related magmatism and tectonothermal events in the Kontum Massif, central Vietnam. Journal of Mineralogical and Petrological Sciences, **111**: 181-195.

Palin, R. M., Weller, O. M., Waters, D. J., and Dyck, B. 2016. Quantifying geological uncertainty in metamorphic phase equilibria modelling; a Monte Carlo assessment and implications for tectonic interpretations. Geoscience Frontiers, **7**(4): 591-607.

Paton, C., Hellstrom, J., Paul, B., Woodhead, J., and Hergt, J. 2011. Iolite: Freeware for the visualisation and processing of mass spectrometric data. Journal of Analytical Atomic Spectrometry, **26**: 2508-2518.

Pattison, D. R. M. and Vogl, J. J. 2005. Contrasting sequences of metapelitic mineral-assemblages in the aureole of the tilted Nelson Batholith, British Columbia: implications for phase equilibria and pressure determination in andalusite-sillimanite type settings. Canadian Mineralogist, **43**: 51-88.

Perchuk, L. L., and Lavrent'eva. 1983. Experimental investigation of exchange equilibria in the system cordierite-garnet-biotite. in Saxena, S.K., Ed., Kinetics and Equilibrium in Mineral Reactions, Advances in Physical Geochemistry: **3**, 199-239.

Pollington, A. D., and Baxter, E. F. 2011. High precision microsampling and preparation of zoned garnet porphyroblasts for Sm–Nd geochronology. Chemical Geology, **281**: 270-282.

Powell, R. & Holland, T. J. B. 1988. An internally consistent dataset with uncertainties and correlations: 3. Applications to geobarometry, worked examples and a computer program. Journal of Metamorphic Geology, **6**: 173–204.

Powell, R. and Holland, T.J.B. 2008. On thermobarometry. Journal of Metamorphic Geology, **26**(2): 155-179.

Scherer, E.E., Münker, C., Mezger, K. 2001. Calibration of the lutetium–hafnium clock. Science **295**: 683–686.

Skora, S., Lapen, T. J., Baumgartner, L. P., Johnson, C. M., Hellebrand, E., and Mahlen, N. J. 2008. The duration of prograde garnet crystallization in the UHP eclogites at Lago di Cignana, Italy. Earth and Planetary Science letters, **287**: 402-411.

Shaw. D.M. 1956. Geochemistry of Pelitic Rocks Part III: Major Elements and General Geochemistry. Bulletin of the Geological Society of America, **67**: 919-934.

Smit, M. A., Scherer, E. E., and Mezger, K. 2013. Lu-Hf and Sm-Nd garnet geochronology: Chronometric closure and implications for dating petrological processes. Earth and Planetary Science Letters, **381**: 222-233.

Standing, J.G. 2008. Terrane amalgamation in the Eastern Goldfields Superterrane, Yilgarn Craton: evidence from tectonostratigraphic studies of the Laverton Greenstone Belt. Precambrian Research, **161**: 114–134

Symmes, G. H., and Ferry, J. M. 1995. Metamorphism, Fluid Flow and Partial Metling in Pelitic Rocks from the Onawa Contact Aureole, Central Maine, USA. Journal of Petrology, **36**: 587-612.

Thompson, A.B. 1975. Mineral reactions in pelitic rocks: II. Calculation of some P--T--X(Fe--Mg) phase relations. American Journal of Science, **276**: 425-454.

Van Kranendonk, M.J., & Ivanic, T.J. 2009. A new lithostratigraphic scheme for the northeastern Murchison Domain, Yilgarn Craton: Geological Survey of Western Australia, Annual Review 2007-2008, p 34-53.

Van Kranendonk, M. J., Ivanic, T. J., Wingate, M.T. D., Kirkland, C. L., and Wyche. S. 2013. Long-lived, autochthonous development of the Archean Murchison Domain, and implications for the Yilgarn Craton tectonics. Precambrian Research, 229: 49- 92.

Vervoort, J. D., Patchett, P. J., Söderlund, U. and Baker, M. 2004. Isotopic composition of Yb and the determination of Lu concentrations and Lu/Hf ratios by isotope dilution using MC-ICPMS. Geochemistry, Geophysics, Geosystems, **5**: doi:10.1029/2004GC000721.

Wang, Q. 1998. Geochronology of the granite-greenstone terranes in the Murchison and Southern Cross Provinces of the Yilgarn Craton, Western Australia: Australia National University, Canaberra, Australia, Ph.D. thesis, 186p.

Watkins, K.P., & Hickman, A.H. 1990. Geological Evolution and Mineralization of the Murchison Province Western Australia: Geological Survey of Western Australia, Bulletin 137.

Webb G., Powell, R. and McLaren, S. 2015. Phase equilibria constraints on the melt fertility of crustal rocks: The effect of subsolidus water loss. Journal of Metamorphic geology, **33**(2): 147-165.

Weis, D., Kieffer, B., Hanano, D., Nobre Silva, I., Barling, J., Pretorius, W., Maerschalk, C. and Mattielli, N. 2007. Hf isotope compositions of U.S. Geological Survey reference materials. Geochemistry, Geophysics, Geosystems, **8**(6): Q06006.

White, R.W., Pomroy, N.E. and Powell, R. 2005. An in-situ metatexite-diatexite transition in upper amphibolite facies rocks from Broken Hill, Australia. Journal of Metamorphic Geology, **23**: 579-602.

White, R.W., Powell, R., Holland, T.J.B., & Worley, B.A. 2000. The effect of TiO2 and Fe2O3 on metapelitic assemblages at greenschist and amphibolite facies conditions: mineral equilibria calculations in the system K2O-FeO-MgO-Al2O3-SiO2-H2O-TiO2-Fe2O3. Journal of Metamorphic Geology, **18**: 497-511.

White, R.W., Powell, R., and Holland, T.J.B. 2007. Progress relating to calculation of partial melting equilibria for metapelites. Journal of Metamorphic Geology, **25**: 511-527.

Wilde, S. A., Middleton, M, F., Evans, B. J. 1996. Terrane accretion in the southwestern Yilgarn Craton: evidence from a deep seismic crustal profile. Precambrian Research, 78: 179-196.

Wingate, M.T.D., Kirkland, C.L., and Ivanic, T.J. 2014. 207630: porphyritic monzogranite, Garden Pool Well; Geochronology Record 1215: Geological Survey of Western Australia, p.4.

Wingate, M.T.D., Lu, Y., and Ivanic, T.J. 2018. 207628: altered metamonzogranite, Mulgine Hill; Geochronology Record 1460: Geological Survey of Western Australia, p.4.

Wu, C. 2017. Calibration of the garnet-biotite-Al_2SiO_5-quartz geobarometer for metapelites. Journal of Metamorphic geology, **35**: 983-998.

Wyman, D. 2018. Do Cratons preserve evidence of stagnant lid tectonics? Geoscience Frontiers, **9**: 3-17.

Yeats, C. J., McNaughton, N. J., and Groves, D. I. 1996. SHRIMP U-Pb geochronological constraints on Archean volcanic-hosted massive sulphide and lode gold mineralization at Mount Gibson, Yilgarn Craton, Western Australia. Economic Geology, 91: 1354- 1371.

Zibra, I., Clos, F., Weinberg, R. F., and Peternell, M. 2017a. The ~2730 Ma onset of the Neoarchean Yilgarn Orogeny. AGU Tectonics, **36**: 1787-1813.

Zibra, I., Korhonen, F. J., Peternell, M., Weinberg, R. F., Romano, S. S., Braga, R., De Paoli, M. C., and Roberts, M. 2017b. On thrusting, regional unconformaties and exhumation of high-grade greenstones in Neoarchean orogens. The case of the Waroonga Shear Zone, Yilgarn Craton. Tectonophysics, **712**: 362-365.

Zibra, I., Peternell, M., Schiller, M., Wingate, M. T. D., Lu, Y., and Clos, F. 2018. Tectono-magmatic evolution of the Neoarchean Yalgoo Dome (Yilgarn Craton): Diapirism in a pre-orogenic setting; Geological Report 176: Geological Survey of Western Australia.

Zirakparvar, N. A., Vervoort, J. D., McClelland, W. and Lewis, R. S. 2010. Insights into the metamorphic evolution of the Belt–Purcell basin; evidence from Lu–Hf garnet geochronology. Canadian Journal of Earth Sciences, **47**(2): 161-179.

Appendix A: Sample Information

Table A1.1. Sample information (GDA94, MDA zone 50).

Sample	Easting	Northing	Thin Section	Whole rock geochemistry
207602	507755	6780386	Y	Y
207691	500197	6801963	Y	Y
207697	500197	6801963	Y	N
207692	516595	6756846	Y	Y
207694	516888	6756813	Y	Y
207695	517089	6757120	Y	Y
211117	512517	6744201	Y	Y
211116	512517	6744201	Y	Y
207689	497923	6771884	Y	N
207690	500499	6772698	Y	Y
207693	516664	6756852	Y	Y
207688	478026	6770990	Y	Y
207672	449809	6839648	Y	N
207676	446237	6839490	Y	N
229101	516597	6756844	Y	Y
229102	480180	6868911	Y	N
229103	480282	6868885	Y	N
229104	500315	6801970	N	N
229105	500197	6801963	Y	Y
229106	509123	6780266	Y	N
229107	509123	6780266	Y	N
229109	509658	6779783	Y	Y
229110	518345	6745826	Y	N
229111	516588	6756937	Y	Y
229112	516588	6756937	Y	N
229113	516648	6756904	Y	Y
229114	516834	6756895	Y	N
229115	516916	6756901	Y	Y
229116	516953	6756901	Y	N
229117	517089	6756978	Y	Y
229118	517049	6757076	N	N
229119	516597	6756844	Y	Y
229120	516597	6756844	Y	Y
229121	516957	6756784	N	N
229122	517268	6755655	N	N
229123	516969	6756597	N	N

Table A1.1. (continued)

Sample	Easting	Northing	Thin Section	Whole rock geochemistry
229124	516959	6756401	Y	Y
229125	517116	6756110	Y	N
229126	517268	6755655	Y	N
229127	518293	6751231	Y	Y
229128	518108	6751557	N	N
229129	518027	6751737	Y	N
229130	518043	6752074	Y	Y
229131	518149	6752002	Y	Y
229132	518076	6751728	Y	N
229133	512564	6744224	Y	N
229134	512564	6744224	Y	N
229135	512295	6744251	Y	Y
229136	512382	6744132	Y	Y
229137	509616	6779803	Y	N
229139	507755	6780386	Y	N
229140	518334	6745748	N	N
229141	518334	6745748	N	N
229142	518334	6745748	N	N
229143	518334	6745748	N	N
229144	518334	6745748	N	N
229145	525078	6782488	Y	Y
229146	501062	6772484	Y	Y
229147	501357	6772462	Y	Y
229148	497923	6771884	Y	Y
229149	497923	6771884	Y	Y
229150	497940	6771912	Y	N
229151	500499	6772698	Y	Y
229152	503577	6781411	Y	Y
229153	516946	6756330	Y	Y
229154	516888	6755993	N	N
229155	516996	6755779	Y	N
229157	517216	6755692	Y	Y
229157B	517216	6755692	Y	Y

Appendix B: Whole-rock trace element geochemistry

Table B1.1. Trace element compositions for rocks of the Mougooderra Formation and select underlying greenstone material.

	Au	Pt	Pd	Ag	As	Ba	Be	Bi	Cd	Ce	Co	Cr	Cs	Cu
UNITS	ppb	ppb	ppb	ppm	ppm	ppm	ppm	ppm	ppm	ppm	ppm	ppm	ppm	ppm
DETECTION	1	1	1	0.1	0.2	0.5	0.2	0.02	0.1	0.02	0.1	1	0.01	2
METHOD	FA003	FA003	FA003	LA101	LA101	LA101	LA101	LA101	LA101	LA101	LA101	LA101	LA101	LA101
229101	1	2	2	<0.1	14	86.5	1.6	0.8	<0.1	39.5	17.7	210	0.95	6
229105	<1	<1	<1	0.2	4.4	82.5	4.8	0.46	0.3	139	0.6	8	0.28	6
229109	<1	7	5	<0.1	42	436	1.4	0.2	<0.1	10.2	8.5	511	3.22	30
229111	2	4	6	<0.1	37.8	468	3.2	0.34	0.2	43.6	50.3	505	6.76	<2
229113	5	9	28	<0.1	33.8	454	1.4	0.34	<0.1	26.8	78.2	849	5.47	44
229115	1	2	1	<0.1	18	305	1	0.24	0.1	28.9	18.4	247	3.1	<2
229117	7	3	4	<0.1	96.8	397	1.8	0.08	<0.1	75.6	33.3	355	1.62	<2
229119	2	5	6	0.2	35.6	343	2.2	0.24	0.1	33.9	39.7	448	4.98	22
229120	6	8	10	<0.1	38.4	438	3.4	0.2	0.4	36.2	43.8	537	6.07	<2
229124	3	5	11	<0.1	3.8	38.5	0.4	0.04	<0.1	8.52	35.6	528	0.25	<2
229127	3	6	8	<0.1	7.4	775	0.4	0.28	0.1	68.7	0.4	386	5.42	8
229130	1	7	11	<0.1	2	291	0.4	0.02	<0.1	24.1	20.4	498	3.86	36
229131	2	2	4	<0.1	10.8	362	0.6	<0.02	<0.1	31.1	11.9	214	64.5	<2
229135	2	8	4	0.1	7	1930	1.2	0.86	0.2	25.2	1.7	187	0.53	52
229136	2	1	2	<0.1	29.8	753	1	2.02	<0.1	34.5	4.5	243	5.74	56
229138	1	6	4	0.3	62.6	957	1.2	0.18	1.1	98.8	8.7	359	1.16	18
229146	2	4	5	<0.1	19.4	217	1.8	0.28	<0.1	47.8	12.6	230	5.62	188
229147	1	6	3	<0.1	36.8	359	1	0.1	<0.1	3.9	3.9	795	0.42	108
229149	1	6	4	<0.1	3.2	165	14.6	1.28	0.1	6.06	38	2160	74.4	60
229152	1	6	5	<0.1	100	363	1.6	0.74	<0.1	50	4.2	244	6.91	86
229157	3	5	10	0.2	9.8	216	0.8	0.24	0.2	43.1	15.5	335	7.51	46
229158	5	1	1	<0.1	2.2	220	1.2	0.12	<0.1	56	20	180	6.5	58

Table B1.1. (continued)

	Au	Pt	Pd	Ag	As	Ba	Be	Bi	Cd	Ce	Co	Cr	Cs	Cu
211117	<1	<1	<1	0.03	7.1	771.6	2.85	0.42	0.03	81.5	3.8	69	3.3	14.2
211116	<1	<1	<1	0.03	33.7	768.2	2.47	1.03	0.08	34.8	3.4	234	2.4	39.3
207695	<1	<1	<1	0.03	30.9	405.2	2.45	0.13	0.22	45.2	59.4	220	2.5	34.1
207694	<1	<1	<1	0.03	12	1386.3	1.07	0.13	0.04	10.8	20.4	292	2.3	47.7
207693	<1	<1	<1	0.03	1.2	173.7	0.21	0.15	0.07	8.3	64.5	278	0.6	23.7
207692	<1	<1	<1	0.02	98.3	379.1	2.24	0.43	0.29	40.7	59.8	536	6.3	7.5
207691	<1	<1	<1	0.02	4.1	35	0.52	0.11	-0.02	197.5	29.2	47	0.4	2.3
207690	<1	<1	<1	0.1	16.1	292.3	1.19	0.33	0.53	29.1	53.7	357	23.8	59.7
207602	<1	<1	<1	0.02	3.5	2719	0.98	0.43	0.05	33.5	8.1	156	2.7	4.7

Table B1.1. (continued)

	Dy	Er	Eu	Ga	Gd	Ge	Hf	Ho	In	La	Lu	Mn	Mo	Nb
UNITS	ppm	ppm	ppm	ppm	ppm	ppm	ppm	ppm	ppm	ppm	ppm	ppm	ppm	ppm
DETECTION	0.01	0.01	0.01	0.1	0.01	0.05	0.01	0.01	0.05	0.01	0.01	1	0.2	0.01
METHOD	LA101	LA101	LA101	LA101	LA101	LA101	LA101	LA101	LA101	LA101	LA101	LA101	LA101	LA101
229101	2.96	2.12	1.19	14.6	3.26	0.5	4.55	0.61	<0.05	20.2	0.3	1650	<0.2	6.6
229105	16.6	13.3	5.77	34.9	20.7	2.6	8.65	4.02	0.1	60.6	2.06	12	1	12.6
229109	1.67	1.21	0.58	20.6	1.15	9.4	3.09	0.36	0.15	19.2	0.18	98	2	5.2
229111	3.52	2.28	0.96	21.7	3.22	4.6	4.25	0.68	0.1	23.5	0.32	811	1.6	6.25
229113	4.88	3.04	1.05	25.1	3.74	7.6	3.18	1.14	0.1	14.3	0.48	470	0.6	4.37
229115	3.87	2.34	1.11	19.7	3.24	1.35	4.36	0.92	0.1	16.2	0.34	1860	0.4	6.96
229117	5.12	3.3	1.45	28.4	5.29	1.6	6.1	1.06	<0.05	40.2	0.46	870	1.6	11
229119	2.46	1.49	0.69	18.4	2.39	3.7	3.32	0.62	<0.05	19.3	0.24	641	1	4.74
229120	2.86	2.06	0.88	19.7	2.62	4.6	3.39	0.66	<0.05	20.7	0.27	764	1.2	5.38
229124	1.98	1.34	0.49	11.8	1.48	14.4	1.44	0.37	<0.05	2.97	0.19	1500	<0.2	2.06
229127	5.28	3.53	1.01	32.4	3.32	2.15	6.62	1.19	0.2	49.5	0.48	35	0.6	10.1
229130	3.07	2.4	1	23	3.09	2.55	2.52	0.7	0.1	11.9	0.32	1280	<0.2	4.57
229131	2.09	1.85	0.51	17.9	1.84	0.85	3.37	0.56	<0.05	15.6	0.23	342	<0.2	5.5
229135	1.86	1.05	0.51	18.4	1.5	1.95	3.44	0.35	0.45	28.3	0.16	43	3.4	5.94
229136	1.63	1.11	0.45	22.5	1.56	2.5	3.29	0.39	4.9	21	0.19	142	2.8	5.37
229138	6.13	3.7	1.91	31.1	6.22	1.75	6.59	1.28	0.1	54.5	0.48	56	1.6	12.6
229146	3.56	2.2	1.21	19.2	3.67	2.75	4.43	0.69	<0.05	28.3	0.31	225	3.8	9.7
229147	0.53	0.42	0.1	17.2	0.2	1.8	3.44	0.09	<0.05	1.98	0.07	57	39.6	7.8
229149	1.98	1.09	0.49	10.3	1.55	3.55	1	0.45	<0.05	4.29	0.17	1620	5.6	2.87
229152	2.22	1.24	0.61	21.5	1.95	2.65	3.3	0.4	0.15	34.6	0.19	25	6	7.08
229157	3.69	2.87	1.18	23.9	4.1	2.1	4.31	0.86	0.2	22	0.36	576	1.2	6.89
229158	4.44	2.9	1.04	25	4.61	2.4	4.87	0.89	0.1	29.4	0.38	614	0.8	8.25

Table B1.1. (continued)

	Dy	Er	Eu	Ga	Gd	Ge	Hf	Ho	In	La	Lu	Mn	Mo	Nb
211117	2.9	1.5	0.7	19	2.3	1.22	3.4	0.5	0.24	50	0.3	<1	2.3	13.1
211116	2.3	1.4	0.5	18.3	1.7	1.52	3.2	0.5	0.91	22.2	0.2	<1	2.5	6
207695	3	1.8	1	22.3	3.6	1.39	4.7	0.6	0.15	21.8	0.3	<1	1	7
207694	1.6	1	0.4	22.6	1.7	0.84	5.3	0.4	0.12	7.8	0.3	<1	0.7	9.4
207693	1.8	1	0.4	8.1	1.5	7.67	1	0.3	0.06	3.9	0.1	<1	0.2	1.5
207692	3.1	1.9	0.8	20.4	3.4	3.22	3.5	0.7	0.04	21.4	0.4	<1	1.7	5.3
207691	9.2	4.5	3.5	26.2	14.6	1.21	9.1	1.7	0.03	98.9	0.6	<1	0.5	10.8
207690	2.8	1.7	0.9	14.1	3	2.54	3.1	0.6	0.07	13.9	0.3	<1	12	6.1
207602	2.6	1.8	0.6	24.9	2.3	1.02	6.1	0.6	0.1	20.8	0.3	<1	1.2	10.1

Table B1.1. (continued)

	Nd	Ni	Pb	Pr	Rb	Re	Sb	Sc	Se	Sm	Sn	Sr	Ta	Tb
UNITS	ppm	ppm	ppm	ppm	ppm	ppm	ppm	ppm	ppm	ppm	ppm	ppm	ppm	ppm
DETECTION	0.01	2	1	0.01	0.05	0.01	0.1	0.1	5	0.01	0.2	0.1	0.01	0.01
METHOD	LA101	LA101	LA101	LA101	LA101	LA101	LA101	LA101	LA101	LA101	LA101	LA101	LA101	LA101
229101	18.2	104	7	4.86	15.8	<0.01	0.3	12.7	<5	3.99	2.4	5.8	0.45	0.57
229105	88.8	4	15	20.4	2.95	0.02	14.6	29.7	<5	24.4	1.8	107	1.04	2.95
229109	7.94	10	30	2.43	154	<0.01	5	35.3	<5	1.34	2	61.2	0.4	0.26
229111	18.4	320	10	5.23	108	<0.01	7.7	26.5	<5	3.52	2	10.7	0.5	0.52
229113	15.3	334	3	3.46	254	<0.01	3.5	64	<5	3.25	1.6	66.5	0.3	0.65
229115	15.1	96	79	4	33	<0.01	0.2	19.3	<5	3.16	3	22.8	0.53	0.64
229117	33.9	112	8	9.53	19.6	<0.01	6.4	27.6	<5	6.06	1.4	11.7	0.85	0.82
229119	13	248	10	3.91	102	<0.01	6.8	23.5	<5	2.67	1.6	5.9	0.41	0.34
229120	15.5	284	11	4.15	129	<0.01	7.2	27.6	<5	2.9	1.8	7	0.43	0.49
229124	4.53	170	2	1.17	5.1	<0.01	1.7	27.6	<5	1.39	0.6	22.2	0.11	0.31
229127	19.7	4	35	6.83	61.3	<0.01	3.7	46	<5	3.51	4.6	177	0.91	0.76
229130	12.6	182	12	3.15	65.7	<0.01	1.3	45.5	<5	2.6	1.8	60.9	0.33	0.47
229131	12.3	78	10	3.65	139	0.02	0.5	25.7	<5	2.63	2	43.2	0.45	0.33
229135	8.4	4	58	2.81	35.5	<0.01	0.9	17.6	<5	1.41	5.2	52.4	0.55	0.26
229136	12.5	20	79	3.97	117	<0.01	3.4	16.8	<5	2.3	14.2	50.4	0.52	0.18
229138	38.2	16	93	11.2	57.9	<0.01	4.1	20.9	<5	6.36	1.8	58.9	0.94	1.18
229146	26.1	128	34	7.25	51.5	<0.01	<0.1	21	<5	4.85	2.2	40.3	0.84	0.62
229147	1.68	56	10	0.37	5.05	<0.01	<0.1	27.8	<5	0.36	1.6	36.7	0.63	0.07
229149	4.64	674	17	1.09	231	<0.01	4.1	25.7	<5	1.58	2.4	54.4	0.13	0.31
229152	15.5	38	57	5.31	94.1	<0.01	7	20.2	<5	2.65	4.6	93.1	0.51	0.45
229157	20.4	34	13	5.43	86.9	0.02	1	34.6	<5	4.96	2	44.2	0.59	0.62
229158	23.9	64	15	6.61	76.2	0.02	0.5	20.6	<5	4.6	2.2	6.3	0.62	0.8

Table B1.1. (continued)

	Nd	Ni	Pb	Pr	Rb	Re	Sb	Sc	Se	Sm	Sn	Sr	Ta	Tb
211117	25.2	15.3	148.8	7.7	161.6	<0.01	1.54	-10	-0.5	4.2	3	63.3	1.3	0.5
211116	13.4	17	31.5	3.9	96.3	<0.01	1.83	13	0.9	2.6	5	43.1	0.6	0.4
207695	18.4	122.5	20.1	5	58.9	<0.01	1.49	18	-0.5	3.5	2	60	0.7	0.6
207694	7.8	59.2	13.7	1.9	133.2	<0.01	0.5	24	0.5	1.6	2	35.4	0.8	0.2
207693	4.6	73.4	1.3	1.1	3.2	<0.01	1.45	19	-0.5	1.2	-1	24	0.2	0.3
207692	16.1	316.4	11	4.5	117.3	<0.01	15.23	28	-0.5	3.3	1	13.4	0.6	0.5
207691	85.6	5.1	11	22.3	1.9	<0.01	12.43	23	0.5	16.6	3	65.4	1	1.7
207690	13.3	117.3	15	3.4	86.1	<0.01	0.1	18	-0.5	2.9	1	82	0.6	0.4
207602	10.6	10.7	34.1	3.3	115.5	<0.01	0.31	21	0.9	2	2	98.9	0.9	0.4

Table B1.1. (continued)

	Te	Th	Ti	Tl	Tm	U	V	W	Y	Yb	Zn	Zr
UNITS	ppm	ppm	ppm	ppm	ppm	ppm	ppm	ppm	ppm	ppm	ppm	ppm
DETECTION	0.2	0.01	1	0.2	0.01	0.01	0.1	0.5	0.02	0.01	5	0.5
METHOD	LA101	LA101	LA101	LA101	LA101	LA101	LA101	LA101	LA101	LA101	LA101	LA101
229101	<0.2	6.85	4320	<0.2	0.34	1.74	114	<0.5	20.8	2.37	85	160
229105	<0.2	14.5	12400	<0.2	1.98	2.4	177	1.5	128	13.4	<5	367
229109	<0.2	2.47	6240	0.6	0.17	0.73	259	2	10.4	1.6	35	104
229111	<0.2	8.07	4610	1	0.31	2.04	201	0.5	21.6	2.18	130	147
229113	<0.2	2.57	7980	0.8	0.49	0.69	430	<0.5	29.7	3.5	80	107
229115	<0.2	7.1	4940	<0.2	0.38	2.05	147	<0.5	27.3	2.44	110	143
229117	<0.2	10.6	7990	0.4	0.54	2.87	228	<0.5	34.1	3.74	90	236
229119	<0.2	5.87	3760	1	0.2	1.59	169	<0.5	16.5	1.85	80	111
229120	<0.2	6.44	4410	1	0.26	1.78	188	<0.5	19.9	2.02	75	125
229124	<0.2	0.98	3600	<0.2	0.17	0.18	177	<0.5	11.9	1.3	25	49
229127	<0.2	12.4	7650	5.2	0.47	2.03	297	2.5	30.8	3.38	10	225
229130	<0.2	3.49	6690	<0.2	0.32	0.51	328	1	20.1	2.5	95	82.5
229131	<0.2	5.85	4310	1.2	0.21	1.32	163	0.5	15.6	1.84	65	116
229135	1.8	7.92	3750	0.6	0.15	1.96	82	1	9.1	1.06	30	120
229136	1.8	8.54	3170	1.8	0.16	1.97	83.4	2	9.42	1.41	485	108
229138	0.4	12.4	6420	0.6	0.49	2.82	192	4.5	35.5	3.57	105	216
229146	<0.2	8.55	5640	0.4	0.34	2.68	164	<0.5	17	2.86	170	153
229147	<0.2	5.2	6030	<0.2	0.07	3.19	195	<0.5	2.72	0.54	35	121
229149	0.4	0.24	2680	1.8	0.19	0.47	151	59	14.3	1.24	165	27
229152	0.6	11.5	3650	3.4	0.22	2.21	162	1	11.2	1.33	145	113
229157	0.4	7.12	5780	1	0.41	2.1	204	<0.5	25.1	2.72	90	153
229158	0.4	9.43	5530	1	0.3	2.22	149	0.5	27.7	2.69	85	173

Table B1.1. (continued)

	Te	Th	Ti	Tl	Tm	U	V	W	Y	Yb	Zn	Zr
211117	0.2	22.8	<1	1	0.2	4.1	28	3	14.9	1.7	71	91
211116	1.2	8.3	<1	0.78	0.3	2.2	95	3	12.6	1.4	175	101
207695	-0.1	6.5	<1	0.89	0.3	2	136	<0.5	16.3	1.6	197	162
207694	-0.1	8.1	<1	1.01	0.2	2.1	181	<0.5	8.3	1.3	123	174
207693	0.1	0.8	<1	-0.02	0.2	0.2	106	<0.5	8.5	1	27	32
207692	-0.1	6.5	<1	1.01	0.3	1.6	178	<0.5	16.2	1.8	92	118
207691	-0.1	9.6	<1	0.04	0.7	3.6	159	<0.5	43.8	4.1	2	339
207690	0.1	4.6	<1	0.57	0.3	1.4	130	<0.5	14.1	1.7	93	95
207602	0.1	10.7	<1	0.84	0.3	1.4	129	<0.5	15.6	1.8	9	223

Appendix C: EPMA Data

Table C1.1. EPMA analyses of cordierite.

Sample	**207692**									**229111**			
wt%													
SiO2	47.64	47.91	49.62	47.59	47.71	47.78	46.99	47.70	47.93	47.20	46.78	47.48	47.54
TiO_2	0.02	0.00	-0.01	0.00	0.00	0.01	0.02	0.00	0.01	0.02	0.02	0.00	0.01
Al_2O_3	32.90	33.01	31.71	33.09	33.14	32.92	32.84	32.74	33.18	32.22	31.81	32.84	32.56
FeO	9.03	8.73	8.91	9.16	9.21	9.02	8.95	9.05	8.84	8.38	8.03	8.69	8.63
MnO	0.05	0.00	0.04	0.02	0.02	0.03	0.03	0.02	0.02	0.04	0.01	0.01	0.01
MgO	7.95	8.04	7.65	7.86	7.99	7.99	7.66	7.96	7.90	7.90	7.57	8.00	7.94
CaO	0.01	0.00	0.01	0.01	0.00	0.01	0.06	0.02	0.02	0.01	0.01	0.01	0.02
K_2O	0.00	0.01	0.00	-0.01	0.00	-0.01	0.02	0.01	0.01	0.10	0.07	0.01	0.02
Total	97.60	97.71	97.93	97.71	98.06	97.74	96.57	97.51	97.91	95.88	94.30	97.03	96.72
cations													
Si	4.96	4.97	5.13	4.95	4.95	4.96	4.94	4.97	4.96	4.99	5.02	4.96	4.98
Ti	0.00	0.00	0.00	0.00	0.00	0.00	0.00	0.00	0.00	0.00	0.00	0.00	0.00
Al	4.04	4.04	3.86	4.06	4.05	4.03	4.07	4.02	4.05	4.01	4.02	4.05	4.02
Fe	0.79	0.76	0.77	0.80	0.80	0.78	0.79	0.79	0.77	0.74	0.72	0.76	0.76
Mn	0.00	0.00	0.00	0.00	0.00	0.00	0.00	0.00	0.00	0.00	0.00	0.00	0.00
Mg	1.23	1.24	1.18	1.22	1.23	1.24	1.20	1.24	1.22	1.24	1.21	1.25	1.24
Ca	0.00	0.00	0.00	0.00	0.00	0.00	0.01	0.00	0.00	0.00	0.00	0.00	0.00
K	0.00	0.00	0.00	0.00	0.00	0.00	0.00	0.00	0.00	0.01	0.01	0.01	0.00
Total	11.02	11.01	10.94	11.02	11.03	11.02	11.02	11.02	11.01	11.01	10.98	11.03	11.01
$X_{(Mg)}$	0.61	0.62	0.60	0.60	0.61	0.61	0.60	0.61	0.61	0.63	0.63	0.62	0.62
O value	18	18	18	18	18	18	18	18	18	18	18	18	18

Table C1.1. (continued)

Sample	**229119**					**229120**									
wt%															
SiO2	47.35	47.46	47.38	47.43	47.12	48.56	45.96	46.30	47.70	47.53	47.93	47.35	47.15	47.40	47.53
TiO_2	0.01	0.00	0.00	0.01	0.00	0.00	0.01	-0.01	0.01	-0.01	0.01	0.00	0.00	0.00	-0.01
Al_2O_3	32.51	32.59	32.40	32.50	32.61	33.48	31.86	31.36	32.88	32.85	33.01	32.71	32.51	32.69	32.81
FeO	8.06	8.25	7.59	8.60	8.62	8.69	8.38	7.97	8.66	9.17	8.91	9.68	9.48	9.40	9.38
MnO	0.02	0.02	0.03	0.03	0.02	0.02	0.03	0.02	0.01	0.02	0.02	0.06	0.04	0.06	0.05
MgO	7.72	7.67	7.68	8.10	7.89	7.80	7.85	7.60	8.04	7.95	8.00	7.35	7.30	7.29	7.33
CaO	0.02	0.02	0.02	0.01	0.01	0.01	0.02	0.02	0.01	0.01	0.00	0.01	0.02	0.01	0.01
K_2O	0.01	0.01	0.17	0.02	0.02	0.01	0.01	1.64	0.00	0.01	0.01	0.01	0.01	0.02	0.00
Total	95.69	96.02	95.28	96.70	96.29	98.57	94.12	94.91	97.31	97.53	97.90	97.17	96.51	96.86	97.10
cations															
Si	5.00	5.00	5.02	4.97	4.96	4.99	4.95	4.99	4.97	4.95	4.97	4.97	4.97	4.98	4.98
Ti	0.00	0.00	0.00	0.00	0.00	0.00	0.00	0.00	0.00	0.00	0.00	0.00	0.00	0.00	0.00
Al	4.05	4.05	4.04	4.02	4.05	4.05	4.05	3.98	4.04	4.04	4.03	4.04	4.04	4.05	4.05
Fe	0.71	0.73	0.67	0.75	0.76	0.75	0.76	0.72	0.75	0.80	0.77	0.85	0.84	0.83	0.82
Mn	0.00	0.00	0.00	0.00	0.00	0.00	0.00	0.00	0.00	0.00	0.00	0.01	0.00	0.01	0.00
Mg	1.21	1.20	1.21	1.27	1.24	1.19	1.26	1.22	1.25	1.23	1.24	1.15	1.15	1.14	1.14
Ca	0.00	0.00	0.00	0.00	0.00	0.00	0.00	0.00	0.00	0.00	0.00	0.00	0.00	0.00	0.00
K	0.00	0.00	0.02	0.00	0.00	0.00	0.00	0.23	0.00	0.00	0.00	0.00	0.00	0.00	0.00
Total	10.98	10.98	10.97	11.02	11.01	10.99	11.02	11.14	11.01	11.03	11.02	11.01	11.01	11.00	11.00
$X_{(Mg)}$	0.63	0.62	0.64	0.63	0.62	0.62	0.63	0.63	0.62	0.61	0.62	0.58	0.58	0.58	0.58
O value	18	18	18	18	18	18	18	18	18	18	18	18	18	18	18

Table C1.2. EPMA analyses of grunerite.

Sample	**207692**														
Wt%															
SiO_2	52.57	52.46	52.59	52.60	52.31	52.51	49.80	51.96	52.15	52.30	52.12	52.61	52.45	53.50	54.96
TiO_2	0.06	0.11	0.06	0.08	0.10	0.07	0.09	0.05	0.08	0.06	0.08	0.08	0.06	0.08	0.12
Al_2O_3	1.83	1.98	1.71	1.65	2.00	2.13	3.18	2.14	2.08	1.88	2.23	2.11	1.82	1.52	1.50
FeO	29.25	29.13	29.00	29.15	29.57	29.56	29.12	29.94	29.31	30.27	29.62	29.79	29.74	25.57	25.33
MnO	0.06	0.10	0.07	0.07	0.10	0.06	0.09	0.07	0.09	0.07	0.08	0.07	0.06	0.06	0.07
MgO	13.41	13.37	13.85	13.32	13.21	13.19	12.10	12.81	13.04	12.93	13.02	13.00	13.05	16.37	17.21
CaO	0.20	0.20	0.16	0.18	0.20	0.20	0.22	0.21	0.20	0.21	0.21	0.22	0.20	0.19	0.19
Na_2O	0.05	0.09	0.12	0.09	0.06	0.11	0.08	0.09	0.15	0.10	0.13	0.13	0.10	0.09	0.07
K_2O	0.00	0.01	0.00	0.00	0.01	0.00	0.01	0.00	0.00	0.00	0.00	0.00	0.00	0.00	0.00
Total	96.45	96.47	96.55	96.16	96.61	96.90	93.80	96.52	96.09	96.94	96.58	97.09	96.57	96.35	98.40
cations															
Si	7.89	7.87	7.88	7.92	7.86	7.86	7.73	7.85	7.87	7.86	7.84	7.87	7.89	7.89	7.90
Ti	0.01	0.01	0.01	0.01	0.01	0.01	0.01	0.01	0.01	0.01	0.01	0.01	0.01	0.01	0.01
Al	0.32	0.35	0.30	0.29	0.35	0.38	0.58	0.38	0.37	0.33	0.40	0.37	0.32	0.26	0.25
Fe	3.67	3.66	3.63	3.67	3.71	3.70	3.78	3.78	3.70	3.81	3.73	3.73	3.74	3.15	3.05
Mn	0.01	0.01	0.01	0.01	0.01	0.01	0.01	0.01	0.01	0.01	0.01	0.01	0.01	0.01	0.01
Mg	3.00	2.99	3.09	2.99	2.96	2.94	2.80	2.88	2.93	2.90	2.92	2.90	2.93	3.60	3.69
Ca	0.03	0.03	0.03	0.03	0.03	0.03	0.04	0.03	0.03	0.03	0.03	0.04	0.03	0.03	0.03
Na	0.02	0.03	0.03	0.03	0.02	0.03	0.03	0.03	0.04	0.03	0.04	0.04	0.03	0.03	0.02
K	0.00	0.00	0.00	0.00	0.00	0.00	0.00	0.00	0.00	0.00	0.00	0.00	0.00	0.00	0.00
Total	14.95	14.95	14.98	14.94	14.96	14.96	14.98	14.97	14.96	14.98	14.97	14.96	14.96	14.98	14.96
$X_{(Mg)}$	0.45	0.45	0.46	0.45	0.44	0.44	0.43	0.43	0.44	0.43	0.44	0.44	0.44	0.53	0.55
O value	23	23	23	23	23	23	23	23	23	23	23	23	23	23	23

Table C1.2. (continued)

Sample	**229111**		**207693**										
Wt%													
SiO_2	49.6093	52.6501	51.9107	52.0472	51.9568	51.9614	52.0259	52.7289	52.4048	52.1587	52.587	52.6581	52.4844
TiO_2	0.0383	0.0181	0.0938	0.0461	0.085	0.0797	0.0392	0.0142	0.0337	0.0815	0.048	0.0496	0.0213
Al_2O_3	4.1218	1.5326	1.1459	0.903	1.3087	1.1057	2.0357	0.6448	1.0887	2.0965	1.232	1.0471	1.1521
FeO	27.8725	27.3681	32.2018	31.8927	32.286	32.4818	29.3772	30.0515	31.8421	32.464	29.7063	31.8265	31.9054
MnO	0.1975	0.124	0.1069	0.0595	0.1365	0.0435	0.0403	0.0807	0.0902	0.0298	0.1212	0.0684	0.0398
MgO	13.9622	14.9574	10.8324	10.6879	10.6216	10.7741	13.3086	12.6253	10.7915	10.7814	12.989	11.0161	10.9107
CaO	0.3595	0.3918	0.1781	0.1566	0.177	0.1901	0.186	0.2348	0.1657	0.1733	0.1572	0.1693	0.1723
Na_2O	0.053	0.0557	0.0952	0.0298	0.0715	0.0597	0.0674	0.0585	0.042	0.0534	0.0183	0.0474	0.056
K_2O	0.0017	0.0012	-0.001	0.0018	-0.0004	0.0034	0	-0.0032	-0.0087	0.0023	-0.0021	0.0008	0.0033
Total	95.2169	96.0856	96.5638	95.8246	96.6427	96.6994	97.08029	96.4355	96.45	97.8409	96.85691	96.88329	96.74531
cations													
Si	7.5418	7.8734	11.1157	11.207	11.1164	11.1204	10.9229	11.1783	11.1953	11.0073	11.0769	11.1914	11.1773
Ti	0.0044	0.002	0.0151	0.0075	0.0137	0.0128	0.0062	0.0023	0.0054	0.0129	0.0076	0.0079	0.0034
Al	0.7386	0.2701	0.2892	0.2292	0.33	0.2789	0.5038	0.1611	0.2741	0.5215	0.3059	0.2623	0.2892
Fe	3.5437	3.4228	5.7668	5.7433	5.7771	5.8137	5.1583	5.328	5.6891	5.7297	5.2331	5.657	5.6826
Mn	0.0254	0.0157	0.0194	0.0109	0.0247	0.0079	0.0072	0.0145	0.0163	0.0053	0.0216	0.0123	0.0072
Mg	3.1641	3.3343	3.4578	3.4306	3.3877	3.4372	4.1652	3.9898	3.4366	3.3917	4.0785	3.4901	3.4637
Ca	0.0586	0.0628	0.0409	0.0361	0.0406	0.0436	0.0418	0.0533	0.0379	0.0392	0.0355	0.0385	0.0393
Na	0.0156	0.0161	0.0395	0.0124	0.0297	0.0248	0.0274	0.024	0.0174	0.0218	0.0075	0.0195	0.0231
K	0.0003	0.0002	-0.0003	0.0005	-1E-04	0.0009	0	-0.0009	-0.0024	0.0006	-0.0006	0.0002	0.0009
Total	15.0925	14.9974	20.7441	20.6775	20.7198	20.7402	20.8328	20.7504	20.6697	20.73	20.766	20.6792	20.6867
$X_{(Mg)}$	0.471705	0.493451	0.374846	0.373952	0.369643	0.371553	0.446742	0.428191	0.376585	0.37184	0.438002	0.381553	0.3787
O value	23	23	32	32	32	32	32	32	32	32	32	32	32

Table C1.2. (continued)

Sample	**229120**							
Wt%								
SiO_2	51.74	51.67	51.95	51.42	51.47	51.12	51.66	51.30
TiO_2	0.05	0.08	0.08	0.11	0.09	0.09	0.08	0.10
Al_2O_3	2.38	2.22	2.31	2.74	2.19	2.63	2.66	2.70
FeO	28.87	28.74	30.83	31.36	30.88	31.03	31.09	31.06
MnO	0.11	0.09	0.11	0.11	0.14	0.13	0.15	0.13
MgO	12.11	12.11	11.98	11.68	11.96	11.69	11.68	11.77
CaO	0.27	0.20	0.25	0.29	0.26	0.28	0.31	0.31
Na_2O	0.11	0.07	0.11	0.17	0.09	0.13	0.17	0.15
K_2O	0.00	0.00	0.00	0.00	0.00	-0.01	0.00	0.00
Total	94.88	94.40	96.66	96.99	96.12	96.15	96.91	96.59
cations								
Si	7.91	7.93	7.85	7.78	7.84	7.79	7.81	7.78
Ti	0.01	0.01	0.01	0.01	0.01	0.01	0.01	0.01
Al	0.43	0.40	0.41	0.49	0.39	0.47	0.47	0.48
Fe	3.69	3.69	3.90	3.97	3.93	3.95	3.93	3.94
Mn	0.01	0.01	0.01	0.01	0.02	0.02	0.02	0.02
Mg	2.76	2.77	2.70	2.63	2.71	2.66	2.63	2.66
Ca	0.04	0.03	0.04	0.05	0.04	0.05	0.05	0.05
Na	0.03	0.02	0.03	0.05	0.03	0.04	0.05	0.04
K	0.00	0.00	0.00	0.00	0.00	0.00	0.00	0.00
Total	14.89	14.87	14.95	14.99	14.97	14.98	14.97	14.99
$X_{(Mg)}$	0.43	0.43	0.41	0.40	0.41	0.40	0.40	0.40
O value	23	23	23	23	23	23	23	23

Table C1.2. (continued)

Sample	**229151**								
Wt%									
SiO_2	52.56	52.15	52.28	51.44	51.61	52.00	50.69	50.95	50.27
TiO_2	0.03	0.05	0.03	0.02	0.05	0.00	0.11	0.14	0.11
Al_2O_3	0.79	1.66	0.96	1.44	1.56	1.07	2.46	2.24	2.78
FeO	31.93	30.96	32.76	32.76	32.87	32.50	32.10	32.86	31.85
MnO	0.15	0.14	0.18	0.16	0.16	0.15	0.13	0.14	0.12
MgO	11.65	11.80	10.82	10.61	10.56	10.83	10.18	10.31	9.92
CaO	0.38	0.48	0.54	0.37	0.56	0.45	0.90	0.44	0.92
Na_2O	0.06	0.22	0.08	0.26	0.15	0.15	0.34	0.28	0.35
K_2O	-0.01	0.00	0.00	0.01	0.01	0.01	0.01	0.00	0.00
Total	96.66	96.50	96.74	96.22	96.66	96.26	96.07	96.44	95.44
cations									
Si	7.99	7.91	7.98	7.92	7.90	7.97	7.81	7.82	7.79
Ti	0.00	0.01	0.00	0.00	0.01	0.00	0.01	0.02	0.01
Al	0.14	0.30	0.17	0.26	0.28	0.19	0.45	0.41	0.51
Fe	4.06	3.93	4.18	4.22	4.21	4.17	4.14	4.22	4.13
Mn	0.02	0.02	0.02	0.02	0.02	0.02	0.02	0.02	0.02
Mg	2.64	2.67	2.46	2.43	2.41	2.47	2.34	2.36	2.29
Ca	0.06	0.08	0.09	0.06	0.09	0.07	0.15	0.07	0.15
Na	0.02	0.06	0.02	0.08	0.04	0.04	0.10	0.08	0.11
K	0.00	0.00	0.00	0.00	0.00	0.00	0.00	0.00	0.00
Total	14.94	14.97	14.94	14.99	14.97	14.95	15.01	15.00	15.00
$X_{(Mg)}$	0.39	0.40	0.37	0.37	0.36	0.37	0.36	0.36	0.36
O value	23	23	23	23	23	23	23	23	23

Table C1.3. EPMA analyses of biotite.

Sample	**207692**					**229111**				
Wt%										
SiO_2	34.98	35.16	34.45	34.35	34.00	33.38	34.46	34.49	32.67	27.55
TiO_2	1.37	1.43	1.41	1.46	1.54	1.45	1.31	1.45	0.96	0.35
Al_2O_3	19.52	18.87	18.76	18.76	18.62	18.77	18.82	18.55	18.31	19.15
FeO	21.53	21.31	21.90	20.81	20.69	21.13	19.47	20.26	18.97	27.68
MnO	0.02	0.03	0.01	0.01	0.03	0.02	0.00	0.02	0.00	0.26
MgO	9.86	9.55	9.29	9.45	9.43	10.99	9.56	9.51	13.59	9.22
CaO	0.54	0.04	0.09	0.20	0.30	0.09	0.00	0.15	0.16	0.50
Na_2O	0.29	0.20	0.17	0.24	0.21	0.13	0.13	0.21	0.12	0.03
K_2O	5.53	7.58	7.29	7.15	6.98	5.47	8.13	7.75	5.15	1.75
Total	93.73	94.17	93.37	92.45	91.81	91.34	91.86	92.34	89.97	86.39
cations										
Si	5.36	5.41	5.36	5.38	5.36	5.25	5.41	5.40	5.18	4.72
Ti	0.16	0.17	0.17	0.17	0.18	0.17	0.15	0.17	0.11	0.05
Al	3.52	3.42	3.44	3.46	3.46	3.48	3.49	3.43	3.42	3.87
Fe	2.76	2.74	2.85	2.72	2.73	2.78	2.56	2.65	2.51	3.97
Mn	0.00	0.00	0.00	0.00	0.00	0.00	0.00	0.00	0.00	0.04
Mg	2.25	2.19	2.16	2.20	2.21	2.58	2.24	2.22	3.21	2.36
Ca	0.09	0.01	0.01	0.03	0.05	0.01	0.00	0.03	0.03	0.09
Na	0.09	0.06	0.05	0.07	0.06	0.04	0.04	0.06	0.04	0.01
K	1.08	1.49	1.45	1.43	1.40	1.10	1.63	1.55	1.04	0.38
Total	15.31	15.49	15.50	15.47	15.46	15.41	15.52	15.52	15.54	15.49
$X_{(Mg)}$	0.45	0.44	0.43	0.45	0.45	0.48	0.47	0.46	0.56	0.37
O value	22	22	22	22	22	22	22	22	22	22

Table C1.3. (continued)

Sample	**229119**								
Wt%									
SiO_2	34.95	34.72	34.40	34.58	35.32	35.02	32.55	34.77	35.33
TiO_2	2.07	1.39	1.50	1.48	1.39	1.91	0.82	0.87	1.47
Al_2O_3	18.72	18.76	18.83	18.34	18.52	18.67	17.15	18.60	19.14
FeO	20.44	19.93	20.10	19.06	17.96	19.33	16.93	17.94	20.03
MnO	0.03	0.00	0.03	0.00	0.01	0.02	0.03	0.03	0.00
MgO	9.25	9.75	9.68	9.51	11.38	11.70	12.74	14.39	9.98
CaO	0.01	0.01	0.01	0.01	0.02	0.03	0.36	0.09	0.01
Na_2O	0.16	0.12	0.15	0.11	0.12	0.10	0.02	0.11	0.20
K_2O	8.08	7.80	7.02	7.56	8.10	7.49	7.10	6.07	8.45
Total	93.67	92.46	91.64	90.59	92.84	94.30	87.87	92.96	94.64
cations									
Si	5.40	5.42	5.40	5.48	5.44	5.33	5.31	5.30	5.40
Ti	0.24	0.16	0.18	0.18	0.16	0.22	0.10	0.10	0.17
Al	3.41	3.45	3.48	3.42	3.36	3.35	3.30	3.34	3.45
Fe	2.64	2.60	2.64	2.53	2.31	2.46	2.31	2.29	2.56
Mn	0.00	0.00	0.00	0.00	0.00	0.00	0.00	0.00	0.00
Mg	2.13	2.27	2.26	2.24	2.61	2.66	3.10	3.27	2.27
Ca	0.00	0.00	0.00	0.00	0.00	0.01	0.06	0.01	0.00
Na	0.05	0.04	0.05	0.03	0.04	0.03	0.01	0.03	0.06
K	1.59	1.55	1.40	1.53	1.59	1.46	1.48	1.18	1.65
Total	15.47	15.49	15.41	15.41	15.53	15.51	15.68	15.53	15.56
$X_{(Mg)}$	0.45	0.47	0.46	0.47	0.53	0.52	0.57	0.59	0.47
O value	22	22	22	22	22	22	22	22	22

Table C1.3. (continued)

Sample	**229120**												
Wt%													
SiO_2	55.59	35.39	27.06	34.18	35.21	34.33	35.04	34.30	35.25	35.23	33.79	31.01	33.37
TiO_2	0.71	1.19	0.51	1.31	1.39	1.33	1.33	1.50	1.67	1.36	1.31	1.31	1.42
Al_2O_3	12.28	18.14	18.46	18.40	18.79	19.58	18.71	18.95	18.92	19.20	19.02	17.43	18.67
FeO	17.50	21.31	24.22	20.33	19.77	19.79	20.13	20.00	19.90	19.75	22.32	23.70	22.87
MnO	0.00	0.13	0.03	-0.01	0.00	0.00	0.02	0.00	0.02	0.00	0.03	0.02	0.03
MgO	7.36	10.03	11.61	10.50	10.20	9.32	9.78	9.96	9.72	10.06	8.90	9.31	9.41
CaO	0.06	0.17	0.03	0.01	0.00	0.18	0.06	0.06	0.00	0.00	0.03	0.04	0.02
Na_2O	0.07	0.01	0.03	0.09	0.21	0.20	0.17	0.19	0.29	0.17	0.13	0.09	0.14
K_2O	2.38	4.37	1.34	7.13	7.93	7.70	7.69	7.42	8.29	8.11	7.27	5.87	7.16
Total	95.93	90.67	83.17	91.93	93.48	92.41	92.90	92.35	94.05	93.84	92.76	88.74	93.11
cations													
Si	7.59	5.54	4.72	5.37	5.43	5.36	5.44	5.36	5.42	5.41	5.31	5.15	5.25
Ti	0.07	0.14	0.07	0.15	0.16	0.16	0.16	0.18	0.19	0.16	0.15	0.16	0.17
Al	1.98	3.35	3.80	3.40	3.41	3.60	3.42	3.49	3.43	3.47	3.53	3.41	3.46
Fe	2.00	2.79	3.54	2.67	2.55	2.58	2.61	2.61	2.56	2.54	2.93	3.29	3.01
Mn	0.00	0.02	0.00	0.00	0.00	0.00	0.00	0.00	0.00	0.00	0.00	0.00	0.00
Mg	1.50	2.34	3.02	2.46	2.34	2.17	2.26	2.32	2.23	2.30	2.09	2.31	2.21
Ca	0.01	0.03	0.00	0.00	0.00	0.03	0.01	0.01	0.00	0.00	0.00	0.01	0.00
Na	0.02	0.00	0.01	0.03	0.06	0.06	0.05	0.06	0.09	0.05	0.04	0.03	0.04
K	0.41	0.87	0.30	1.43	1.56	1.53	1.52	1.48	1.63	1.59	1.46	1.24	1.44
Total	13.57	15.08	15.46	15.51	15.52	15.48	15.48	15.49	15.53	15.52	15.52	15.61	15.59
$X_{(Mg)}$	0.43	0.46	0.46	0.48	0.48	0.46	0.46	0.47	0.47	0.48	0.42	0.41	0.42
O value	22	22	22	22	22	22	22	22	22	22	22	22	22

Table C1.4. EPMA garnet traverses.

Sample	**207692 grt 1**												
Wt%	**Rim**												**Rim**
SiO_2	38.41	38.43	38.15	38.61	38.51	38.66	38.76	38.66	38.76	38.55	38.67	38.86	38.63
Al_2O_3	21.68	21.56	21.46	21.58	21.54	21.58	21.55	21.57	21.56	21.66	21.38	21.57	21.72
FeO	36.54	36.52	36.15	36.28	35.98	35.99	36.34	36.15	35.79	36.21	36.34	36.64	36.86
MnO	0.44	0.39	0.42	0.43	0.44	0.41	0.45	0.44	0.39	0.39	0.41	0.39	0.41
MgO	3.02	2.97	3.02	2.96	2.85	2.68	2.58	2.81	2.84	2.91	2.81	2.82	2.57
CaO	1.43	1.22	1.27	1.39	1.60	1.78	1.51	1.81	1.74	1.48	1.33	1.34	1.29
Total	101.51	101.09	100.47	101.25	100.92	101.10	101.19	101.44	101.07	101.20	100.94	101.61	101.48
cations													
Si	3.03	3.04	3.04	3.05	3.05	3.06	3.06	3.05	3.06	3.04	3.06	3.06	3.05
Al	2.02	2.01	2.01	2.01	2.01	2.01	2.01	2.00	2.01	2.02	2.00	2.00	2.02
Fe	2.41	2.42	2.41	2.40	2.38	2.38	2.40	2.38	2.36	2.39	2.41	2.41	2.43
Mn	0.03	0.03	0.03	0.03	0.03	0.03	0.03	0.03	0.03	0.03	0.03	0.03	0.03
Mg	0.36	0.35	0.36	0.35	0.34	0.32	0.30	0.33	0.33	0.34	0.33	0.33	0.30
Ca	0.12	0.10	0.11	0.12	0.14	0.15	0.13	0.15	0.15	0.13	0.11	0.11	0.11
Total	7.96	7.95	7.95	7.95	7.94	7.94	7.93	7.95	7.94	7.95	7.94	7.94	7.94
O value	12	12	12	12	12	12	12	12	12	12	12	12	12

Table C1.4. (continued)

Sample	**207692 grt 2**													
Wt%	**Rim**													**Rim**
SiO_2	38.26	38.25	38.21	38.24	37.99	38.01	38.33	38.15	38.50	38.34	37.68	37.08	38.60	38.50
Al_2O_3	21.71	21.62	21.64	21.77	21.60	21.48	21.62	21.48	21.67	21.85	21.22	21.05	21.69	21.62
FeO	37.09	36.39	36.29	36.33	35.95	36.00	35.69	36.50	36.34	36.60	36.32	36.20	36.17	36.52
MnO	0.46	0.42	0.46	0.44	0.40	0.41	0.42	0.43	0.42	0.44	0.42	0.42	0.40	0.42
MgO	2.69	2.96	2.96	2.98	2.82	2.85	2.93	2.79	2.97	2.94	3.10	3.33	2.86	2.95
CaO	1.16	1.30	1.72	1.22	1.88	2.03	1.90	1.63	1.58	1.25	1.42	1.82	1.78	1.34
Total	101.38	100.95	101.27	100.97	100.65	100.77	100.89	100.99	101.49	101.42	100.17	99.91	101.49	101.35
cations														
Si	3.03	3.03	3.02	3.03	3.02	3.02	3.04	3.03	3.04	3.03	3.02	2.99	3.04	3.04
Al	2.03	2.02	2.02	2.03	2.03	2.01	2.02	2.01	2.01	2.03	2.00	2.00	2.01	2.01
Fe	2.46	2.41	2.40	2.41	2.39	2.39	2.36	2.42	2.40	2.42	2.43	2.44	2.38	2.41
Mn	0.03	0.03	0.03	0.03	0.03	0.03	0.03	0.03	0.03	0.03	0.03	0.03	0.03	0.03
Mg	0.32	0.35	0.35	0.35	0.33	0.34	0.35	0.33	0.35	0.35	0.37	0.40	0.34	0.35
Ca	0.10	0.11	0.15	0.10	0.16	0.17	0.16	0.14	0.13	0.11	0.12	0.16	0.15	0.11
Total	7.96	7.96	7.97	7.95	7.96	7.97	7.95	7.96	7.96	7.96	7.98	8.01	7.95	7.95
O value	12	12	12	12	12	12	12	12	12	12	12	12	12	12

Table C1.4. (continued)

Sample	**207692 grt 4**											
Wt%	**Rim**											**Rim**
SiO_2	38.19	38.21	38.09	37.71	37.22	37.18	37.90	37.89	33.32	38.29	38.04	38.01
Al_2O_3	21.25	21.32	21.24	21.25	20.93	20.59	21.27	21.06	23.66	21.33	21.09	21.16
FeO	37.12	36.28	36.04	36.79	35.72	35.43	36.00	35.80	34.15	36.16	36.66	36.84
MnO	0.42	0.38	0.41	0.49	0.38	0.46	0.51	0.41	0.44	0.44	0.45	0.42
MgO	2.77	3.08	3.04	2.49	2.88	3.18	3.13	3.24	3.18	3.05	3.02	2.90
CaO	1.07	1.54	1.54	1.32	1.69	1.37	1.25	1.20	1.53	1.41	1.06	1.03
Total	100.83	100.81	100.36	100.06	98.82	98.21	100.06	99.60	96.29	100.68	100.34	100.37
cations												
Si	3.04	3.04	3.04	3.03	3.02	3.04	3.03	3.04	2.78	3.04	3.04	3.04
Al	2.00	2.00	2.00	2.01	2.00	1.98	2.01	1.99	2.33	2.00	1.99	2.00
Fe	2.47	2.41	2.40	2.47	2.43	2.42	2.41	2.40	2.38	2.40	2.45	2.46
Mn	0.03	0.03	0.03	0.03	0.03	0.03	0.03	0.03	0.03	0.03	0.03	0.03
Mg	0.33	0.37	0.36	0.30	0.35	0.39	0.37	0.39	0.40	0.36	0.36	0.35
Ca	0.09	0.13	0.13	0.11	0.15	0.12	0.11	0.10	0.14	0.12	0.09	0.09
Total	7.96	7.97	7.96	7.96	7.98	7.97	7.96	7.96	8.06	7.96	7.96	7.96
O value	12	12	12	12	12	12	12	12	12	12	12	12

Table C1.4. (continued)

Sample	**207693 grt 1**												
Wt%	**Rim**									**Core**			
SiO_2	38.70	37.03	36.51	38.50	38.36	37.86	39.99	40.86	38.35	44.05	38.43	39.16	38.66
Al_2O_3	21.57	21.13	22.67	21.66	21.51	21.15	22.36	17.15	21.32	18.30	21.37	21.87	21.27
FeO	37.94	37.69	36.92	37.97	38.27	38.32	38.24	36.46	37.65	34.68	37.57	38.00	38.20
MnO	0.47	0.53	0.47	0.49	0.54	0.50	0.54	0.51	0.49	0.48	0.46	0.61	0.57
MgO	2.12	2.34	2.17	2.17	2.16	1.84	1.66	4.42	2.09	2.10	2.10	2.02	1.78
CaO	1.11	0.99	0.79	0.69	0.85	0.93	1.03	0.93	1.38	1.18	1.28	1.18	1.02
Total	101.91	99.72	99.53	101.49	101.69	100.60	103.81	100.32	101.29	100.79	101.21	102.84	101.49
cations													
Si	3.06	3.00	2.95	3.05	3.04	3.04	3.09	3.26	3.05	3.43	3.05	3.06	3.07
Al	2.01	2.02	2.16	2.02	2.01	2.00	2.03	1.61	2.00	1.68	2.00	2.01	1.99
Fe	2.50	2.56	2.50	2.52	2.54	2.58	2.47	2.43	2.50	2.26	2.50	2.48	2.54
Mn	0.03	0.04	0.03	0.03	0.04	0.03	0.04	0.03	0.03	0.03	0.03	0.04	0.04
Mg	0.25	0.28	0.26	0.26	0.26	0.22	0.19	0.52	0.25	0.24	0.25	0.24	0.21
Ca	0.09	0.09	0.07	0.06	0.07	0.08	0.09	0.08	0.12	0.10	0.11	0.10	0.09
Total	7.94	7.99	7.97	7.94	7.95	7.96	7.90	7.94	7.95	7.73	7.94	7.93	7.93
O value	12	12	12	12	12	12	12	12	12	12	12	12	12

Table C1.4. (continued)

Sample	**207693**	**grt 1 cont**							**207693**	**grt 2**	**207693**	**Grt 3**
Wt%								**Rim**	**Rim**	**Core**	**Rim**	**Core**
SiO_2	37.30	38.86	38.82	34.63	33.43	39.92	38.77	38.81	38.56	38.20	35.57	38.55
Al_2O_3	20.89	21.37	21.40	24.88	29.89	22.55	21.37	21.60	21.39	21.40	26.57	21.36
FeO	37.74	37.52	37.73	34.98	31.68	37.73	37.79	37.65	37.77	37.88	35.20	37.77
MnO	0.54	0.56	0.50	0.48	0.42	0.48	0.48	0.51	0.49	0.51	0.49	0.51
MgO	2.31	2.17	2.20	1.63	1.25	2.19	2.31	2.23	2.27	2.40	1.80	2.09
CaO	0.98	1.08	1.01	0.88	0.74	0.91	1.01	1.09	1.17	1.14	1.05	1.38
Total	99.75	101.55	101.65	97.49	97.42	103.77	101.73	101.89	101.65	101.52	100.68	101.66
cations												
Si	3.02	3.07	3.07	2.84	2.69	3.07	3.06	3.06	3.05	3.03	2.81	3.05
Al	2.00	1.99	1.99	2.41	2.83	2.05	1.99	2.01	2.00	2.00	2.48	1.99
Fe	2.56	2.48	2.49	2.40	2.13	2.43	2.50	2.48	2.50	2.51	2.33	2.50
Mn	0.04	0.04	0.03	0.03	0.03	0.03	0.03	0.03	0.03	0.03	0.03	0.03
Mg	0.28	0.26	0.26	0.20	0.15	0.25	0.27	0.26	0.27	0.28	0.21	0.25
Ca	0.09	0.09	0.09	0.08	0.06	0.07	0.09	0.09	0.10	0.10	0.09	0.12
Total	7.98	7.93	7.93	7.96	7.89	7.90	7.94	7.94	7.95	7.97	7.95	7.95
O value	12	12	12	12	12	12	12	12	12	12	12	12

Table C1.4. (continued)

Sample	**229111**									
Wt%	**Rim**									**Core**
SiO_2	36.77	37.07	36.94	36.86	36.94	36.54	36.74	36.89	36.84	36.77
TiO_2	-0.01	0.05	0.04	0.10	0.11	0.15	0.10	0.11	0.10	0.08
Al_2O_3	21.28	21.18	21.12	21.23	21.07	20.96	21.00	21.02	21.17	21.18
FeO	36.41	36.01	36.34	36.00	35.73	35.70	35.53	35.82	35.74	35.58
MnO	0.37	0.50	0.64	0.71	0.72	0.78	0.87	0.96	0.96	0.92
MgO	3.19	3.47	3.31	3.38	3.23	3.19	3.08	3.09	3.00	3.04
CaO	1.29	1.42	1.23	1.51	1.83	1.80	1.91	1.91	1.97	2.03
Total	99.31	99.71	99.62	99.79	99.61	99.11	99.24	99.81	99.78	99.61
cations										
Si	2.98	2.99	2.99	2.97	2.98	2.97	2.98	2.98	2.98	2.97
Ti	0.00	0.00	0.00	0.01	0.01	0.01	0.01	0.01	0.01	0.01
Al	2.03	2.01	2.01	2.02	2.01	2.01	2.01	2.00	2.02	2.02
Fe	2.47	2.43	2.46	2.43	2.41	2.43	2.41	2.42	2.41	2.41
Mn	0.03	0.03	0.04	0.05	0.05	0.05	0.06	0.07	0.07	0.06
Mg	0.39	0.42	0.40	0.41	0.39	0.39	0.37	0.37	0.36	0.37
Ca	0.11	0.12	0.11	0.13	0.16	0.16	0.17	0.17	0.17	0.18
Total	8.00	8.00	8.01	8.01	8.01	8.01	8.01	8.01	8.01	8.01
O value	12	12	12	12	12	12	12	12	12	12

Table C1.4. (continued)

Sample	**229111 cont.**									
Wt%										**Rim**
SiO_2	36.67	36.81	36.65	36.78	36.80	36.65	36.68	36.63	36.82	36.91
TiO_2	0.12	0.14	0.12	0.13	0.10	0.05	0.04	0.03	0.02	0.02
Al_2O_3	21.05	21.03	21.08	21.05	21.06	21.03	21.18	21.14	21.15	21.03
FeO	35.76	35.67	35.74	35.95	35.92	36.22	36.50	35.89	36.23	36.15
MnO	0.94	0.86	0.95	0.86	0.83	0.77	0.79	0.62	0.47	0.40
MgO	3.02	3.05	3.01	3.00	3.01	3.05	3.04	3.17	3.30	3.30
CaO	1.94	1.90	1.96	1.83	1.79	1.45	1.21	1.68	1.38	1.41
Total	99.50	99.45	99.52	99.60	99.51	99.22	99.44	99.16	99.37	99.24
cations										
Si	2.97	2.98	2.97	2.98	2.98	2.98	2.98	2.97	2.98	2.99
Ti	0.01	0.01	0.01	0.01	0.01	0.00	0.00	0.00	0.00	0.00
Al	2.01	2.01	2.01	2.01	2.01	2.02	2.03	2.02	2.02	2.01
Fe	2.42	2.42	2.42	2.43	2.43	2.46	2.48	2.44	2.45	2.45
Mn	0.06	0.06	0.07	0.06	0.06	0.05	0.05	0.04	0.03	0.03
Mg	0.37	0.37	0.36	0.36	0.36	0.37	0.37	0.38	0.40	0.40
Ca	0.17	0.17	0.17	0.16	0.16	0.13	0.11	0.15	0.12	0.12
Total	8.01	8.01	8.01	8.01	8.01	8.01	8.01	8.01	8.01	8.00
O value	12	12	12	12	12	12	12	12	12	12

Table C1.4. (continued)

Sample	**229115 grt 1**													
Wt%	**Rim**										**Core**			
SiO_2	37.25	37.20	31.87	40.02	37.17	37.56	37.64	37.47	37.82	37.52	37.43	37.74	37.44	37.67
TiO_2	0.01	0.04	0.04	0.01	0.00	-0.02	0.02	-0.01	0.02	0.01	-0.01	0.03	0.04	0.02
Al_2O_3	20.75	20.61	32.27	19.07	20.56	20.89	20.62	20.71	20.74	20.52	20.58	20.80	20.58	20.56
FeO	37.09	36.71	30.70	35.42	35.55	35.48	35.51	35.46	35.30	35.48	35.61	35.55	35.67	35.71
MnO	2.28	2.24	1.94	2.68	3.09	3.24	3.42	3.48	3.41	3.49	3.38	3.37	3.16	2.98
MgO	1.90	1.98	1.54	1.79	2.02	1.98	2.05	2.02	2.00	2.12	2.05	2.03	1.91	1.99
CaO	0.94	1.18	1.17	1.19	1.25	1.47	1.54	1.49	1.42	1.46	1.48	1.50	1.41	1.62
Total	100.23	99.96	99.53	100.19	99.64	100.61	100.79	100.62	100.72	100.61	100.52	101.02	100.21	100.55
cations														
Si	3.02	3.02	2.52	3.21	3.03	3.03	3.03	3.02	3.04	3.03	3.02	3.03	3.03	3.04
Ti	0.00	0.00	0.00	0.00	0.00	0.00	0.00	0.00	0.00	0.00	0.00	0.00	0.00	0.00
Al	1.98	1.97	3.01	1.80	1.97	1.98	1.96	1.97	1.97	1.95	1.96	1.97	1.96	1.95
Fe	2.51	2.49	2.03	2.38	2.42	2.39	2.39	2.39	2.37	2.39	2.41	2.39	2.42	2.41
Mn	0.16	0.15	0.13	0.18	0.21	0.22	0.23	0.24	0.23	0.24	0.23	0.23	0.22	0.20
Mg	0.23	0.24	0.18	0.21	0.24	0.24	0.25	0.24	0.24	0.26	0.25	0.24	0.23	0.24
Ca	0.08	0.10	0.10	0.10	0.11	0.13	0.13	0.13	0.12	0.13	0.13	0.13	0.12	0.14
Total	7.99	7.99	7.97	7.89	7.99	7.98	7.99	7.99	7.97	8.00	8.00	7.99	7.98	7.98
O value	12	12	12	12	12	12	12	12	12	12	12	12	12	12

Table C1.4. (continued)

Sample	**229115 grt 1 cont.**				**229115 grt 2**							
Wt%				**Rim**	**Rim**							
SiO_2	37.13	38.02	37.30	37.19	37.49	37.45	37.31	37.24	37.27	37.38	37.62	37.36
TiO_2	0.07	0.03	0.07	0.01	-0.01	0.04	0.04	0.05	0.06	0.05	0.04	0.04
Al_2O_3	20.57	20.74	20.80	20.48	20.65	20.70	20.66	20.58	20.53	20.54	20.69	20.63
FeO	36.09	36.21	36.65	37.22	37.34	37.02	36.91	36.82	36.74	36.85	36.66	36.82
MnO	2.74	2.61	2.34	2.23	2.11	2.16	2.18	2.24	2.31	2.25	2.23	2.29
MgO	2.01	2.02	1.97	1.87	1.89	2.03	2.01	2.05	2.08	2.05	2.02	1.98
CaO	1.50	1.44	1.25	1.05	0.95	1.10	1.12	1.09	1.15	1.14	1.25	1.32
Total	100.11	101.06	100.37	100.06	100.43	100.49	100.23	100.06	100.14	100.25	100.50	100.44
cations												
Si	3.01	3.05	3.02	3.03	3.03	3.03	3.02	3.02	3.02	3.03	3.03	3.02
Ti	0.00	0.00	0.00	0.00	0.00	0.00	0.00	0.00	0.00	0.00	0.00	0.00
Al	1.97	1.96	1.98	1.96	1.97	1.97	1.97	1.97	1.96	1.96	1.97	1.97
Fe	2.45	2.43	2.48	2.53	2.53	2.50	2.50	2.50	2.49	2.50	2.47	2.49
Mn	0.19	0.18	0.16	0.15	0.14	0.15	0.15	0.15	0.16	0.15	0.15	0.16
Mg	0.24	0.24	0.24	0.23	0.23	0.24	0.24	0.25	0.25	0.25	0.24	0.24
Ca	0.13	0.12	0.11	0.09	0.08	0.09	0.10	0.09	0.10	0.10	0.11	0.11
Total	8.00	7.97	7.99	7.99	7.98	7.99	7.99	7.99	7.99	7.99	7.98	7.99
O value	12	12	12	12	12	12	12	12	12	12	12	12

Table C1.4. (continued)

Sample	**229115 grt 2 cont.**									
Wt%	**Core**									**Rim**
SiO_2	37.43	37.34	37.64	37.59	37.58	37.39	37.42	37.36	37.57	37.25
TiO_2	0.06	0.01	0.00	0.02	0.04	0.06	0.03	-0.02	0.04	0.01
Al_2O_3	20.73	20.77	20.68	20.73	20.56	20.84	20.54	20.85	20.63	20.65
FeO	36.20	36.20	36.31	36.22	36.54	36.29	36.52	37.13	37.06	37.43
MnO	2.27	2.42	2.35	2.37	2.33	2.34	2.23	2.25	2.15	2.12
MgO	1.99	1.99	2.00	2.00	1.99	2.01	2.06	2.04	2.04	1.81
CaO	1.65	1.65	1.43	1.53	1.40	1.54	1.42	1.01	1.06	0.87
Total	100.32	100.37	100.41	100.46	100.44	100.47	100.23	100.61	100.57	100.14
cations										
Si	3.02	3.02	3.04	3.03	3.04	3.02	3.03	3.02	3.03	3.03
Ti	0.00	0.00	0.00	0.00	0.00	0.00	0.00	0.00	0.00	0.00
Al	1.97	1.98	1.97	1.97	1.96	1.98	1.96	1.98	1.96	1.98
Fe	2.45	2.45	2.45	2.44	2.47	2.45	2.47	2.51	2.50	2.54
Mn	0.16	0.17	0.16	0.16	0.16	0.16	0.15	0.15	0.15	0.15
Mg	0.24	0.24	0.24	0.24	0.24	0.24	0.25	0.25	0.25	0.22
Ca	0.14	0.14	0.12	0.13	0.12	0.13	0.12	0.09	0.09	0.08
Total	7.99	7.99	7.98	7.98	7.98	7.99	7.99	7.99	7.98	7.99
O value	12	12	12	12	12	12	12	12	12	12

Table C1.4. (continued)

Sample	**229119 grt 1**													
Wt%	**Rim**										**Core**			
SiO_2	37.00	37.18	37.50	37.08	37.17	37.13	37.04	36.87	37.02	36.99	37.12	37.02	37.03	37.09
TiO_2	0.05	0.02	0.06	0.07	0.03	0.05	0.01	0.01	0.05	0.05	0.03	0.07	0.06	0.10
Al_2O_3	21.40	21.34	21.74	21.40	21.27	21.53	21.52	21.37	21.48	21.43	21.59	21.36	21.42	21.43
FeO	35.34	35.70	35.82	35.75	35.84	35.69	36.04	35.93	35.83	35.86	36.01	35.83	35.88	35.63
MnO	0.37	0.42	0.50	0.59	0.61	0.65	0.78	0.80	0.77	0.73	0.73	0.72	0.73	0.71
MgO	3.58	3.22	3.00	2.92	2.94	2.72	2.81	2.74	2.86	3.06	3.01	3.01	2.97	3.00
CaO	1.83	2.04	2.04	2.04	2.14	2.07	2.05	2.00	2.02	1.92	1.67	1.88	1.93	2.00
Total	99.58	99.92	100.67	99.85	100.00	99.85	100.26	99.73	100.02	100.04	100.16	99.88	100.03	99.96
cations														
Si	2.98	2.99	2.99	2.99	2.99	2.99	2.98	2.98	2.98	2.98	2.98	2.98	2.98	2.98
Ti	0.00	0.00	0.00	0.00	0.00	0.00	0.00	0.00	0.00	0.00	0.00	0.00	0.00	0.01
Al	2.03	2.02	2.04	2.03	2.02	2.04	2.04	2.04	2.04	2.03	2.04	2.03	2.03	2.03
Fe	2.38	2.40	2.39	2.41	2.41	2.40	2.42	2.43	2.41	2.41	2.42	2.41	2.41	2.40
Mn	0.03	0.03	0.03	0.04	0.04	0.04	0.05	0.05	0.05	0.05	0.05	0.05	0.05	0.05
Mg	0.43	0.39	0.36	0.35	0.35	0.33	0.34	0.33	0.34	0.37	0.36	0.36	0.36	0.36
Ca	0.16	0.18	0.17	0.18	0.18	0.18	0.18	0.17	0.17	0.17	0.14	0.16	0.17	0.17
Total	8.00	8.00	7.99	7.99	8.00	7.99	8.00	8.00	8.00	8.01	8.00	8.00	8.00	8.00
O value	12	12	12	12	12	12	12	12	12	12	12	12	12	12

Table C1.4. (continued)

Sample	**229119 grt 1 cont.**				**229119 grt 2**						
Wt%				**Rim**	**Rim**						
SiO_2	37.27	37.20	37.02	37.16	37.09	37.51	37.12	36.53	37.17	37.38	36.89
TiO_2	0.04	0.07	0.07	0.04	0.01	0.04	0.06	0.11	0.06	0.04	0.09
Al_2O_3	21.40	21.22	21.22	21.30	21.22	21.55	21.39	21.09	21.41	21.43	21.29
FeO	35.74	35.48	35.64	35.39	35.68	35.34	35.58	35.72	35.88	35.79	35.54
MnO	0.74	0.72	0.62	0.48	0.44	0.47	0.57	0.86	0.86	0.90	0.92
MgO	2.98	3.08	3.11	3.27	3.25	3.24	3.06	2.93	2.97	2.95	2.92
CaO	1.97	1.97	1.97	2.08	1.83	2.05	1.99	1.93	1.90	1.83	2.15
Total	100.14	99.74	99.65	99.73	99.53	100.20	99.77	99.16	100.24	100.32	99.80
cations											
Si	2.99	3.00	2.99	2.99	2.99	3.00	2.99	2.97	2.98	3.00	2.98
Ti	0.00	0.00	0.00	0.00	0.00	0.00	0.00	0.01	0.00	0.00	0.01
Al	2.02	2.01	2.02	2.02	2.02	2.03	2.03	2.02	2.03	2.02	2.03
Fe	2.40	2.39	2.40	2.38	2.41	2.36	2.40	2.43	2.41	2.40	2.40
Mn	0.05	0.05	0.04	0.03	0.03	0.03	0.04	0.06	0.06	0.06	0.06
Mg	0.36	0.37	0.37	0.39	0.39	0.39	0.37	0.35	0.35	0.35	0.35
Ca	0.17	0.17	0.17	0.18	0.16	0.18	0.17	0.17	0.16	0.16	0.19
Total	7.99	7.99	8.00	8.00	8.00	7.99	7.99	8.01	8.00	7.99	8.01
O value	12	12	12	12	12	12	12	12	12	12	12

Table C1.4. (continued)

Sample	**229119 grt 2 cont.**										
Wt%	**Core**										**Rim**
SiO_2	37.28	36.93	37.00	36.89	37.00	37.12	36.58	37.11	36.85	37.39	36.98
TiO_2	0.12	0.07	0.05	0.11	0.10	0.08	0.09	0.04	0.07	0.06	0.04
Al_2O_3	21.42	21.25	21.26	21.14	21.27	21.22	21.06	21.29	21.33	21.37	21.38
FeO	35.28	35.63	36.09	35.53	35.16	35.41	35.26	35.31	35.46	35.51	35.45
MnO	1.00	1.05	1.10	1.02	0.95	0.88	0.73	0.60	0.49	0.50	0.47
MgO	2.91	2.94	2.49	2.87	2.99	3.07	3.24	3.24	3.38	3.32	3.32
CaO	2.29	1.98	1.93	2.05	2.23	2.08	2.11	1.90	1.79	1.98	1.90
Total	100.30	99.85	99.93	99.60	99.71	99.86	99.07	99.48	99.36	100.12	99.54
cations											
Si	2.99	2.98	2.99	2.98	2.98	2.99	2.97	2.99	2.98	2.99	2.98
Ti	0.01	0.00	0.00	0.01	0.01	0.01	0.01	0.00	0.00	0.00	0.00
Al	2.02	2.02	2.02	2.02	2.02	2.01	2.02	2.02	2.03	2.02	2.03
Fe	2.36	2.40	2.44	2.40	2.37	2.38	2.40	2.38	2.40	2.38	2.39
Mn	0.07	0.07	0.07	0.07	0.07	0.06	0.05	0.04	0.03	0.03	0.03
Mg	0.35	0.35	0.30	0.35	0.36	0.37	0.39	0.39	0.41	0.40	0.40
Ca	0.20	0.17	0.17	0.18	0.19	0.18	0.18	0.16	0.15	0.17	0.16
Total	7.99	8.01	8.00	8.00	8.00	8.00	8.02	7.99	8.00	7.99	8.00
O value	12	12	12	12	12	12	12	12	12	12	12

Table C1.4. (continued)

Sample	229120 grt 1											229120 grt 2		229120 grt 3	
Wt%	Rim										Core	Rim	Core	Rim	Core
SiO_2	37.60	36.91	36.98	37.48	37.74	37.91	38.13	38.12	101.37	38.50	38.45	36.33	36.05	37.89	37.87
TiO_2	0.07	0.06	0.05	0.07	0.06	0.04	0.05	0.01	-0.01	0.00	0.00	0.02	0.04	0.02	0.01
Al_2O_3	20.81	20.12	20.34	20.57	20.82	20.90	20.99	21.21	0.18	21.65	21.40	19.89	20.01	20.85	20.90
FeO	35.91	36.03	36.27	36.24	36.41	36.20	36.19	36.09	1.05	35.72	36.40	36.99	36.71	36.78	36.46
MnO	1.06	0.92	0.93	0.84	0.76	0.69	0.60	0.57	0.00	0.47	0.52	0.76	0.68	0.68	0.64
MgO	2.86	2.80	2.77	2.83	2.88	2.90	3.09	3.18	-0.02	3.42	2.78	2.18	2.45	2.41	2.82
CaO	1.92	2.03	1.96	1.84	1.84	1.95	1.90	1.85	0.02	1.74	1.85	1.65	1.63	1.62	1.60
Total	100.23	98.86	99.30	99.87	100.50	100.58	100.96	101.03	102.59	101.50	101.41	97.81	97.57	100.26	100.30
cations															
Si	3.02	3.02	3.01	3.03	3.02	3.03	3.03	3.03	5.97	3.03	3.04	3.02	3.00	3.04	3.04
Ti	0.00	0.00	0.00	0.00	0.00	0.00	0.00	0.00	0.00	0.00	0.00	0.00	0.00	0.00	0.00
Al	1.97	1.94	1.95	1.96	1.97	1.97	1.97	1.98	0.01	2.01	1.99	1.95	1.96	1.97	1.98
Fe	2.41	2.46	2.47	2.45	2.44	2.42	2.41	2.40	0.05	2.35	2.41	2.57	2.55	2.47	2.44
Mn	0.07	0.06	0.06	0.06	0.05	0.05	0.04	0.04	0.00	0.03	0.04	0.05	0.05	0.05	0.04
Mg	0.34	0.34	0.34	0.34	0.34	0.35	0.37	0.38	0.00	0.40	0.33	0.27	0.30	0.29	0.34
Ca	0.17	0.18	0.17	0.16	0.16	0.17	0.16	0.16	0.00	0.15	0.16	0.15	0.14	0.14	0.14
Total	7.99	8.01	8.01	7.99	7.99	7.98	7.98	7.98	6.03	7.97	7.96	8.01	8.02	7.97	7.98
O value	12	12	12	12	12	12	12	12	12	12	12	12	12	12	12

Table C1.4. (continued)

Sample	**229151 grt 1**										
Wt%	**Rim**										**Rim**
SiO_2	37.70	37.74	37.83	37.85	37.89	38.03	37.93	38.03	38.21	37.99	37.90
TiO_2	0.05	0.02	0.03	0.04	0.09	0.03	0.03	0.05	0.00	0.14	0.05
Al_2O_3	20.78	20.65	20.59	20.81	20.46	20.77	20.84	20.86	21.03	20.78	20.85
FeO	36.61	36.38	36.78	36.44	35.95	36.09	36.43	36.40	36.65	36.66	36.64
MnO	0.77	0.71	0.76	0.73	0.72	0.73	0.74	0.77	0.77	0.74	0.72
MgO	2.05	2.21	2.13	2.10	2.09	2.23	2.31	2.17	1.85	1.79	2.20
CaO	2.53	2.43	2.38	2.52	3.04	2.48	2.29	2.47	2.53	2.47	2.43
Total	100.48	100.15	100.49	100.49	100.24	100.35	100.56	100.75	101.03	100.58	100.81
cations											
Si	3.03	3.04	3.04	3.04	3.05	3.05	3.04	3.04	3.05	3.05	3.03
Ti	0.00	0.00	0.00	0.00	0.01	0.00	0.00	0.00	0.00	0.01	0.00
Al	1.97	1.96	1.95	1.97	1.94	1.96	1.97	1.97	1.98	1.97	1.97
Fe	2.46	2.45	2.47	2.45	2.42	2.42	2.44	2.44	2.45	2.46	2.45
Mn	0.05	0.05	0.05	0.05	0.05	0.05	0.05	0.05	0.05	0.05	0.05
Mg	0.25	0.26	0.25	0.25	0.25	0.27	0.28	0.26	0.22	0.21	0.26
Ca	0.22	0.21	0.21	0.22	0.26	0.21	0.20	0.21	0.22	0.21	0.21
Total	7.98	7.98	7.98	7.97	7.98	7.97	7.97	7.97	7.96	7.96	7.98
O value	12	12	12	12	12	12	12	12	12	12	12

Table C1.5. EPMA analyses of chlorite.

Sample	229111				229115							
Wt%												
SiO_2	23.66	24.12	24.07	23.87	22.08	22.11	22.88	23.46	22.71	22.90	21.94	22.40
TiO_2	0.12	0.11	0.08	0.08	0.04	0.02	0.04	0.12	0.13	0.12	0.06	0.09
Al_2O_3	22.46	22.06	21.81	22.20	21.02	20.83	22.74	22.35	22.48	22.59	22.86	22.12
FeO	25.31	25.29	22.86	24.97	34.18	35.53	28.79	27.82	28.64	28.88	28.88	29.02
MnO	0.02	0.00	0.02	0.04	1.65	1.62	0.15	0.27	0.15	0.17	0.22	0.16
MgO	14.49	14.01	16.55	15.70	5.65	4.86	10.92	11.64	10.88	11.04	10.42	11.37
CaO	0.01	0.00	0.03	0.05	0.04	0.03	0.02	0.04	0.01	0.02	0.04	0.01
Na_2O	0.00	-0.01	-0.01	0.01	-0.01	0.01	0.02	0.00	-0.02	0.00	0.02	0.02
K_2O	0.00	0.00	0.02	0.00	0.02	0.02	0.01	0.01	0.00	0.01	0.01	0.00
Total	86.08	85.57	85.42	86.93	84.68	85.01	85.56	85.70	84.98	85.73	84.44	85.20
cations												
Si	6.55	6.71	6.63	6.53	6.63	6.66	6.51	6.62	6.51	6.51	6.35	6.43
Ti	0.03	0.02	0.02	0.02	0.01	0.00	0.01	0.02	0.03	0.03	0.01	0.02
Al	7.33	7.23	7.08	7.16	7.44	7.40	7.63	7.44	7.59	7.57	7.80	7.48
Fe	5.86	5.88	5.27	5.72	8.59	8.96	6.85	6.57	6.86	6.86	6.99	6.97
Mn	0.01	0.00	0.00	0.01	0.42	0.41	0.04	0.06	0.04	0.04	0.05	0.04
Mg	5.98	5.81	6.80	6.41	2.53	2.18	4.63	4.90	4.65	4.68	4.50	4.86
Ca	0.00	0.00	0.01	0.01	0.01	0.01	0.01	0.01	0.00	0.00	0.01	0.00
Na	0.00	-0.01	-0.01	0.01	0.00	0.00	0.01	0.00	-0.01	0.00	0.01	0.01
K	0.00	0.00	0.01	0.00	0.01	0.01	0.00	0.00	0.00	0.00	0.00	0.00
Total	25.76	25.65	25.81	25.87	25.64	25.64	25.68	25.63	25.67	25.69	25.74	25.82
O value	36	36	36	36	36	36	36	36	36	36	36	36

Table C1.5. (continued).

Sample	229119							229120				
Wt%												
SiO_2	24.47	24.03	24.33	24.83	23.33	24.83	24.63	30.24	24.11	24.05	25.24	24.16
TiO_2	0.23	0.32	0.17	0.15	0.05	0.05	0.05	0.03	0.10	0.08	0.07	0.07
Al_2O_3	21.90	22.28	22.22	21.77	21.44	23.94	22.48	20.74	22.22	22.56	22.95	22.23
FeO	24.88	25.09	24.91	24.94	24.12	24.07	24.73	27.56	25.34	25.25	24.61	25.47
MnO	0.02	0.02	0.01	0.00	0.07	0.06	0.06	0.04	-0.02	0.01	0.01	0.00
MgO	13.96	14.25	14.22	13.69	13.76	13.66	15.21	9.77	14.26	14.37	13.75	13.87
CaO	0.00	0.02	0.01	0.08	0.03	0.11	0.03	0.04	0.01	0.01	0.02	0.01
Na_2O	0.03	0.00	0.01	0.01	0.01	0.01	0.03	0.01	-0.01	0.01	0.04	0.02
K_2O	0.13	0.00	0.01	0.04	0.01	0.02	0.00	0.00	0.01	0.03	0.39	0.01
Total	85.61	86.01	85.88	85.52	82.81	86.73	87.21	88.44	86.04	86.38	87.08	85.83
cations												
Si	6.79	6.64	6.72	6.89	6.70	6.73	6.69	8.07	6.67	6.62	6.86	6.70
Ti	0.05	0.07	0.03	0.03	0.01	0.01	0.01	0.01	0.02	0.02	0.01	0.01
Al	7.16	7.26	7.24	7.12	7.25	7.65	7.20	6.52	7.25	7.32	7.35	7.27
Fe	5.77	5.80	5.76	5.79	5.79	5.46	5.62	6.15	5.86	5.82	5.59	5.91
Mn	0.01	0.00	0.00	0.00	0.02	0.01	0.01	0.01	0.00	0.00	0.00	0.00
Mg	5.77	5.88	5.86	5.66	5.89	5.52	6.16	3.89	5.88	5.90	5.57	5.74
Ca	0.00	0.01	0.00	0.02	0.01	0.03	0.01	0.01	0.00	0.00	0.00	0.00
Na	0.01	0.00	0.00	0.01	0.01	0.00	0.01	0.01	0.00	0.01	0.02	0.01
K	0.04	0.00	0.00	0.01	0.00	0.01	0.00	0.00	0.00	0.01	0.14	0.00
Total	25.61	25.66	25.62	25.53	25.67	25.43	25.71	24.67	25.68	25.71	25.54	25.65
O value	36	36	36	36	36	36	36	36	36	36	36	36

Table C1.6. EPMA analyses of apatite.

Sample	229111			229115			229119			229120				
Wt%														
P_2O_5	41.80	39.11	37.95	41.61	42.08	41.70	39.97	42.84	43.26	42.64	42.21	42.01	42.18	43.09
FeO	1.14	1.07	3.01	0.00	0.00	0.01	1.92	0.46	0.67	0.93	1.14	0.93	0.99	0.70
MnO	0.03	0.05	0.09	0.04	0.06	0.04	0.23	-0.01	-0.01	0.07	0.01	0.03	0.03	-0.02
MgO	0.02	0.02	0.21	0.02	0.00	0.01	0.07	0.00	0.02	0.02	0.03	0.01	0.00	0.01
CaO	55.43	53.97	51.77	55.23	55.18	55.18	53.00	55.36	55.86	55.15	54.71	54.94	55.74	56.43
Cl	0.05	0.04	0.05	0.01	0.00	0.00	0.02	0.02	0.03	0.05	0.09	0.06	0.05	0.03
F	2.77	3.12	1.92	3.26	3.20	3.20	2.69	3.19	3.09	2.44	2.05	3.07	3.11	3.29
Total	100.06	96.07	94.18	98.79	99.17	98.79	96.77	100.52	101.60	100.26	99.36	99.74	100.78	102.14
cations														
P	2.97	2.92	2.90	2.99	3.00	2.99	2.95	3.02	3.01	3.00	3.00	2.99	2.98	3.00
Fe	0.08	0.08	0.23	0.00	0.00	0.00	0.14	0.03	0.05	0.07	0.08	0.07	0.07	0.05
Mn	0.00	0.00	0.01	0.00	0.00	0.00	0.02	0.00	0.00	0.00	0.00	0.00	0.00	0.00
Mg	0.00	0.00	0.03	0.00	0.00	0.00	0.01	0.00	0.00	0.00	0.00	0.00	0.00	0.00
Ca	4.99	5.11	5.00	5.02	4.99	5.01	4.95	4.93	4.92	4.92	4.92	4.95	4.98	4.96
Cl	0.01	0.01	0.01	0.00	0.00	0.00	0.00	0.00	0.00	0.01	0.01	0.01	0.01	0.00
F	0.69	0.81	0.52	0.82	0.80	0.80	0.70	0.79	0.76	0.61	0.52	0.77	0.77	0.80
Total	8.74	8.93	8.69	8.83	8.79	8.81	8.78	8.77	8.74	8.61	8.53	8.79	8.81	8.81
O value	12.5	12.5	12.5	12.5	12.5	12.5	12.5	12.5	12.5	12.5	12.5	12.5	12.5	12.5

Appendix D: Lu-Hf and Sm-Nd isotope data

Table D1.1. Lu-Hf and Sm-Nd isotope data.

Sample	Lu(ppm)	Hf (ppm)	$^{176}Lu/^{177}Hf$	$^{176}Hf/^{177}Hf$	2SE error		Sm (ppm)	Nd (ppm)	$^{147}Sm/^{144}Nd$	$^{143}Nd/^{144}Nd$	2SE error
207692											
whole-rock B	0.211	2.814	0.0106	0.28162	0.000004		2.00	9.50	0.1249	0.511139	0.000009
whole-rock TT	0.250	2.867	0.0124	0.28163	0.000006		2.60	13.3	0.1192	0.511183	0.000008
garnet 1	1.007	2.938	0.0486	0.2835	0.000008		3.70	11.3	0.1981	0.512542	0.000014
garnet 2	0.960	2.951	0.0461	0.28336	0.000011		3.90	12.8	0.1869	0.512353	0.000009
garnet 3	1.017	2.989	0.0483	0.28347	0.000005		4.00	13.0	0.1871	0.512360	0.000012
garnet 4	1.006	2.971	0.0481	0.28346	0.000005		4.00	12.6	0.1898	0.512387	0.000013
garnet 5	1.025	2.834	0.0513	0.28363	0.000004		3.91	12.6	0.1879	0.512365	0.000005
229151											
whole-rock B	0.259	3.035	0.0121	0.28151	0.000007		3.03	14.1	0.1300	0.511260	0.000003
whole-rock TT	0.269	2.874	0.0133	0.28156	0.000011		2.99	13.9	0.1301	0.511266	0.000005
garnet 1	0.868	2.598	0.0474	0.28331	0.000005		2.94	7.87	0.2262	0.512912	0.000004
garnet 2	0.647	2.358	0.039	0.2829	0.000006		3.28	8.36	0.2374	0.513103	0.000003
garnet 3	0.781	2.499	0.0443	0.28317	0.000006		3.09	8.07	0.2318	0.512999	0.000004
garnet 4	0.845	2.508	0.0478	0.28333	0.000003		3.15	8.06	0.2365	0.513075	0.000003
garnet 5	0.822	2.380	0.049	0.2834	0.000005		2.03	5.10	0.2401	0.513139	0.000003

Appendix E: Garnet trace element analysis

Table E1.1. Garnet REE and Hf analyses in ppm.

Sample	^{139}La	±	^{140}Ce	±	^{141}Pr	±	^{146}Nd	±	^{147}Sm	±
207692 grt a.1										1.2
207692 grt a.2							0.27	0.39	2.8	1.3
207692 grt a.3					0.015	0.026	0.59	0.49	2.81	0.97
207692 grt a.4			0.035	0.058	0.009	0.025	0.71	0.47	2.2	1
207692 grt a.5	330	150	630	340	69	34	240	120	52	25
207692 grt a.6	55	13	149	48	12.2	3.7	49	18	10.6	2.6
207692 grt a.7	19.9	5.4	40	11	3.39	0.97	15.4	3.7	5.6	1.4
207692 grt a.8	10.9	4.1	38	13	2.63	0.77	10.5	3.3	3.97	0.79
207692 grt a.9	6.7	1.1	19.9	6.4	2.33	0.79	8.4	2.9	3.6	1.1
207692 grt a.10	3.3	2.1	12	4.9	1.24	0.71	3.4	2	3.2	1.8
207692 grt a.11	2.1	2	7.7	4.4	1.8	1.5	1.9	1.3	3.1	1.1
207692 grt b.1			0.1	0.24			0.19	0.37	0.67	0.47
207692 grt b.2	2.2	1.1	5.2	4.3	0.7	0.54	1.1	1.6	0.9	0.44
207692 grt b.3	76	86	160	180	18	20	69	76	14	13
207692 grt b.4	6	2.6	25.7	8.6	1.79	0.8	6.8	3	3.4	1.2
207692 grt b.5	3.5	2.4	20	10	1.55	0.77	7.9	3.8	3.6	1.9
207692 grt b.6	3.8	1.6	13.3	5.8	1.56	0.67	4.3	1.4	3.6	1.4
207692 grt b.7	3.21	0.96	6.5	1.4	0.83	0.28	2.7	1.2	2.8	1
207692 grt b.8	2.6	1.6	6.5	2.7	0.66	0.35	2.5	1.1	2.8	1.8
207692 grt b.9	2.4	1.5	5.6	2.4	0.38	0.2	2.3	1	2.22	0.82
207692 grt b.10	0.72	0.33	2.08	0.84	0.37	0.2	1.45	0.66	1.8	0.7
207692 grt b.11	0.8	0.5	2.9	2	0.2	0.15	1.42	0.64	2.69	0.94
207692 grt b.12	0.48	0.27	1.4	0.66	0.16	0.11	0.79	0.72	2.6	1.1
207692 grt b.13	0.61	0.46	2.4	2	0.18	0.12	1.39	0.88	2.54	0.85
207692 grt b.14	1.08	0.91	0.99	0.59	0.14	0.14	1.08	0.73	1.71	0.79
207692 grt c.1					0.016	0.057			1.81	0.8
207692 grt c.2			0.06	0.079			0.36	0.35	1.31	0.63
207692 grt c.3							0.49	0.39	1.47	0.9
207692 grt c.4					0.007	0.024	0.54	0.44	2.12	0.87
207692 grt c.5			0.131	0.069	0.034	0.062	1.24	0.53	2.07	0.8
207692 grt c.6					0.009	0.027	0.68	0.45	2.19	0.97
207692 grt c.7	0.004	0.027	0.14	0.11	0.007	0.025	0.3	0.33	1.8	1.1
207692 grt c.8	0.003	0.023	0.018	0.034			0.19	0.16	1.92	0.88

Blanks indicate below detection limit.

Table E1.1. (continued)

Sample	^{153}Eu	±	^{157}Gd	±	^{159}Tb	±	^{163}Dy	±	^{165}Ho	±
207692 grt a.1	1.65	0.58	9.3	1.7	0.94	0.26	6.7	1.4	1.18	0.39
207692 grt a.2	2.06	0.42	15.2	3.5	4.8	0.5	39.7	4	6.75	0.6
207692 grt a.3	1.89	0.48	8	1.8	1.68	0.31	18.1	2	4.31	0.53
207692 grt a.4	2.13	0.41	5.3	1	1.25	0.23	9.9	1.1	2.23	0.35
207692 grt a.5	10.4	6	40	15	6.7	1.8	40.1	6.7	9.2	1
207692 grt a.6	3.99	0.74	8.9	1.9	1.65	0.35	11.4	1.5	2.53	0.32
207692 grt a.7	3.05	0.43	5.3	1.3	0.87	0.2	5.8	1.2	1.05	0.27
207692 grt a.8	3.38	0.54	4.1	1.1	0.51	0.14	3.51	0.88	0.7	0.14
207692 grt a.9	3	0.5	3.12	0.81	0.48	0.16	2.82	0.97	0.55	0.15
207692 grt a.10	1.96	0.37	14.9	2	3.3	0.4	21.2	2	2.46	0.46
207692 grt a.11	1.74	0.4	8.8	1.2	1.54	0.24	9.1	1.2	1.42	0.17
207692 grt b.1	1.6	0.62	6.8	2.2	1.18	0.28	8.6	1.9	2.25	0.64
207692 grt b.2	1.21	0.36	8	2.9	1.12	0.31	11.8	1.5	2.42	0.78
207692 grt b.3	3.7	1.6	20.8	8.4	3.99	0.9	33.3	7.1	7.2	1.1
207692 grt b.4	2.04	0.33	9.3	1.7	2.69	0.39	23.2	2.9	5.52	0.47
207692 grt b.5	2.69	0.73	12.4	2.5	2.46	0.44	18.7	3.6	4.42	0.86
207692 grt b.6	2.11	0.44	7.8	2.2	2.09	0.33	15.6	1.9	3.41	0.47
207692 grt b.7	2.1	0.49	8.9	2.1	2.49	0.34	23.7	2.4	5.32	0.49
207692 grt b.8	2.48	0.5	13.2	3	2.74	0.36	26.1	5.9	4.48	0.73
207692 grt b.9	1.84	0.41	10.2	1	2.77	0.33	27.2	2.8	7.49	0.89
207692 grt b.10	2.43	0.5	9.1	1.6	2.77	0.29	27.4	2.1	6.38	0.4
207692 grt b.11	2.52	0.54	8.6	1.3	2.22	0.22	19.6	2.3	3.89	0.48
207692 grt b.12	2.22	0.54	13.6	1.7	3.56	0.44	24.6	2.5	4.93	0.45
207692 grt b.13	1.99	0.34	8.2	1.7	1.09	0.21	6.8	1.1	1.28	0.21
207692 grt b.14	1.37	0.63	6.3	1.2	0.84	0.19	6.5	1.1	1.49	0.4
207692 grt c.1	1.04	0.61	5.1	2.3	0.62	0.31	5.8	2.3	1.04	0.32
207692 grt c.2	2.45	0.56	5.5	1.2	1.14	0.26	7.2	1.2	1.26	0.31
207692 grt c.3	1.4	0.32	6.1	1.5	1.19	0.29	10.3	1.1	2.7	0.35
207692 grt c.4	2.43	0.56	3.88	0.97	0.99	0.27	7.4	1.3	1.62	0.26
207692 grt c.5	2.99	0.53	3.4	1.1	0.84	0.19	5.07	0.66	1.3	0.29
207692 grt c.6	2.06	0.34	4.3	1.2	0.96	0.16	10.7	2.3	2.86	0.53
207692 grt c.7	2.52	0.5	5.5	1.2	1.05	0.23	11.7	0.99	2.65	0.41
207692 grt c.8	1.29	0.3	3.27	0.99	0.75	0.18	5.6	1.4	0.98	0.24

Table E1.1. (continued)

Sample	^{166}Er	±	^{169}Tm	±	^{172}Yb	±	^{175}Lu	±	^{178}Hf	±
207692 grt a.1	3.48	0.66	0.51	0.23	4.3	1.5	0.61	0.22	4.8	5.5
207692 grt a.2	16.4	1.9	2.6	0.57	14.3	2.7	2.09	0.31	2.6	2.7
207692 grt a.3	16	1.7	2.4	0.3	18	2.3	2.73	0.27	1.61	0.8
207692 grt a.4	5.87	0.83	0.83	0.18	5.2	1.1	0.83	0.24	0.97	0.35
207692 grt a.5	25.1	2.8	2.77	0.35	20.8	2.5	2.87	0.25	1.72	0.83
207692 grt a.6	7.6	1.5	1.13	0.19	6.1	0.76	0.93	0.2	1.85	0.53
207692 grt a.7	2.55	0.38	0.4	0.1	2.87	0.97	0.36	0.14	2.11	0.94
207692 grt a.8	1.72	0.48	0.18	0.12	1.26	0.68	0.24	0.12	1.18	0.42
207692 grt a.9	1.5	0.45	0.32	0.12	1.27	0.53	0.31	0.1	1.08	0.42
207692 grt a.10	5.9	1	0.51	0.16	2.36	0.61	0.324	0.098	1.85	0.74
207692 grt a.11	2.67	0.43	0.294	0.084	1.71	0.66	0.37	0.12	1.03	0.55
207692 grt b.1	8.4	1.4	0.98	0.24	8.9	2.5	1.42	0.55	0.39	0.47
207692 grt b.2	7.4	2.2	1.38	0.36	10.8	2.4	1.28	0.19	0.27	0.28
207692 grt b.3	26.9	2.3	4.06	0.49	32.4	2.9	4.97	0.61	3.1	1.1
207692 grt b.4	18.8	1.6	2.69	0.35	20	1.9	2.54	0.41	3.9	1.2
207692 grt b.5	11.8	1.7	1.52	0.33	12.7	1.3	1.5	0.37	1.72	0.76
207692 grt b.6	11.1	1.1	1.6	0.38	9.8	1.8	1.6	0.3	3.2	1.2
207692 grt b.7	16.1	2.1	2.4	0.41	16	2	2.27	0.28	1.83	0.56
207692 grt b.8	16	1.8	2.38	0.46	16.9	3.4	2.13	0.74	3	1.6
207692 grt b.9	24.5	2.4	3.47	0.52	25.2	3	3.61	0.33	1.55	0.58
207692 grt b.10	22.2	2.2	3.16	0.39	21.4	3.2	3.15	0.45	1.58	0.55
207692 grt b.11	12.8	1.5	1.82	0.36	14	1.9	1.97	0.25	1.39	0.72
207692 grt b.12	14.1	2.1	2.09	0.28	12.7	2	1.98	0.25	0.92	0.47
207692 grt b.13	3.09	0.63	0.33	0.11	2.66	0.87	0.36	0.14	1.66	0.74
207692 grt b.14	3.52	0.55	0.64	0.18	5.2	1.1	0.59	0.11	0.94	0.66
207692 grt c.1	1.59	0.73	0.17	0.1	2.62	0.83	0.19	0.14	1.9	1.4
207692 grt c.2	2.94	0.59	0.28	0.12	2.74	0.64	0.53	0.24	0.4	0.27
207692 grt c.3	7.78	0.84	1.22	0.24	8.9	1.6	1.45	0.24	0.55	0.43
207692 grt c.4	5.67	0.73	0.57	0.19	5	1	0.65	0.17	0.93	0.52
207692 grt c.5	2.82	0.47	0.41	0.15	3.26	0.74	0.31	0.11	1.92	0.7
207692 grt c.6	9.1	1.4	1.61	0.26	9.4	1.2	1.2	0.16	0.83	0.52
207692 grt c.7	9.2	1.6	1.31	0.19	9.3	1.3	1.31	0.33	0.66	0.35
207692 grt c.8	3.45	0.99	0.39	0.17	2.94	0.78	0.31	0.12	0.77	0.41

Table E1.1. (continued)

Sample	^{139}La	±	^{140}Ce	±	^{141}Pr	±	^{146}Nd	±	^{147}Sm	±
229151 grt a.1	0.042	0.045	0.22	0.11	0.012	0.017	0.36	0.2	0.52	0.28
229151 grt a.2					0.024	0.019	1.16	0.3	4.19	0.74
229151 grt a.3			0.01	0.019			1.04	0.37	4.12	0.84
229151 grt a.4			0.003	0.017			0.85	0.36	2.21	0.74
229151 grt a.5					0.014	0.014	0.99	0.27	2.66	0.52
229151 grt b.1					0.025	0.03	1.1	0.37	2.89	0.6
229151 grt b.2					0.005	0.011	0.81	0.32	2.7	0.73
229151 grt b.3	0.198	0.072	0.57	0.14	0.128	0.047	1.87	0.47	4.83	0.72
229151 grt b.4	0.067	0.061	0.145	0.095	0.047	0.047	0.75	0.43	2.53	0.92
229151 grt c.1	0.272	0.083	0.95	0.22	0.124	0.053	1.28	0.35	2.4	0.56
229151 grt c.2	0.045	0.029	0.203	0.066	0.009	0.014	0.94	0.31	2.32	0.52
229151 grt c.3	0.019	0.036	0.063	0.068	0.051	0.055	1.53	0.67	4.2	1.1
229151 grt c.4	0.39	0.18	0.65	0.24	0.05	0.048	1.59	0.6	3.72	0.91
229151 grt c.5			0.019	0.036	0.016	0.03	1.26	0.98	3.4	1.2
229151 grt c.6					0.031	0.021	1.29	0.39	4.95	0.9
229151 grt c.7			0.006	0.016	0.032	0.028	0.62	0.21	3.91	0.66
229151 grt c.8			0.022	0.027	0.018	0.022	0.76	0.24	6.3	1
207690 grt a.1	0.065	0.061	0.46	0.21	0.115	0.068	0.27	0.19	1.48	0.66
207690 grt a.2			0.25	0.14	0.034	0.024	1.41	0.38	4.13	0.78
207690 grt a.3					0.061	0.063	1.34	0.66	4.3	1.5
207690 grt a.4			0.021	0.025	0.016	0.024	0.95	0.32	3.31	0.89
207690 grt a.5			0.041	0.046	0.019	0.023	0.84	0.31	3.4	0.76
207690 grt a.6	0.021	0.053	0.11	0.12	0.034	0.051	0.76	0.53	3.5	1.5
207690 grt b.1	0.027	0.031	0.031	0.062	0.03	0.036	0.79	0.41	4.1	1
207690 grt b.2	0.13	0.12	0.64	0.42	0.082	0.048	2.02	0.55	5.66	0.86
207690 grt b.3			0.057	0.041	0.043	0.027	1.72	0.44	6.12	0.88
207690 grt b.4	0.025	0.034	0.066	0.042	0.022	0.021	1.14	0.33	3.22	0.69
207690 grt b.5	1.42	0.33	3.94	0.87	0.57	0.17	4.5	1.4	4.15	0.94

Table E1.1. (continued)

Sample	^{153}Eu	±	^{157}Gd	±	^{159}Tb	±	^{163}Dy	±	^{165}Ho	±
229151 grt a.1	0.18	0.082	1.08	0.47	0.136	0.061	1.14	0.43	0.212	0.06
229151 grt a.2	0.79	0.13	6.18	0.83	0.76	0.11	4.09	0.49	1.03	0.13
229151 grt a.3	0.9	0.22	4.8	1	0.79	0.13	4.77	0.72	1.02	0.16
229151 grt a.4	0.65	0.17	4.2	1.1	0.62	0.13	3.98	0.8	1.12	0.15
229151 grt a.5	0.6	0.13	3.3	0.55	0.634	0.09	4.35	0.54	1.4	0.17
229151 grt b.1	1.07	0.18	4.11	0.84	0.72	0.15	4.28	0.57	0.75	0.15
229151 grt b.2	1.1	0.16	5.32	0.78	1.23	0.15	7.74	0.81	1.5	0.18
229151 grt b.3	1.6	0.22	7.2	0.92	1.29	0.14	9.3	0.76	1.97	0.17
229151 grt b.4	0.83	0.2	5.5	1	0.81	0.19	5.44	0.86	1.23	0.17
229151 grt c.1	0.63	0.16	4.41	0.82	0.84	0.13	6.32	0.69	1.53	0.17
229151 grt c.2	0.66	0.15	4.82	0.85	1.3	0.16	12.1	1.3	3.19	0.27
229151 grt c.3	1.41	0.35	8.9	1.5	2.1	0.33	18.8	1.9	4.71	0.53
229151 grt c.4	1.84	0.49	9.4	1.4	1.99	0.29	19.5	2.1	4.38	0.39
229151 grt c.5	1.39	0.41	1.65	0.67	0.24	0.12	0.58	0.29	0.053	0.04
229151 grt c.6	1.56	0.19	11.9	0.98	2.17	0.24	16.1	1.3	3.15	0.29
229151 grt c.7	1.61	0.27	3.78	0.79	0.502	0.086	2.3	0.48	0.43	0.089
229151 grt c.8	1.68	0.23	15.8	2	3.23	0.31	20.7	2.1	4.28	0.51
207690 grt a.1	0.35	0.18	2.19	0.92	0.318	0.093	1.45	0.53	0.19	0.066
207690 grt a.2	2.23	0.23	5.44	0.76	0.85	0.12	3.85	0.45	0.465	0.081
207690 grt a.3	2.56	0.5	7.2	1.6	1.16	0.18	6.3	1.1	1.03	0.15
207690 grt a.4	2.18	0.3	5.49	0.85	1.01	0.15	6.5	0.76	1.21	0.2
207690 grt a.5	2.8	0.39	12.4	1.8	2.42	0.26	18.6	2.1	3.54	0.42
207690 grt a.6	3.08	0.61	14.8	4.5	2.9	0.5	16.8	2.2	3.73	0.81
207690 grt b.1	1.37	0.3	2.98	0.76	0.38	0.12	1.77	0.5	0.434	0.085
207690 grt b.2	2.02	0.22	5.04	0.91	0.51	0.11	2.51	0.44	0.458	0.091
207690 grt b.3	2.21	0.26	4.5	0.75	0.524	0.098	2.21	0.34	0.384	0.069
207690 grt b.4	2.68	0.28	5.3	0.83	0.8	0.14	4.29	0.59	0.8	0.13
207690 grt b.5	3.62	0.53	11.1	1.6	2.24	0.25	16.2	1.6	4.18	0.35

Table E1.1. (continued)

Sample	^{166}Er	±	^{169}Tm	±	^{172}Yb	±	^{175}Lu	±	^{178}Hf	±
229151 grt a.1	0.71	0.2	0.121	0.044	0.95	0.3	0.13	0.024	0.024	0.03
229151 grt a.2	3.54	0.4	0.59	0.11			0.791	0.053	0.104	0.029
229151 grt a.3	4.54	0.64	0.68	0.11	5.79	0.69	0.959	0.076	0.137	0.036
229151 grt a.4	3.61	0.61	0.66	0.13	5.7	1.1	0.883	0.057	0.126	0.043
229151 grt a.5	5.35	0.57	0.93	0.11	7.59	0.68	1.33	0.1	0.138	0.032
229151 grt b.1	2.21	0.41	0.287	0.07	2.25	0.44	0.29	0.032	0.204	0.051
229151 grt b.2	4.38	0.56	0.64	0.1	4.21	0.59	0.533	0.053	0.209	0.056
229151 grt b.3	7.02	0.56	1.02	0.13	7.63	0.94	1.142	0.061	0.148	0.041
229151 grt b.4	3.12	0.5	0.69	0.19	3.3	0.82	0.636	0.073	0.163	0.063
229151 grt c.1	7.69	0.68	1.39	0.15	11.2	1	2.315	0.098	0.083	0.034
229151 grt c.2	10.13	0.69	1.52	0.17	10.8	1.2	1.562	0.077	0.057	0.022
229151 grt c.3	14.3	1.4	2.19	0.33	13	2	1.81	0.14	0.208	0.075
229151 grt c.4	13.6	1.3	2.04	0.27	13	1.5	1.79	0.12	0.175	0.069
229151 grt c.5	0.21	0.17			0.1	0.13	0.019	0.013	0.082	0.047
229151 grt c.6	8.08	0.63	1.1	0.14	7.6	0.88	1.115	0.066	0.19	0.044
229151 grt c.7	0.93	0.23	0.11	0.041	0.49	0.18	0.064	0.014	0.256	0.047
229151 grt c.8	10.6	1.2	1.43	0.19	8.9	1.2	1.2	0.14	0.218	0.047
207690 grt a.1	0.74	0.32	0.152	0.078	1	0.35	0.227	0.054	0.125	0.053
207690 grt a.2	1.22	0.21	0.138	0.047	1.11	0.27	0.215	0.03	0.18	0.045
207690 grt a.3	2.19	0.42	0.36	0.15	2.6	1.1	0.378	0.059	0.7	0.19
207690 grt a.4	3.5	0.66	0.58	0.13	4.87	0.87	0.66	0.057	0.204	0.057
207690 grt a.5	10.6	1.1	1.51	0.2	11.5	1.6	1.54	0.17	0.22	0.054
207690 grt a.6	11.9	2.3	2	0.54	11.8	1.9	1.86	0.16	0.24	0.13
207690 grt b.1	1.15	0.28	0.222	0.076	1.78	0.59	0.378	0.064	0.18	0.058
207690 grt b.2	1.33	0.27	0.204	0.059	1.43	0.32	0.244	0.025	0.175	0.04
207690 grt b.3	1.12	0.24	0.152	0.045	1.21	0.26	0.204	0.026	0.172	0.043
207690 grt b.4	2.43	0.36	0.45	0.11	2.89	0.51	0.388	0.048	0.204	0.045
207690 grt b.5	11.9	1.2	1.92	0.24	12	1.3	1.89	0.13	0.221	0.064

RECORD 2019/3

METAMORPHIC HISTORY OF THE MOUGOODERRA FORMATION, YLGARN CRATON, WESTERN AUSTRALIA

This Record is published in digital format (PDF) and is available as a free download from the DMIRS website at <www.dmp.wa.gov.au/GSWApublications>.

Further details of geological products can be obtained by contacting:

Information Centre
Department of Mines, Industry Regulation and Safety
100 Plain Street
EAST PERTH WESTERN AUSTRALIA 6004
Phone: +61 8 9222 3459 Fax: +61 8 9222 3444
www.dmp.wa.gov.au/GSWApublications

Parmenter